



TECHNISCHE
UNIVERSITÄT
WIEN

INSTITUT FÜR
MECHANIK UND
MECHATRONIK
Mechanics & Mechatronics



DISSERTATION

Advanced Control and Online Monitoring of Fuel Cell Systems

ausgeführt zum Zwecke der Erlangung des akademischen Grades
eines Doktors der technischen Wissenschaften (Dr.techn.)
unter der Leitung von

Univ.Prof. Dipl.-Ing. Dr.techn. Stefan Jakubek

am Institut für Mechanik und Mechatronik,
Forschungsbereich Regelungstechnik und Prozessautomatisierung,

eingereicht an der Technischen Universität Wien,
Fakultät für Maschinenwesen und Betriebswissenschaften,

von

Martin Vrlić, mag.phys.

Matrikelnummer 01652342

Brnaze 179

Sinj, Croatia

Wien, 29. November 2024

To my family,
without whom I would not be where I am

Acknowledgments

I want to express my deep gratitude to Professor Stefan Jakubek for his unique and excellent mentorship, which extends beyond the scientific and educational work we did together over the past few years. His guidance has been very important in guiding my doctoral studies.

Thanks to Professor Christoph Hametner for his motivational conversations and his trust in me during our collaborations, especially in the recent years. His support has been of big help.

Special thanks to Dr. Daniel Ritzberger for his mentorship and patience from the very beginning of my studies. Our discussions have been invaluable, both academically and personally. Additionally, I want to thank one of my dearest colleagues, Dr. Zhang Peng Du, for his relaxed and humorous approach, which lightened difficult moments and provided much-needed encouragement.

I am thankful to Dr. Andraž Kravos from the University of Ljubljana for his insights into fuel cells and our fruitful collaboration. I extend my gratitude to Dr. Alexander Schirrer for his practical advice that often saved me significant time and effort and extended my horizons.

Finally, I am incredibly grateful to my family, especially my beloved wife Rahela and our (for now) two children, Emilija and Rafael, for standing (and crawling) by me throughout my PhD journey and giving me the strength to overcome any challenge. Their constant support has been my firm standing place. I want to thank my family, friends and teammates. Their help and support over the past few years have meant a lot to me. They've all been a big part of my journey, and I'm really grateful for everything they've done.

Diese Arbeit wurde von der Österreichischen Forschungsförderungsgesellschaft (“PROTECT” Projektnummer 865181 und “AlpeDHues” Projektnummer 884322), der Christian Doppler Gesellschaft und der TU Wien Bibliothek (Open Access Funding Program und Lektoratsservice) unterstützt.

Ich nehme zur Kenntnis, dass ich zur Drucklegung meiner Arbeit unter der Bezeichnung Dissertation nur mit Bewilligung der Prüfungskommission berechtigt bin.

Eidesstattliche Erklärung

Ich erkläre an Eides statt, dass die vorliegende Arbeit nach den anerkannten Grundsätzen für wissenschaftliche Abhandlungen von mir selbstständig erstellt wurde. Alle verwendeten Hilfsmittel, insbesondere die zugrunde gelegte Literatur, sind in dieser Arbeit genannt und aufgelistet. Die aus den Quellen wörtlich entnommenen Stellen, sind als solche kenntlich gemacht.

Das Thema dieser Arbeit wurde von mir bisher weder im In- noch Ausland einer Beurteilerin/einem Beurteiler zur Begutachtung in irgendeiner Form als Prüfungsarbeit vorgelegt. Diese Arbeit stimmt mit der von den Begutachterinnen/Begutachtern beurteilten Arbeit überein.

Ich nehme zur Kenntnis, dass die vorgelegte Arbeit mit geeigneten und dem derzeitigen Stand der Technik entsprechenden Mitteln (Plagiat-Erkennungssoftware) elektronisch-technisch überprüft wird. Dies stellt einerseits sicher, dass bei der Erstellung der vorgelegten Arbeit die hohen Qualitätsvorgaben im Rahmen der geltenden Regeln zur Sicherung guter wissenschaftlicher Praxis „Code of Conduct“ an der TU Wien eingehalten wurden. Zum anderen werden durch einen Abgleich mit anderen studentischen Abschlussarbeiten Verletzungen meines persönlichen Urheberrechts vermieden.

Wien, 29. November 2024

Martin Vrlić

Kurzfassung

Diese Dissertation untersucht intelligente Methoden zur Steuerung und Überwachung von Brennstoffzellensystemen mit Polymer-Elektrolyt-Membran (PEMFC), wobei der Schwerpunkt auf deren Einsatz in Fahrzeuganwendungen liegt. Das Hauptziel ist, den sicheren und effizienten Betrieb von Brennstoffzellenfahrzeugen zu gewährleisten.

Im ersten Teil der Arbeit wird die Bereitstellung dynamischer Leistungsanforderungen eines realen Brennstoffzellenfahrzeugs behandelt. Dabei geht es insbesondere um schnelle Änderungen der inneren Zustände der Brennstoffzelle. Mithilfe einer modellprädiktiven Regelung basierend auf sukzessiver Linearisierung (SLMPC) wird nicht nur die benötigte Leistung bereitgestellt, sondern es werden auch Sicherheitsgrenzen eingehalten und der Wasserstoffverbrauch im Vergleich zu einem Referenzfahrzeug reduziert.

Im zweiten Teil wird ein echtzeitfähiger modellprädiktiver Referenzregler (RG-MPC) für die Steuerung von Brennstoffzellen in Fahrzeuganwendungen vorgestellt. Dieser neue Ansatz bietet Referenztrajektorien für untergeordnete Regler und ermöglicht die Anpassung von Mehrgrößensystemen sowie die Handhabung von Einschränkungen. Durch die sukzessive Linearisierung wird die Echtzeitfähigkeit gewährleistet, was im Wesentlichen ein Upgrade bestehender Regelungskonzepte darstellt, ohne dass ein vollständiges Systemdesign erforderlich ist.

Der dritte Teil der Dissertation konzentriert sich auf die Online-Überwachung von Brennstoffzellensystemen. Hierfür wird ein nichtlinearer Beobachter mit reduzierter Dimensionalität und verteilten Parametern eingeführt, der interne Phänomene wie Reaktantenmangel und Membrantrocknung/-flutung effizient erkennen kann. Mithilfe virtueller Sensorik und eines hochauflösenden Modells mit verteilten Parametern korrigiert der Beobachteralgorithmus effizient die vorhergesagten Zustandsverteilungen und zeigt in detaillierten Simulationen eine hohe Rechenleistung und robuste Leistung.

Diese umfangreiche Forschung bietet einen Rahmen für die Weiterentwicklung der Steuerung und Überwachung von PEMFC-Systemen in Fahrzeuganwendungen. Die hier vorgestellten Strategien versprechen eine Steigerung der Effizienz, Sicherheit und Gesamtleistung von Brennstoffzellenfahrzeugen.

Abstract

This dissertation aims to investigate smart ways to control and monitor polymer electrolyte membrane fuel cell (PEMFC) systems, focusing on their use in automotive applications. The main goal is to make sure fuel cell vehicles operate safely and efficiently.

The first part of the research addresses the delivering of dynamic power demands of a real fuel cell vehicle, dealing with fast transients in the internal states of the fuel cell. Using successive linearization based model predictive control (SLMPC), the resulting work not only delivers the power demand but also enforces safety constraints, reducing the hydrogen consumption compared to a reference vehicle.

In the second part, a real-time capable reference governor superordinate model predictive controller (RG-MPC) for fuel cell control in automotive applications is introduced. This novel approach provides reference trajectories for subordinate controllers, offering the possibility to adapt multivariable control systems and constraint handling. The use of successive linearization ensures real-time feasibility, essentially offering an upgrade to existing control schemes without requiring a complete system redesign.

The dissertation concludes with the third part, focusing on online monitoring of fuel cell systems. For this purpose, a reduced-dimensionality nonlinear distributed-parameter observer is introduced to efficiently detect internal phenomena such as reactants' starvation and membrane dryout/flooding. Using virtual sensing and a high-order distributed-parameter model, the observer algorithm efficiently corrects predicted internal state distributions, demonstrating computational efficiency and robust performance through detailed simulations.

This extended research provides a framework for advancing the control and monitoring of PEMFC systems in automotive applications. The strategies presented here hold the promise of increasing efficiency, safety, and overall performance of fuel cell vehicles.

Contents

1	Overview	1
1.1	Motivation and Problem Statement	2
1.1.1	State-of-the-Art Review	3
1.1.2	Problem Statement	6
1.2	Goals	7
1.3	Methodology	8
1.3.1	Fuel Cell System Modeling	8
1.3.2	Model Predictive Control (MPC) Techniques	12
1.3.3	Reduced-dimensionality Distributed-parameter Observer	19
1.3.4	Validation and Simulation Framework	21
1.4	Summary of Scientific Publications	25
1.5	Scientific Contribution of This Thesis	26
	Bibliography	27
2	Publications	33
2.1	Publication A	34
2.2	Publication B	51
2.3	Publication C	69
	Curriculum Vitae	84
	List of Scientific Publications	86

List of Figures

1.1	Fuel cell zero-dimensional model	10
1.2	The quasi-2D fuel cell model and its spatial discretization	11
1.3	Refernce governor MPC scheme	17
1.4	Distributed observer scheme	20
1.5	Net power tracking	21
1.6	Performance in pressure difference control	22
1.7	Membrane water content distribution	23

List of Abbreviations

The following abbreviations are used in this manuscript:

CFD	Computational fluid dynamics
EKF	Extended Kalman filter
FC	Fuel cell
GDL	Gas diffusion layer
MPC	Model predictive control
PEMFC	Polymer electrolyte membrane fuel cell
PI	Proportional-integral
QP	Quadratic programming
RG-MPC	Reference governor model predictive control
SLMPC	Successive linearization model predictive control

List of Symbols

The following symbols are used in this manuscript:

Subscripts

an	Anode
ca	Cathode
em	Exhaust manifold
GDL	Gas diffusion layer
liq	Liquid
N ₂	Nitrogen
O ₂	Oxygen
ref	Reference
sm	Supply manifold

vap Water vapor

Symbols

α_{ca}	Cathode backpressure valve opening
$\Delta \mathbf{u}_i$	Control input increment
\mathbf{A}_d	Discretized state matrix
\mathbf{A}_k	State matrix at time step k
\mathbf{B}_d	Discretized input matrix
\mathbf{B}_k	Input matrix at time step k
\mathbf{C}_d	Discretized output matrix
\mathbf{C}_k	Output matrix at time step k
\mathbf{D}_d	Discretized feedthrough matrix
\mathbf{D}_k	Feedthrough matrix at time step k
\mathbf{f}	State equation function
\mathbf{f}_{Q2D}	State transition function for quasi-2D model
\mathbf{h}	Output equation function
\mathbf{Q}	Output weighting matrix
\mathbf{R}	Control effort weighting matrix
\mathbf{u}	Input vector
\mathbf{x}	State vector
\mathbf{y}	Output vector
Δp	Pressure difference
$\dot{\mathbf{x}}$	Time derivative of the state vector
η_{sys}	System efficiency
$a_{m,d}$	Water activity
I	Current
I_{an}	Integral term for anode PI controller
I_{ca}	Integral term for cathode PI controller
J	Objective cost
k	Time step index
$K_{i,an}$	Integral gain for anode pressure PI controller
$K_{i,ca}$	Integral gain for cathode pressure PI controller
$K_{p,an}$	Proportional gain for anode pressure PI controller
$K_{p,ca}$	Proportional gain for cathode pressure PI controller
m	Mass of reactants
N_c	Control horizon
N_p	Prediction horizon
p	Absolute pressure

P_{net}	Net system power
W_{in}^{an}	Inlet flow rate of the anode
W_{in}^{ca}	Inlet flow rate of the cathode

Chapter 1

Overview

For sustainable no emission transportation, Polymer Electrolyte Membrane Fuel Cells (PEMFCs) have become a promising option compared to conventional internal combustion engines. In this dissertation, the use of PEMFCs in automotive applications is examined.

An important part of this thesis is the development and use of safe and efficient control strategies, addressing the various operating limits found in real vehicles. The complex dynamics of PEMFCs, as an important part in no emission vehicles, requires careful control for best performance and lifespan. Advanced control methods are used, addressing challenges caused by temperature changes, different power demands, and other operating conditions during the specific automotive application. By focusing on the importance of control strategies, this research helps to improve the overall efficiency and reliability of PEMFCs in automotive applications.

In addition, the thesis investigates on online monitoring of fuel cell distributed internal states using state observers. Due to the fast dynamic operation of PEMFCs, online monitoring is crucial. State observers act as tools to provide real-time insights into the system's internal states. This part of the research wants to develop an observer for monitoring and analyzing fuel cell internal states, enabling the detection of critical or even faulty conditions. The use of state observers helps in understanding the PEMFC operation, useful for the overall system health and efficiency.

Together, this thesis highlights the link between control strategies and state observer-based monitoring, setting the stage for a combined system. This combination not only meets immediate operational needs but also anticipates and adjusts to the changing conditions found in automotive applications. By combining advanced control techniques with real-time monitoring using state observers, this research's goal is to advance the field of PEMFCs towards practical and efficient use in automotive applications.

To sum up, this thesis offers a detailed look at the progress in Polymer Electrolyte Membrane Fuel Cells, emphasizing their potential as a sustainable replacement for in-

ternal combustion engines in automotive applications. Through the investigation of safe and efficient control strategies and the use of state observers for online monitoring, the research contributes to ongoing efforts in creating sustainable energy solutions for the future of transportation.

Chapter 1 provides an overview of this work by presenting the motivation, problem statement, and goals. It also provides a brief introduction into the developed methods, followed by a summary of the scientific publications and the unique contribution of this research. The main focus of this thesis, comprised of the selected journal publications, is outlined in Chapter 2, along with a description of the author's specific contributions to each publication.

1.1 Motivation and Problem Statement

Successfully using fuel cell systems in automotive applications requires an advanced control system, capable of delivering the requested power, while at the same time ensuring both safety and efficiency requirements are met. This thesis addresses this important question with the approach outlined in the three constituting publications.

Publication A introduces a new strategy using a nonlinear state space model along with successive linearization-based model predictive control (SLMPC). This method improves the control of fuel cell systems in dynamic automotive applications. Therefore, in Publication A the initial contributions for safe and efficient fuel cell control are presented, setting the stage for the subsequent parts of this research.

In Publication B, the challenge of avoiding a complete replacement of a Proportional-Integral (PI) based controller, is addressed. Publication B introduces a higher-level reference governor model predictive controller (RG-MPC). This top-level controller is designed to easily work with existing PI controllers, providing the lower level PIs the reference trajectories that align with the goals outlined in Publication A. This cooperative interaction between the top-level controller and PI controllers ensures a successful use of the proposed control strategy without having to rebuild the existing control setup.

In Publication C, the focus moves to online monitoring through the use of a distributed state observer. Using a distributed parameter nonlinear fuel cell model and applying model reduction methods, such as Balanced Truncation, this state observer estimates the distributed internal states of the fuel cell. The described online monitoring, is used in the control system, providing real-time insights on the fuel cell's behavior and alerting the system to any faulty or critical conditions.

To sum up, the following sections of this thesis build on the ideas presented in Publications A, B, and C. The use of a nonlinear state space model for predictive control, the creation of a higher-level reference governor to work with existing PI controllers, and

the use of a state observer for online monitoring together constitute a complex dynamic system. This thesis has the goal of contributing to the improvement of control methods for fuel cell systems in automotive applications, ensuring an optimal approach to power delivery, safety, and efficiency.

1.1.1 State-of-the-Art Review

Overview of Modeling Approaches in PEMFC Systems

Modeling is a fundamental aspect of understanding and optimizing PEMFC systems. Accurate models are essential for predicting system behavior, designing control strategies, and diagnosing issues [1]. Two primary modeling approaches are used in PEMFC research and application: lumped parameter models and distributed parameter models.

Lumped parameter models simplify the representation of a fuel cell by aggregating all the physical phenomena into a single or a few states, often neglecting spatial variations [2]. These models are typically zero-dimensional, treating the system as if it has no spatial extension. This simplification makes lumped models computationally efficient, allowing for real-time simulation and control applications [3]. They are particularly useful in control design due to their reduced complexity and ease of integration into control algorithms like Proportional-Integral-Derivative (PID) and Model Predictive Control (MPC) [4]. However, the primary limitation of lumped models is their inability to capture spatial variations within the cell, such as temperature gradients and uneven reactant distribution, which can lead to less accurate predictions under varying operating conditions [5].

In contrast, distributed parameter models provide a more detailed representation by incorporating spatial dimensions into the model [6]. These models are typically one-dimensional (1D), two-dimensional (2D), or even three-dimensional (3D), capturing the variations in physical properties across the fuel cell [7]. For example, quasi-2D models can describe phenomena like gas distribution and membrane hydration more accurately, which are crucial for understanding and predicting fuel cell performance and degradation [8]. Distributed models are more complex and computationally intensive, making them less suitable for real-time control applications but invaluable for detailed analysis and design optimization [9].

Lumped and distributed models serve different purposes in PEMFC research and application [10]. Lumped models are favored for their simplicity and real-time applicability, while distributed models are essential for detailed studies and precise diagnostics [11]. Hybrid modeling approaches aim to combine the strengths of both, using lumped models for control and distributed models for monitoring and diagnostics [12]. These integrated models allow for comprehensive system analysis and control, balancing the need for

detail and computational efficiency [13].

Control Strategies for PEMFC Systems

Classical control techniques, such as Proportional-Integral-Derivative (PID) controllers, have been widely used in PEMFC systems due to their simplicity and ease of implementation [14]. These controllers adjust the control inputs based on the error between a measured process variable and a desired setpoint, providing a straightforward mechanism to maintain desired operating conditions [15]. However, PID controllers may struggle with the nonlinearities and multivariable interactions inherent in fuel cell systems [16]. The tuning of PID parameters involves balancing response time, stability, and overshoot, which can be challenging to optimize [17].

Model Predictive Control (MPC) offers a significant advancement over classical control methods, particularly for complex systems like PEMFCs [18]. MPC uses a dynamic model of the system to predict future behavior and optimize control inputs over a specified time horizon [19]. Notable variants of MPC in PEMFC applications include SLMPC and RG-MPC [20, 21]. SLMPC effectively handles the nonlinear characteristics of fuel cells by updating the linear model at each control step, reflecting the current operating point [22]. RG-MPC provides setpoints for subordinate controllers, ensuring safe and efficient system operation through a layered approach that handles constraints and disturbances, enhancing system robustness [21, 23].

Adaptive and robust control strategies address uncertainties and variabilities in PEMFC systems [24]. Adaptive control adjusts its parameters in real-time based on changes in system dynamics, making it suitable for scenarios with varying system characteristics, such as load changes or degradation over time [25]. Robust control aims to maintain performance despite uncertainties and disturbances, with techniques like H-infinity control and sliding mode control being explored in PEMFC applications [26]. These approaches ensure system stability and performance under adverse conditions [27].

In summary, the choice of control strategy for PEMFC systems depends on the specific requirements of the application, including the need for real-time response, robustness to disturbances, and computational resources. The trend towards integrating advanced control methods with classical approaches offers a balance between simplicity and performance [28].

Monitoring and Diagnostic Techniques in PEMFC Systems

State estimation, virtual sensing, and diagnostic algorithms are critical aspects for the effective monitoring and control of PEMFC systems [29]. Due to the inherent complexity of these systems, not all internal states can be directly measured [30]. State observers,

such as Kalman filters and Luenberger observers, are commonly used to estimate unmeasurable states [31]. These observers leverage mathematical models and available measurements to provide estimates of crucial internal states like membrane hydration levels, reactant concentrations, and temperature distributions [32]. Advanced observers, including nonlinear and unscented Kalman filters, can accommodate the nonlinearities present in PEMFC systems, offering more accurate and reliable state estimations [33].

Virtual sensing methods have become increasingly significant in PEMFC systems, especially for parameters that are difficult or impossible to measure directly [34]. High-order distributed-parameter models are particularly useful as they account for spatial variations within the fuel cell [35, 36]. Virtual sensors estimate critical internal states such as the local current density and gas concentration profiles, which are essential for optimizing fuel cell performance. There are close to none publications on the topic as the problem of PEMFC distributed states estimation is quite novel and an integral part of this dissertation. The accuracy and reliability of these estimates are to be validated through comparisons with physical sensors and empirical data.

Effective fault detection and diagnosis are essential for maintaining the safety and efficiency of PEMFC systems [37]. Diagnostic algorithms analyze data from sensors and virtual sensors to detect anomalies indicative of faults or degradation. The use of machine learning and data-driven methods in these algorithms enhances the accuracy and speed of fault diagnosis [38]. By learning from historical data, these algorithms can identify patterns associated with specific faults, facilitating early detection and intervention [39]. Additionally, model-based approaches utilize detailed physical models to diagnose faults by identifying deviations from expected behavior [40]. The integration of diagnostic algorithms with control systems allows for proactive management, reducing downtime and extending the life of PEMFC systems [41].

In conclusion, the combination of state estimation, virtual sensing, and diagnostic algorithms provides a robust framework for the real-time monitoring and fault management of PEMFC systems. These techniques are vital for ensuring the reliability and efficiency of fuel cells, supporting their broader adoption in various applications.

Computational and Modeling Challenges

Accurate modeling of PEMFC systems is complex due to the nonlinear and multivariable nature of the processes involved [42]. High-fidelity models that can accurately predict system behavior often require significant computational resources, making real-time application challenging [43]. This is particularly problematic for control and monitoring systems that need to operate in real-time to ensure safe and efficient operation [44]. Model reduction techniques and the development of efficient algorithms are essential to make these high-fidelity models usable in practical applications [45, 35]. However, these

approaches often involve trade-offs between accuracy and computational feasibility.

1.1.2 Problem Statement

As the focus of this dissertation, the following questions explore optimizing the control and monitoring of PEMFC systems in real-world automotive applications. Addressing dynamic challenges posed by varying power demand and internal states, these questions aim to contribute valuable insights to the advancement of fuel cell technology.

Main Question

How can the control and monitoring of polymer electrolyte membrane fuel cell systems in real-world automotive applications be optimized to ensure safe and efficient operation, addressing the dynamic challenges posed by varying power demand and internal states?

Subordinate Questions

1. **What innovative control strategies, especially those utilizing SLMPC, can be employed to effectively track transient power demand in PEMFC stacks while simultaneously ensuring safe operation through adherence to imposed safety constraints?**

Addressing the transient power demand of PEMFC stacks requires innovative control strategies capable of dynamically adjusting to changing conditions. The use of SLMPC, with its ability to linearize the nonlinear fuel cell system in real-time, stands as a potential solution. This question explores the specific control strategies that can robustly track power demand while ensuring the safety of the PEMFC system.

2. **How can existing Proportional-Integral control schemes for fuel cell stacks in automotive applications be upgraded without the need for a complete interface rebuild, and what role does a real-time capable RG-MPC play in providing efficient and safe power control solutions?**

Upgrading existing control schemes without rebuilding interfaces is a challenge in automotive applications. This question delves into the potential of RG-MPC as a real-time capable controller, investigating its role in providing efficient and safe power control solutions. Understanding the mechanisms for upgrading PI control schemes is crucial for practical implementation in real-world fuel cell vehicles.

3. **In the context of online monitoring for fuel cell systems, what approaches, such as the reduced - dimensionality nonlinear distributed - parameter observer, can be utilized to efficiently correct predicted quantities based on high-order distributed-parameter fuel cell models, enabling the robust and computationally efficient monitoring of internal phenomena like reactants' starvation and membrane dryout?**

Monitoring fuel cell systems online is essential for ensuring reliable and efficient operation. This question explores the use of reduced-dimensionality nonlinear distributed-parameter observers to correct predicted quantities. Understanding how such approaches efficiently monitor internal phenomena, including reactants' starvation and membrane dryout, is critical for enhancing the overall performance and longevity of PEMFC systems.

1.2 Goals

The contribution of this dissertation is to better understand and provide improvement to the control as well as the monitoring of fuel cell systems in automotive applications. The main goals are as follows:

- **Real-Time Control Improvement with RG-MPC:** This project is about creating a better way to control fuel cell systems in cars using a real-time reference governor model predictive controller (RG-MPC). The goal is to improve how traditional controllers, like proportional-integral ones, work by adding an extra layer with RG-MPC. This new setup helps make smarter control decisions while handling different factors at the same time. We'll test how well it works and how safe it is by trying it out in real driving situations.
- **Integration of PI Dynamics and Successive Linearization:** This study focuses on combining Proportional-Integral control dynamics into the RG-MPC controller. The aim is to ensure that the control commands work well with existing systems. The technique of successive linearization will be used to handle the complex behavior of the fuel cell model during real-time operations, improving control accuracy.
- **Observer-Based Internal State Estimation:** A key aspect of this research is developing a method to estimate the internal states of fuel cell systems. Using a detailed fuel cell model, the goal is to create an algorithm that predicts and corrects internal conditions. This includes monitoring critical issues like reactant starvation and membrane issues, thus enhancing the reliability and safety of fuel cell operations.
- **Efficient Observer Algorithm with Model Reduction:** The project aims to create a computationally efficient observer algorithm for estimating internal states, using model reduction techniques like Balanced Truncation. This approach will address

the complexity of high-dimensional models and provide accurate state estimates in real-time.

- **Validation and Real-World Application:** The final phase involves validating the proposed control and observation methods through simulations and real-world tests. The goal is to demonstrate the practical benefits of the RG-MPC and observer algorithms in managing safe and efficient fuel cell operations, particularly in automotive contexts.

In summary, this dissertation aims to advance fuel cell control and monitoring methods, setting new standards for their use in automotive applications. The research intends to contribute significantly to the development of cleaner and more sustainable energy solutions.

1.3 Methodology

The main result of this thesis is achieving safe and efficient control by using a high-level controller and internal state monitoring through an observer. This includes specific results in system modeling, controller design, and observer design. Each method is briefly described in this section, and more details can be found in the related publications.

1.3.1 Fuel Cell System Modeling

In this section, two distinct models, integral to our research, will be presented. Firstly, the zero-dimensional lumped parameter model, utilized for the controller design, will be introduced. All the details of this model, including the definitions of the state, input, and output vectors, as well as the state and output equations, can be found in [46, 22].

Next, a quasi two-dimensional model employed in the design of the observer will be discussed. For an in-depth understanding of this model and its intricacies, references [8, 35] are recommended for further exploration of the details and implications. These two models collectively constitute essential components of our research framework, with each playing a unique role in shaping the overall methodology employed in this study.

Zero-dimensional lumped parameter model

The zero-dimensional dynamic fuel cell stack model is mathematically represented as a nonlinear state space model, striking a balance between computational efficiency and accuracy. The model captures fundamental dynamics, denoted by the following state and output equations:

$$\dot{\mathbf{x}} = \mathbf{f}(\mathbf{x}, \mathbf{u}) \quad (1.1)$$

$$\mathbf{y} = \mathbf{h}(\mathbf{x}, \mathbf{u}) \quad (1.2)$$

Here, \mathbf{x} represents the state vector, \mathbf{u} is the input vector, and \mathbf{y} denotes the outputs of the system. The state equation $\dot{\mathbf{x}} = \mathbf{f}(\mathbf{x}, \mathbf{u})$ encapsulates the system's dynamic evolution, while the output equation $\mathbf{y} = \mathbf{h}(\mathbf{x}, \mathbf{u})$ provides a description of the system's outputs. These equations together define the zero-dimensional model, enabling an accurate representation of gas dynamics, diffusion processes, and membrane humidification within the fuel cell stack. The state, input and output vectors are defined as:

$$\mathbf{x} = \begin{bmatrix} p_{sm}^{ca} \\ m_{O_2}^{ca} \\ m_{N_2}^{ca} \\ m_{vap}^{ca} \\ m_{liq}^{ca} \\ p_{em}^{ca} \\ p_{sm}^{an} \\ m_{H_2}^{an} \\ m_{N_2}^{an} \\ m_{vap}^{an} \\ m_{liq}^{an} \\ p_{em}^{an} \\ a_{m,d} \\ m_{O_2}^{GDL} \\ m_{N_2}^{GDL} \\ m_{vap}^{GDL} \end{bmatrix} \quad \mathbf{u} = \begin{bmatrix} W_{in}^{ca} \\ W_{in}^{an} \\ \alpha_{ca} \\ I \end{bmatrix} \quad \mathbf{y} = \begin{bmatrix} P_{net} \\ \Delta p \\ \eta_{sys} \end{bmatrix}. \quad (1.3)$$

The structure of the model is presented in Figure 1.1.

Some key components of the model include:

- **Gas Dynamics in Cathode and Anode:**
 - Described by interconnected zero-dimensional volumes.
 - Captures the essential gas flow and reactions within the cathode and anode compartments.
- **Gas Diffusion Layer on the Cathode Side:**
 - Considers the diffusion of gases through the gas diffusion layer on the cathode side.
 - Accounts for the impact of this diffusion on the overall performance of the fuel cell.

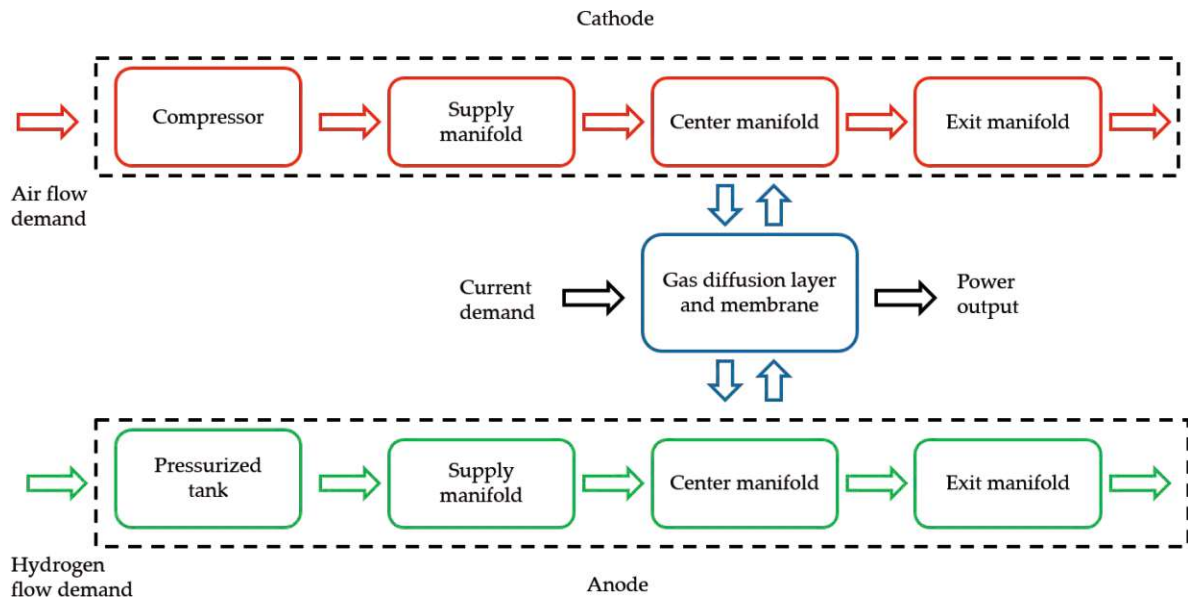


Figure 1.1: Fuel cell zero-dimensional model

- **Transient Membrane Humidification:**

- Models the dynamic humidification of the membrane.
- Recognizes the influence of membrane humidity on the overall behavior of the fuel cell stack.

Parameterization Methodology:

The zero-dimensional model undergoes an experimental parameterization process to align it with real-world behavior. The methodology involves approximating the non-linear fuel cell stack model using multiple local linear models obtained through analytic linearization. These local linear models are then incorporated into the state and output equations, ensuring continuous differentiability for real-time applicability.

Spatial Considerations:

While the zero-dimensional model provides an efficient representation, it does come with inherent limitations. The lumped volume approach restricts the simulation from accounting for spatially resolved information. Pressure and concentration gradients along the channel, as well as the effects and transport mechanisms of liquid water, are not fully captured in this simplified model.

Integration into System Simulation:

Once parameterized, the zero-dimensional stack model is seamlessly integrated into a larger system simulation. This integration considers additional dynamics, such as com-

pressor dynamics, feedback controllers for pressure control, and the purging strategy. The resulting virtual fuel cell system is then subjected to the same dynamic set point demand trajectories as a real fuel cell vehicle, facilitating comprehensive validation.

Role in Model Predictive Control (MPC):

For applications such as Model Predictive Control (MPC), which involves solving an on-line optimization problem for real-time decision-making, the choice of a zero-dimensional model is imperative. The computational demands of MPC necessitate a model that can provide predictive insights in real-time. A higher-dimensional model, while potentially more accurate, would be computationally prohibitive for the real-time constraints imposed by MPC. The zero-dimensional model's ability to balance accuracy and computational efficiency makes it a crucial asset for fuel cell systems where online optimization is essential for dynamic control and decision-making.

Quasi two dimensional distributed parameter model

In this section, the distributed parameter fuel cell model from [8] which is the underlying model of the observer is described. The model is splitted into several domains, shown in Figure 1.2. These domains are the cathode and anode channels, the cathode and anode gas diffusion layers and the membrane.

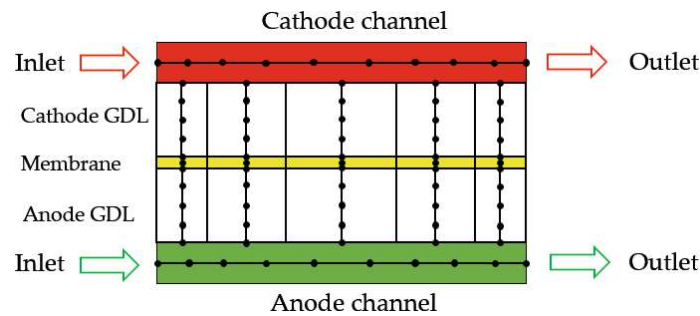


Figure 1.2: The quasi-2D fuel cell model and its spatial discretization

All the details of the model are given in [8, 35]. The model is called quasi-2D because of its independent discretization directions along and across the channels.

The model is assumed to be isothermal, with a controlled temperature. In this case, liquid water is not considered, but membrane drying and flooding can be estimated using the membrane water content.

Gas channels and GDL nodes described by variables such as gas velocity, mass fractions (oxygen, hydrogen, nitrogen, water vapor), gas pressure, and gas density. The model includes local current density computed for each slice and cell voltage as an aggregated

state. The system matrix sparsity pattern shows the interdependency of model domains (gas channels, slices) and their coupling, shown in Figure 3 of Publication C.

The presented model aims to capture the behavior of a fuel cell, considering key physical and operational aspects while facilitating computational efficiency through the use of quasi-2D spatial discretization and linearization techniques.

Considering all the modelling details, the resulting model structure is:

$$\mathbf{x}_k = \mathbf{f}_{\text{Q2D}}(\mathbf{x}_{k-1}, \mathbf{u}_{k-1}) \quad (1.4)$$

$$\mathbf{y}_k = \mathbf{C}\mathbf{x}_k \quad (1.5)$$

with \mathbf{x} containing several hundred states mentioned in the paragraph before, \mathbf{u} containing the boundary conditions of the system such as the pressure and gas composition at the system boundary. The output \mathbf{y} is considered to be the voltage in this research work. This model will later on be used for developing a state observer.

1.3.2 Model Predictive Control (MPC) Techniques

Successive linearization model predictive control

Fuel cell systems are complex, mainly due to their electrochemical processes and dynamic behaviors. Unlike simpler linear systems, fuel cells are inherently nonlinear, making it challenging to optimize their performance using traditional linear Model Predictive Control. To tackle this issue, Successive Linearization Model Predictive Control has become a valuable method specifically designed for the nonlinear dynamics of fuel cells.

Fuel cells play a crucial role in converting chemical energy into electrical power for various applications, from stationary power generation to transportation. However, their nonlinear nature, influenced by intricate electrochemical reactions, heat transfer, and mass transport phenomena, requires control strategies that can adapt to changes and handle complex interactions.

Traditional linear MPC, designed for simpler systems, struggles to effectively manage the complexities of fuel cell dynamics due to the inherent nonlinearities. SLMPC addresses this challenge by iteratively linearizing the nonlinear system dynamics around the current operating point. This iterative approach ensures that the controller remains adaptable to changes in the fuel cell's behavior, providing a robust framework for optimal control.

This explanation explores the mathematical basis of SLMPC for fuel cell systems, showing how it can handle the nonlinearities in these devices. By discussing the limitations of linear MPC and the need for a specialized approach, we introduce SLMPC as a tool that can effectively manage the unique characteristics of nonlinear fuel cell systems.

In this part, the zero-dimensional fuel cell model was used for developing the controller [22, 47, 21]. The continuous-time state space model is shown in Equation (1.2), but it is repeated here for clarity:

$$\dot{\mathbf{x}} = \mathbf{f}(\mathbf{x}, \mathbf{u}) \quad (1.6)$$

$$\mathbf{y} = \mathbf{h}(\mathbf{x}, \mathbf{u}). \quad (1.7)$$

In the process of developing a Successive Linearization Model Predictive Controller for fuel cell systems, the linearization of the model plays a crucial role. Unlike traditional linearization methods, successive linearization adopts a dynamic approach, performing linearization not just at a single operating point but at every time step throughout the system's operation.

At each time step, denoted as k , the model is linearized around the current state \mathbf{x}_k and control input \mathbf{u}_k . This continuous adaptation to the changing operating conditions allows the SLMPC to effectively capture the evolving dynamics of the fuel cell system.

The linearized model takes the form:

$$\dot{\mathbf{x}} \approx \mathbf{A}_k \cdot (\mathbf{x} - \mathbf{x}_k) + \mathbf{B}_k \cdot (\mathbf{u} - \mathbf{u}_k) \quad (1.8)$$

Simultaneously, the linearization of the output equation $\mathbf{y} = \mathbf{h}(\mathbf{x}, \mathbf{u})$ is performed, resulting in:

$$\mathbf{y} \approx \mathbf{C}_k(\mathbf{x} - \mathbf{x}_k) + \mathbf{D}_k(\mathbf{u} - \mathbf{u}_k) \quad (1.9)$$

Here, \mathbf{A}_k , \mathbf{B}_k , \mathbf{C}_k , \mathbf{D}_k represent the Jacobian matrices, which quantify the system's sensitivity to changes in state and control input. This dynamic linearization process ensures that the controller remains responsive to variations in the system, providing a more accurate representation of the fuel cell dynamics at each time step.

This dynamic approach is a key characteristic of the SLMPC, allowing it to adapt to the inherently nonlinear nature of fuel cell systems and enhance its effectiveness in achieving control objectives. The continuous linearization process contributes to the controller's ability to navigate through various operating conditions, making it a robust solution for real-time control in dynamic environments.

The next step in the development of the Successive Linearization Model Predictive Controller for fuel cell systems involves discretizing the continuous-time model. This step is crucial because our model predictive control algorithm is specifically designed and developed in discrete time.

At each time step k , the discretized model is expressed as:

$$\Delta \mathbf{x}_{k+1} = \mathbf{A}_d \Delta \mathbf{x}_k + \mathbf{B}_d \Delta \mathbf{u}_k \quad (1.10)$$

$$\Delta \mathbf{y}_k = \mathbf{C}_d \Delta \mathbf{x}_k + \mathbf{D}_d \Delta \mathbf{u}_k \quad (1.11)$$

Here, \mathbf{A}_d , \mathbf{B}_d , \mathbf{C}_d and \mathbf{D}_d are the discretized versions of the system matrices obtained through discretization. This transformation from continuous to discrete time is imperative to align the fuel cell system model with the discrete-time nature of the model predictive control algorithm. The Δ variables denote the deviation from the current trajectory point.

Discretization allows the SLMPC to effectively operate within the discrete-time framework of the MPC algorithm, ensuring seamless integration between the predictive control strategy and the system dynamics. It facilitates the translation of control actions into discrete steps, enabling the controller to make real-time decisions and adjustments based on the discretized model.

The discrete-time formulation enhances the computational efficiency and practical implementation of the SLMPC, making it well-suited for real-world applications where controllers operate in discrete intervals. The integration of discretization ensures that the fuel cell system responds optimally to control inputs within the discrete-time context, contributing to the overall effectiveness of the SLMPC algorithm in achieving control objectives.

The formulation of the Model Predictive Controller involves defining the prediction and control horizons (N_p and N_c), selecting tuning matrices (\mathbf{Q} and \mathbf{R}), and formulating the cost function:

$$J = \sum_{i=0}^{N_p-1} \left[(\mathbf{y}_i - \mathbf{y}_{\text{ref},i})^T \mathbf{Q} (\mathbf{y}_i - \mathbf{y}_{\text{ref},i}) + (\Delta \mathbf{u}_i)^T \mathbf{R} (\Delta \mathbf{u}_i) \right] \quad (1.12)$$

Here, \mathbf{y}_i is the predicted output at time step i , $\mathbf{y}_{\text{ref},i}$ is the defined control goal, and $\Delta \mathbf{u}_i$ is the predicted control input increment. The matrices \mathbf{Q} and \mathbf{R} weigh the importance of output and control effort, respectively.

The solution for $\Delta \mathbf{u}_i$ is given by the equation:

$$\Delta \mathbf{u}_i = \underset{\Delta \mathbf{u}_i}{\text{argmin}} J \text{ s.t. constraints} \quad (1.13)$$

This optimization process ensures that the control input increment is determined in a way that minimizes the cost function J while satisfying specified constraints, thereby achieving effective control objectives.

Defining control goals is a crucial aspect of the Successive Linearization Model Predictive Controller. The controlled output, represented by \mathbf{y} , encompasses key performance indicators of the fuel cell system. In this context, \mathbf{y} is a vector containing the following physical quantities:

$$\mathbf{y} = \begin{bmatrix} P_{\text{net}} \\ \Delta p \\ \eta_{\text{sys}} \end{bmatrix}$$

Here, P_{net} represents the net system power, and it is noteworthy that, in this research, P_{net} is obtained directly from an actual vehicle. The control objectives for Δp are to maintain it at 200 mbar, and for η_{sys} , the goal is to maximize its value.

These control goals, denoted by \mathbf{y}_{ref} , are summarized in Table 1.1. They create a challenging scenario as delivering the required net power demand, maintaining a specific pressure difference, and maximizing system efficiency are conflicting objectives. The challenge lies in developing a control strategy that optimally balances these competing goals over the prediction horizon. The control objectives guide the SLMPC in minimizing deviations of the predicted output \mathbf{y}_i from the reference trajectory $\mathbf{y}_{\text{ref},i}$, considering the inherent trade-offs between these conflicting goals. This intricate balance is crucial for effective and robust control of the fuel cell system.

Quantity	Variable	Actual Goal
Net System Power	P_{net}	Given by the actual vehicle
Pressure Difference	Δp	Maintain at 200 mbar
System Efficiency	η_{sys}	Maximize

Table 1.1: Control Goals

In the Successive Linearization Model Predictive Controller, constraints play a crucial role in shaping the behavior of the fuel cell system. The system variables, represented by m (masses of the reactants) and p (absolute pressures of the cathode and anode channels), are subject to certain limitations.

The constraints can be explicitly defined as follows:

Variable	Constraint
m	$1 \text{ g} \leq m$ (No upper limit)
p	$1 \text{ bar} \leq p \leq 2.4 \text{ bar}$
Δp	$100 \text{ mbar} \leq \Delta p \leq 300 \text{ mbar}$

Table 1.2: Explicit Constraint Definition

Here, the mass constraint specifies that the mass of oxygen and hydrogen must be at least 1 g, with no upper limit. The absolute pressures p are constrained to be within the range of 1 bar to 2.4 bar, ensuring safe operation. The pressure difference Δp is bounded between 100 mbar and 300 mbar, contributing to the stability of the fuel cell system.

Incorporating these constraints into the optimization problem is essential for the SLMPC algorithm to generate control inputs that meet the control goals while staying within the system's physical limits. This balance between control goals and constraints is key to a strong and effective control strategy for fuel cell systems.

The control problem becomes a quadratic programming (QP) problem when using the Successive Linearization Model Predictive Controller and the **qpOASES** solver. The main goal is to minimize a quadratic cost function, which measures how much the system outputs deviate from the desired paths while also considering the control effort. This cost function has specific constraints, such as keeping reactant masses and channel pressures within set limits. The optimization problem involves finding the best changes to the control inputs, represented by $\Delta \mathbf{u}_i$, over a given prediction horizon. The QP formulation includes weighting matrices, \mathbf{Q} and \mathbf{R} , which balance tracking accuracy and control effort. The **qpOASES** solver efficiently solves this QP problem, providing a solution that respects the system's dynamics and constraints. By using QP techniques, the SLMPC effectively guides the fuel cell system towards the desired performance while adhering to operational limits, showing the effective combination of mathematical optimization and real-time control strategies.

Reference governor model predictive control

This part builds up on the previous one, where the SLMPC is explained. The controller is extended to incorporate PI controllers.

In real-world fuel cell test stations, the implementation of multivariate Proportional-Integral controllers introduces challenges that stem from the lack of coordination between individual controllers. Oscillations, instabilities, and unpredictable interactions emerge as each PI controller operates independently, unaware of the behavior of the others. This uncoordinated approach often leads to suboptimal performance, as the controllers cannot adapt to changes in one another's outputs, creating a system prone to overshooting, undershooting, and oscillatory behavior.

To address the limitations of the conventional multivariate PI control setup, a more sophisticated control strategy is proposed. Building upon the state space model in Equation (1.2), this approach incorporates integrator states corresponding to two PI controllers responsible for regulating cathode and anode pressures. Specifically, one PI controller manipulates the cathode pressure via the backpressure valve, while the other

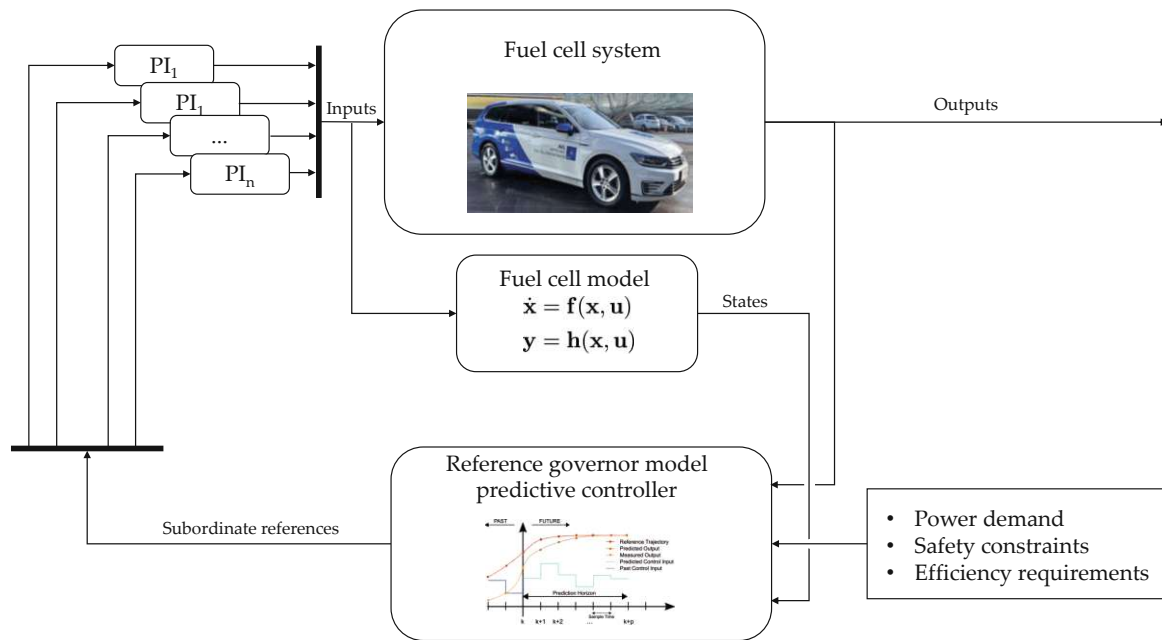


Figure 1.3: Safe and efficient general reference governor model predictive controller

manages the anode pressure by adjusting the inlet hydrogen mass flow. This extension augments the control framework by accounting for the integrative dynamics introduced by the PI controllers, offering a more comprehensive representation of the system.

In order to overcome the challenges associated with multivariate PI control, a superior solution is introduced - the implementation of a Reference Governor Model Predictive Controller. Unlike traditional PI controllers operating in isolation, the Reference Governor MPC acts as a centralized management system. This advanced controller, equipped with a deep understanding of the dynamics of the PI controllers, provides references to the individual controllers. Consequently, the PI controllers are no longer operating in isolation, but rather, they are seamlessly coordinated and managed by the Reference Governor MPC. This integration ensures that each PI controller is cognizant of the actions of the other, facilitating a synchronized and optimized control strategy for the fuel cell system. The result is a more robust and efficient control framework that mitigates the challenges associated with multivariate PI control in fuel cell test stations, offering improved stability and performance. The structure of the RG-MPC is shown in Figure 1.3. The PI controllers do the following action on the cathode backpressure valve

opening α_{ca} and the hydrogen inlet massflow W_{in}^{an} :

$$\alpha_{ca} = K_{p,ca}(p_{sm,ref}^{ca} - p_{sm}^{ca}) + K_{i,ca} \int_0^t (p_{sm,ref}^{ca} - p_{sm}^{ca}) d\tau \quad (1.14)$$

$$W_{in}^{an} = K_{p,an}(p_{sm,ref}^{an} - p_{sm}^{an}) + K_{i,an} \int_0^t (p_{sm,ref}^{an} - p_{sm}^{an}) d\tau. \quad (1.15)$$

The integrals $I_{ca} = \int_0^t (p_{sm,ref}^{ca} - p_{sm}^{ca}) d\tau$ and $I_{an} = \int_0^t (p_{sm,ref}^{an} - p_{sm}^{an}) d\tau$ are included in the state vector of the system. The inputs optimized by the RG-MPC do not longer include the hydrogen inlet massflow and the cathode backpressure valve opening. Instead, the references provided to the PI controllers are being optimized, namely $p_{sm,ref}^{ca}$ and $p_{sm,ref}^{an}$. This is clearly shown in Equation (1.16).

$$\mathbf{x} = \begin{bmatrix} p_{sm}^{ca} \\ m_{O_2}^{ca} \\ m_{N_2}^{ca} \\ m_{vap}^{ca} \\ m_{liq}^{ca} \\ p_{em}^{ca} \\ p_{sm}^{an} \\ m_{H_2}^{an} \\ m_{N_2}^{an} \\ m_{vap}^{an} \\ m_{liq}^{an} \\ p_{em}^{an} \\ a_{m,d} \\ m_{O_2}^{GDL} \\ m_{N_2}^{GDL} \\ m_{vap}^{GDL} \\ I_{ca} \\ I_{an} \end{bmatrix} \quad \mathbf{u} = \begin{bmatrix} W_{in}^{ca} \\ p_{sm,ref}^{an} \\ p_{sm,ref}^{ca} \\ I \end{bmatrix} \quad (1.16)$$

In addition to all the safety requirements already laid out in the SLMPC section, important efficiency requirements are imposed. The reason is obvious. Efficient operation of a fuel cell system involves careful consideration of various components, and one critical aspect is the minimization of compressor power. Compressors play a pivotal role in maintaining optimal operating conditions by ensuring the appropriate pressure levels for reactants. However, excessive power consumption by the compressor can significantly impact the overall efficiency of the system. By optimizing the compressor operation, the system achieves a delicate balance between energy consumption and maintaining the necessary pressures for fuel cell performance.

Operational efficiency is further enhanced by focusing on low electrical currents within the fuel cell system. Lower electrical currents reduce resistive losses, contributing to

improved overall efficiency. This consideration is particularly crucial in the design and implementation of stack configurations, where minimizing internal resistance is key to minimizing hydrogen consumption.

Optimizing voltage levels is a fundamental approach to improving the efficiency of fuel cell systems. By carefully selecting operating conditions, such as higher pressures, the voltage output of the system can be increased. Higher pressures contribute to improved mass transport within the fuel cell, facilitating more efficient electrochemical reactions. This strategic choice of operating conditions allows the system to generate higher voltage levels, enhancing overall energy conversion efficiency. Moreover, this approach aligns with the broader goal of maximizing power density and performance while maintaining system stability.

However, the controller may choose to operate at either lower or higher pressures depending on the dangerous operating zones instructed to the controller. An example can be seen in one of the results of the control operation compared to the reference vehicle in Figure 11 of Publication B.

1.3.3 Reduced-dimensionality Distributed-parameter Observer

Fuel cell systems, crucial for sustainable energy, demand precise monitoring for reliable operation. Traditional lumped-parameter models often employ a single variable to describe internal parameters like hydrogen concentration. However, these models fall short when attempting to capture spatial distribution information crucial for understanding phenomena such as reactants' starvation, membrane dryout/flooding, and nitrogen accumulation within the fuel cell.

The challenge lies in the placement of sensors within the fuel cell to monitor these phenomena directly. To address this, this thesis opts for virtual sensing using a high-order distributed-parameter fuel cell model. Unlike lumped-parameter models, distributed-parameter models account for spatial variations in internal states, making them more suitable for capturing local phenomena within the system. For this reason, the distributed model explained before, is used.

The observer has the job of estimating unmeasurable internal states of the fuel cell system, such as local current density, species concentrations and membrane water content. These states are critical for understanding and optimizing the fuel cell's performance. The employed model is a straight channel isothermal distributed parameter fuel cell model, validated beforehand against Computational Fluid Dynamics (CFD) simulations. For details on this topic, the reader is referred to [8].

The observer's goal is to predict these internal states using available measurement signals (in this case, the voltage signal and the boundary conditions of the system) and an

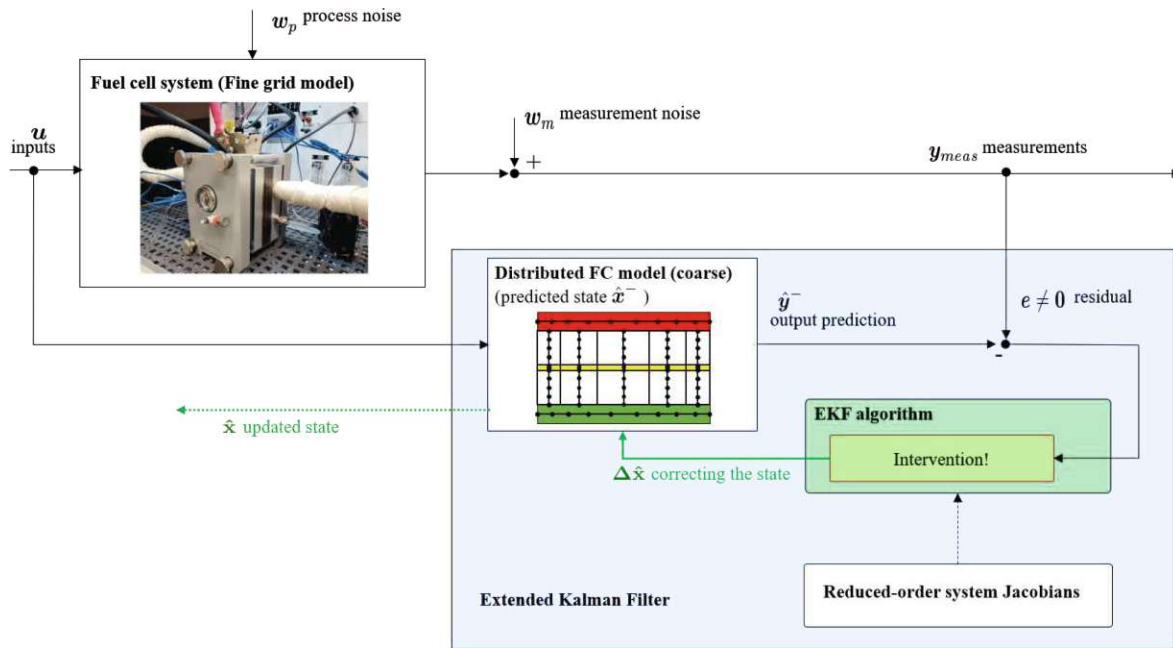


Figure 1.4: Reduced dimensionality distributed nonlinear fuel cell observer.

appropriate algorithm, in this case, the Extended Kalman Filter. The observer operates based on a coarse-grid version of the model, which inherently introduces a plant-model mismatch. The task is to minimize the difference between the measured output signal (voltage) from a fine-grid model (simulated reality) and the predicted output from the coarse-grid model. Successful minimization implies that the coarse-grid model effectively estimates the internal states, considering the model has been validated against reality. The structure of the observer with the two models of different resolutions can be seen in Figure 1.4.

For systems with a large number of states, like the fuel cell system in question, it is impractical to correct each individual state freely. Tuning the observer for hundreds of states becomes a daunting task, risking disproportional corrections that may lead to unrealistic system behavior.

Model reduction becomes necessary to identify and focus on the dominant dynamics of the system. By extracting only a few principal modes of the system, the observer can make corrections in the direction of these modes, avoiding the challenge of individually tuning numerous states. This not only streamlines the computational efficiency of the observer algorithm but also ensures a more realistic and manageable correction process for large-scale systems. The reduction in complexity allows for a more effective estimation of the distribution of internal states in the fuel cell system.

1.3.4 Validation and Simulation Framework

In this part, the validation of the previously explained concepts is detailed. Firstly, the performance of the proposed controller is showcased, accompanied by the presentation of selectively chosen results obtained from Publications A and B. Subsequently, an evaluation of the efficacy of the distributed observer is provided, elucidating upon the investigative outcomes highlighted in Publication C. This segment serves as the conclusion of the Methodology section, laying the groundwork for the subsequent original publications where the comprehensive extent of the research is detailed.

Safe and Efficient MPC

To evaluate the effectiveness of our control algorithm, we used data collected from a real fuel cell vehicle. This included power demand, voltage, pressure difference, and current measurements. This comprehensive dataset was carefully compared to validate our control method and determine its accuracy. However, it's important to note that our model has certain limitations. It cannot fully represent the complexity and unique aspects of the entire vehicle system. The vehicle operates with a sophisticated control structure that includes basic purging strategies, as well as several finely tuned PI controllers, all working together to manage the system.

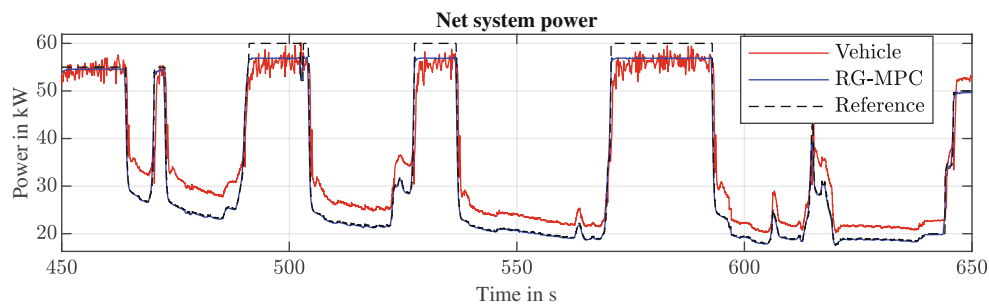


Figure 1.5: Net power tracking compared with a vehicle. (Reproduced from Publication B [21], with permission.)

Despite these complexities, it's encouraging to observe our controller successfully meeting the power demand, mirroring the vehicle's performance (see to Figure 1.5). Notably, our controller achieves this while adhering to the safety and efficiency conditions discussed earlier, underscoring its practical viability.

For a complete understanding of our research findings, readers are referred to Publications A and B, which explore the details of our model. A key example is the control of the pressure difference across the membrane, an important factor in fuel cell operation. With a target value set at 200 mbar and a safety margin of ± 100 mbar in our MPC

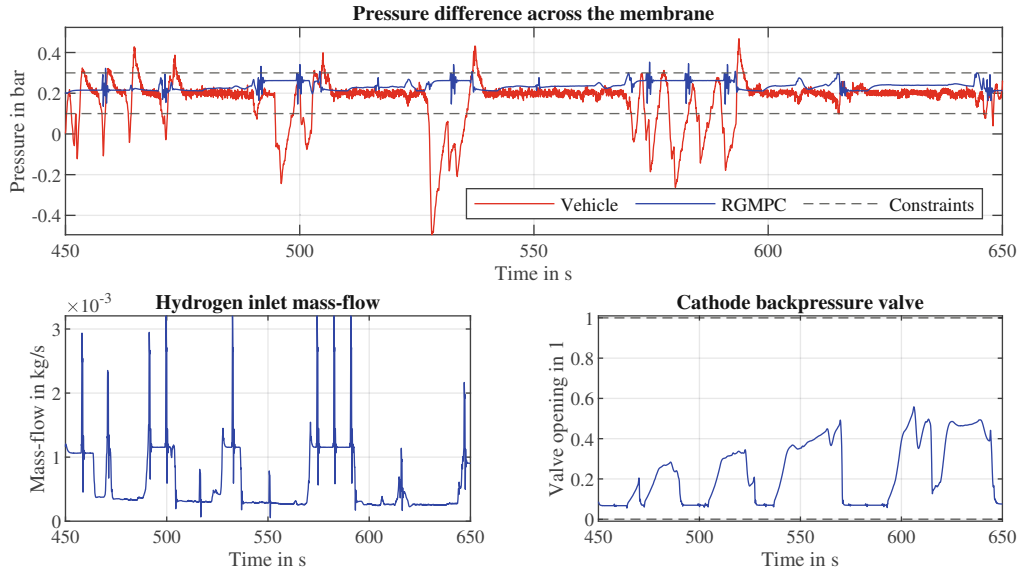


Figure 1.6: Performance in pressure difference control. (Reproduced from Publication B [21], with permission.)

framework, Figure 1.6 clearly shows the challenge faced by the vehicle's controller in keeping within these limits, since it doesn't handle constraints well. In contrast, our controller, based on optimal control ideas, smoothly manages this issue during purging events.

This promising performance extends the applicability of our controller to address the inherent nonlinear and multivariate challenges associated with fuel cell stack applications in vehicles. Furthermore, owing to its reference governor architecture, our controller offers the advantage of potential implementation without necessitating a complete overhaul of the existing interface. This achievement successfully addresses the initial two questions raised in the Problem Statement (section 1.1.2 of this thesis), laying the groundwork for future advancements in fuel cell control technology.

Distributed observer

Upon examining the results in Publications A and B, as well as a thorough review of current literature, it becomes clear that common approaches to management and observation of fuel cell systems mainly use a simplified method. A notable exception is seen in the work by Luna et al., where the tracking of internal conditions is methodically handled [36]. However, when the aim is to manage or observe the spatial details of internal conditions, especially crucial for evaluating wear, turning to a detailed parameter model becomes necessary. In this situation, we use the quasi-two-dimensional model described

in [8] as the basic structure for our state estimation efforts. Our approach incorporates

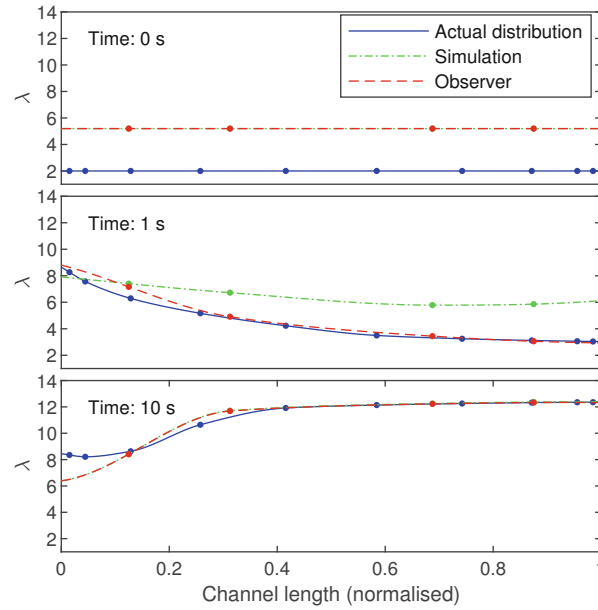


Figure 1.7: Membrane water content distribution along the channel at different times. (Reproduced from Publication C [35], with permission.)

two distinct resolutions of the model. The first, a coarse grid model, serves as the basis for the observer’s predictive function, essentially operating under the assumption that the coarse grid model faithfully represents the reality. The second resolution entails a fine grid model, which encapsulates the actual reality and constitutes the benchmark against which we aspire the observer to align its estimations. Notably, validation of the observer’s capability proves inherently challenging, given the impracticality of obtaining direct measurements within the fuel cell in real-world scenarios. While segmented cells permit local measurements of current density or temperature, real-time assessment of species concentrations or membrane humidity remains elusive. Consequently, for the validation of our conceptual framework, we resort to the utilization of a high-fidelity, fine grid model as a surrogate for our simulated reality.

Detailed information, including video recordings showing the dynamic estimation of fuel cell states’ distribution, is covered in Publication C. Currently, we present select findings. In Figure 1.7, the effectiveness of the observer algorithm in estimating membrane water content over time is evident, shown by the agreement between the red and blue lines. The smoothness of this estimation comes from using model simplification techniques, carefully choosing key system behaviors. Notably, the lack of a zig-zag pattern highlights the comprehensive estimation of membrane water content, rather than the estimation of individual points. The green line, representing simulation without the observer, eventually matches the blue line, indicating stability, though deviations occur

during operation, highlighting the importance of a state estimation tool like an observer.

Additionally, it is significant that the red line matches the blue line even though the detailed grid model, represented by the latter, includes more points. This result emphasizes the strong robustness and observability achieved by our method.

1.4 Summary of Scientific Publications

In Publication A (2.1), the study tackles the issue of managing polymer electrolyte membrane fuel cell stacks for actual fuel cell vehicles, focusing on safe and efficient functioning under varying power demands. The emphasis is on the importance of hydrogen-powered fuel cells in the global shift to clean energy, with a particular focus on PEMFCs due to their high power density and efficiency. The research uses successive linearization-based model predictive control to manage the system's nonlinearity during dynamic power demands. The control concept is validated with real vehicle data from a hydrogen-powered vehicle. The study involves simulations that incorporate safety and efficiency constraints, with SLMPC ensuring valid control across all operational ranges. The findings show that SLMPC effectively tracks power demand while maintaining safe and efficient operations, suggesting its potential for automotive fuel cell control applications.

In Publication B (2.2), a real-time reference governor model predictive controller (RG-MPC) is introduced for managing fuel cell (FC) systems in vehicles. The RG-MPC sets reference points for subordinate proportional-integral controllers, handling system constraints without extra layers. The study underscores the role of hydrogen-powered fuel cells in clean energy, particularly in automotive settings, where zero-emission PEM fuel cells are ideal due to their high power density and low operating temperatures. It reviews control methods, noting that rule-based and PI-based controls are common but highlights MPC's ability to manage complex systems. The RG-MPC provides optimized guidance for PI controllers, as shown through simulations, ensuring efficient and safe power control in automotive FC systems. This approach offers an advanced yet practical upgrade to existing control systems, enhancing vehicle performance and cost-effectiveness.

In Publication C (2.3), a method for monitoring internal states in fuel cell systems is proposed, addressing challenges related to sensor placement. The focus is on virtual sensing via an efficient state observer using a high-order distributed-parameter model. The observer algorithm adjusts predictions based on boundary measurements, emphasizing dominant dynamics from a reduced model for computational efficiency. The study critiques traditional measurement methods for internal states, highlighting their limitations and costs, and proposes a virtual sensing method using a state observer based on a quasi-2D model. The chosen observer algorithm, an extended Kalman filter (EKF), tackles issues associated with high-order models, employing balanced truncation to simplify computations while preserving essential system behaviors. The methodology's validity is confirmed through simulations, demonstrating the observer's effectiveness despite model mismatches. This study highlights the potential for practical applications in automotive settings, with future work aiming to include parameter estimation for enhanced robustness. ““

1.5 Scientific Contribution of This Thesis

In this thorough study of fuel cell control and monitoring within real-world vehicle applications, three main studies have been done, together adding to the understanding and development of polymer electrolyte membrane fuel cell systems.

The research offers the following key scientific contributions:

- **Innovative Control Strategy:** The first study introduces a new method for PEMFC stack control using Successive Linearization Model Predictive Control. This method not only ensures the following of changing power demand but also ensures safe operation by following safety rules.
- **Real-time Ready Reference Governor:** The second study introduces a Reference Governor Model Predictive Controller, setting reference paths for other controllers. This real-time ready controller offers an efficient and safe power control method for fuel cell stacks in vehicle applications, presenting a key improvement over current Proportional-Integral control methods.
- **Effective Online Monitoring:** The third study tackles the problem of online monitoring of fuel cell systems. The suggested lower-dimensionality nonlinear observer effectively corrects predicted values based on a high-order fuel cell model. This method allows monitoring of internal processes, such as fuel shortage and membrane drying, in a fast and strong way.

Together, these studies add significantly to the field of fuel cell technology. The methods introduced provide new control strategies and monitoring methods, enhancing the understanding of fuel cell behaviors and paving the way for safer, more efficient, and real-time control in vehicle applications. This work establishes a solid base for future progress in fuel cell research and technology.

Bibliography

- [1] R. Petrone, Z. Zheng, D. Hissel, M. Péra, C. Pianese, M. Sorrentino, M. Becherif, and N. Yousfi-Steiner. “A review on model-based diagnosis methodologies for PEMFCs”. In: *International Journal of Hydrogen Energy* 38.17 (2013), pp. 7077–7091. DOI: <https://doi.org/10.1016/j.ijhydene.2013.03.106>. URL: <https://www.sciencedirect.com/science/article/pii/S0360319913007465>.
- [2] J. Chen, L. Huang, C. Yan, and Z. Liu. “A dynamic scalable segmented model of PEM fuel cell systems with two-phase water flow”. In: *Mathematics and Computers in Simulation* 167 (2020). INTERNATIONAL CONFERENCE on Emerging and Renewable Energy: Generation and Automation, held in Belfort, France on 4-6 July, 2017, pp. 48–64. DOI: <https://doi.org/10.1016/j.matcom.2018.05.006>. URL: <https://www.sciencedirect.com/science/article/pii/S0378475418301186>.
- [3] X. Xue, J. Tang, A. Smirnova, R. England, and N. Sammes. “System level lumped-parameter dynamic modeling of PEM fuel cell”. In: *Journal of Power Sources* 133.2 (2004), pp. 188–204. DOI: <https://doi.org/10.1016/j.jpowsour.2003.12.064>. URL: <https://www.sciencedirect.com/science/article/pii/S0378775304002782>.
- [4] V. Liso, M. P. Nielsen, S. K. Kær, and H. H. Mortensen. “Thermal modeling and temperature control of a PEM fuel cell system for forklift applications”. In: *International Journal of Hydrogen Energy* 39.16 (2014), pp. 8410–8420. DOI: <https://doi.org/10.1016/j.ijhydene.2014.03.175>. URL: <https://www.sciencedirect.com/science/article/pii/S0360319914008672>.
- [5] E. J. F. Dickinson and G. Smith. “Modelling the Proton-Conductive Membrane in Practical Polymer Electrolyte Membrane Fuel Cell (PEMFC) Simulation: A Review”. In: *Membranes* 10.11 (2020). URL: <https://www.mdpi.com/2077-0375/10/11/310>.
- [6] M. Sarmiento-Carnevali, M. Serra, and C. Batlle. “Distributed parameter model-based control of water activity and concentration of reactants in a polymer electrolyte membrane fuel cell”. In: *International Journal of Hydrogen Energy* 42.42 (2017), pp. 26389–26407. DOI: <https://doi.org/10.1016/j.ijhydene.2017.>

- 08.191. URL: <https://www.sciencedirect.com/science/article/pii/S0360319917334948>.
- [7] R. B. Ferreira, D. Falcão, V. Oliveira, and A. Pinto. “1D+3D two-phase flow numerical model of a proton exchange membrane fuel cell”. In: *Applied Energy* 203 (2017), pp. 474–495. DOI: <https://doi.org/10.1016/j.apenergy.2017.06.048>. URL: <https://www.sciencedirect.com/science/article/pii/S0306261917307997>.
- [8] D. Murschenhofer, D. Kuzdas, S. Braun, and S. Jakubek. “A real-time capable quasi-2D proton exchange membrane fuel cell model”. In: *Energy Conversion and Management* 162. February (2018), pp. 159–175. DOI: 10.1016/j.enconman.2018.02.028. URL: <https://doi.org/10.1016/j.enconman.2018.02.028>.
- [9] S. Zhang, S. Beale, U. Reimer, M. Andersson, and W. Lehnert. “Polymer electrolyte fuel cell modeling - A comparison of two models with different levels of complexity”. In: *International Journal of Hydrogen Energy* 45.38 (2020), pp. 19761–19777. DOI: <https://doi.org/10.1016/j.ijhydene.2020.05.060>. URL: <https://www.sciencedirect.com/science/article/pii/S0360319920318371>.
- [10] M. Guarnieri, P. Alotto, and F. Moro. “Distributed and Lumped Parameter Models for Fuel Cells”. In: *Thermodynamics and Energy Engineering*. Ed. by P. Vizureanu. Rijeka: IntechOpen, 2019. Chap. 2. DOI: 10.5772/intechopen.89048. URL: <https://doi.org/10.5772/intechopen.89048>.
- [11] H. Ju and C.-Y. Wang. “Experimental Validation of a PEM Fuel Cell Model by Current Distribution Data”. In: *Journal of The Electrochemical Society* 151.11 (Oct. 2004), A1954. DOI: 10.1149/1.1805523. URL: <https://dx.doi.org/10.1149/1.1805523>.
- [12] G. Besagni, R. Mereu, F. Inzoli, and P. Chiesa. “Application of an integrated lumped parameter-CFD approach to evaluate the ejector-driven anode recirculation in a PEM fuel cell system”. In: *Applied Thermal Engineering* 121 (2017), pp. 628–651. DOI: <https://doi.org/10.1016/j.applthermaleng.2017.04.111>. URL: <https://www.sciencedirect.com/science/article/pii/S1359431116333981>.
- [13] J. Zhao, X. Li, C. Shum, and J. McPhee. “Control-oriented computational fuel cell dynamics modeling – Model order reduction vs. computational speed”. In: *Energy* 266 (2023), p. 126488. DOI: <https://doi.org/10.1016/j.energy.2022.126488>. URL: <https://www.sciencedirect.com/science/article/pii/S0360544222033746>.
- [14] B. Yang, J. Li, Y. Li, Z. Guo, K. Zeng, H. Shu, P. Cao, and Y. Ren. “A critical survey of proton exchange membrane fuel cell system control: Summaries, advances, and perspectives”. In: *International Journal of Hydrogen Energy* 47.17 (2022), pp. 9986–10020. DOI: <https://doi.org/10.1016/j.ijhydene.2022.>

- 01.065. URL: <https://www.sciencedirect.com/science/article/pii/S0360319922001252>.
- [15] R. Zhang, Y. Jia, T. Zhang, and Z. Fan. “Research on modeling and control of PEMFC cooling system”. In: *Applied Thermal Engineering* 241 (2024), p. 122303. DOI: <https://doi.org/10.1016/j.applthermaleng.2023.122303>. URL: <https://www.sciencedirect.com/science/article/pii/S1359431123023323>.
- [16] M. F. Munir, I. Ahmad, S. A. Siffat, M. A. Qureshi, H. Armghan, and N. Ali. “Non-linear control for electric power stage of fuel cell vehicles”. In: *ISA Transactions* 102 (2020), pp. 117–134. DOI: <https://doi.org/10.1016/j.isatra.2020.02.033>. URL: <https://www.sciencedirect.com/science/article/pii/S0019057820300975>.
- [17] P. Yin, J. Chen, and H. He. “Control of Oxygen Excess Ratio for a PEMFC Air Supply System by Intelligent PID Methods”. In: *Sustainability* 15.11 (2023). URL: <https://www.mdpi.com/2071-1050/15/11/8500>.
- [18] M. Derbeli, A. Charaabi, O. Barambones, and C. Napole. “High-Performance Tracking for Proton Exchange Membrane Fuel Cell System PEMFC Using Model Predictive Control”. In: *Mathematics* 9.11 (2021). URL: <https://www.mdpi.com/2227-7390/9/11/1158>.
- [19] Y. Zhou, A. Ravey, and M.-C. Péra. “Real-time cost-minimization power-allocating strategy via model predictive control for fuel cell hybrid electric vehicles”. In: *Energy Conversion and Management* 229 (2021), p. 113721. DOI: <https://doi.org/10.1016/j.enconman.2020.113721>. URL: <https://www.sciencedirect.com/science/article/pii/S0196890420312450>.
- [20] A. Goshtasbi and T. Ersal. “Degradation-conscious control for enhanced lifetime of automotive polymer electrolyte membrane fuel cells”. In: *Journal of Power Sources* 457 (2020), p. 227996. DOI: <https://doi.org/10.1016/j.jpowsour.2020.227996>. URL: <https://www.sciencedirect.com/science/article/pii/S0378775320302998>.
- [21] M. Vrlić, D. Ritzberger, and S. Jakubek. “Model-predictive-control-based reference governor for fuel cells in automotive application compared with performance from a real vehicle”. In: *Energies* 14.8 (2021). DOI: 10.3390/en14082206.
- [22] M. Vrlić, D. Ritzberger, and S. Jakubek. “Safe and efficient polymer electrolyte membrane fuel cell control using successive linearization based model predictive control validated on real vehicle data”. In: *Energies* 13.20 (2020). DOI: 10.3390/en13205353.

- [23] M. Klaučo, M. Kalúz, and M. Kvasnica. “Real-time implementation of an explicit MPC-based reference governor for control of a magnetic levitation system”. In: *Control Engineering Practice* 60 (2017), pp. 99–105. DOI: <https://doi.org/10.1016/j.conengprac.2017.01.001>. URL: <https://www.sciencedirect.com/science/article/pii/S0967066117300011>.
- [24] L. Huang, J. Chen, Z. Liu, and M. Becherif. “Adaptive thermal control for PEMFC systems with guaranteed performance”. In: *International Journal of Hydrogen Energy* 43.25 (2018). Alternative Energies for Sustainability, pp. 11550–11558. DOI: <https://doi.org/10.1016/j.ijhydene.2017.12.121>. URL: <https://www.sciencedirect.com/science/article/pii/S0360319917348371>.
- [25] C. Jia, W. Qiao, J. Cui, and L. Qu. “Adaptive Model-Predictive-Control-Based Real-Time Energy Management of Fuel Cell Hybrid Electric Vehicles”. In: *IEEE Transactions on Power Electronics* 38.2 (2023), pp. 2681–2694. DOI: 10.1109/TPEL.2022.3214782.
- [26] G. Taneja, V. K. Tayal, and K. Pandey. “Robust Control of Proton Exchange Membrane Fuel Cell (PEMFC) System”. In: *Computational Intelligence*. Ed. by A. Shukla, B. K. Murthy, N. Hasteer, and J.-P. Van Belle. Singapore: Springer Nature Singapore, 2023, pp. 617–628.
- [27] X. Hao, I. Salhi, S. Laghrouche, Y. Ait-Amirat, and A. Djerdir. “Robust control of four-phase interleaved boost converter by considering the performance of PEM fuel cell current”. In: *International Journal of Hydrogen Energy* 46.78 (2021), pp. 38827–38840. DOI: <https://doi.org/10.1016/j.ijhydene.2021.09.132>. URL: <https://www.sciencedirect.com/science/article/pii/S0360319921036594>.
- [28] J. Mao, Z. Li, J. Xuan, X. Du, M. Ni, and L. Xing. “A review of control strategies for proton exchange membrane (PEM) fuel cells and water electrolyser: from automation to autonomy”. In: *Energy and AI* (2024), p. 100406. DOI: <https://doi.org/10.1016/j.egyai.2024.100406>. URL: <https://www.sciencedirect.com/science/article/pii/S2666546824000727>.
- [29] F. Segura and J. Andújar. “Step by step development of a real fuel cell system. Design, implementation, control and monitoring”. In: *International Journal of Hydrogen Energy* 40.15 (2015), pp. 5496–5508. DOI: <https://doi.org/10.1016/j.ijhydene.2015.01.178>. URL: <https://www.sciencedirect.com/science/article/pii/S0360319915002773>.
- [30] H. Yuan, H. Dai, X. Wei, and P. Ming. “Model-based observers for internal states estimation and control of proton exchange membrane fuel cell system: A review”. In: *Journal of Power Sources* 468 (2020), p. 228376. DOI: <https://doi.org/10.1016/j.jpowsour.2020.228376>. URL: <https://www.sciencedirect.com/science/article/pii/S0378775320306807>.

- [31] L. Böhler, D. Ritzberger, C. Hametner, and S. Jakubek. “Constrained extended Kalman filter design and application for on-line state estimation of high-order polymer electrolyte membrane fuel cell systems”. In: *International Journal of Hydrogen Energy* 46.35 (2021), pp. 18604–18614. DOI: <https://doi.org/10.1016/j.ijhydene.2021.03.014>. URL: <https://www.sciencedirect.com/science/article/pii/S0360319921008351>.
- [32] A. Cecilia, M. Serra, and R. Costa-Castelló. “Nonlinear adaptive observation of the liquid water saturation in polymer electrolyte membrane fuel cells”. In: *Journal of Power Sources* 492 (2021), p. 229641. DOI: <https://doi.org/10.1016/j.jpowsour.2021.229641>. URL: <https://www.sciencedirect.com/science/article/pii/S0378775321001853>.
- [33] H. Yue, H. He, M. Han, and S. Gong. “Active disturbance rejection control strategy for PEMFC oxygen excess ratio based on adaptive internal state estimation using unscented Kalman filter”. In: *Fuel* 356 (2024), p. 129619. DOI: <https://doi.org/10.1016/j.fuel.2023.129619>. URL: <https://www.sciencedirect.com/science/article/pii/S0016236123022330>.
- [34] A. Kravos, D. Ritzberger, C. Hametner, S. Jakubek, and T. Katrašnik. “Methodology for efficient parametrisation of electrochemical PEMFC model for virtual observers: Model based optimal design of experiments supported by parameter sensitivity analysis”. In: *International Journal of Hydrogen Energy* 46.26 (2021). European Fuel Cell Conference & Exhibition 2019, pp. 13832–13844. DOI: <https://doi.org/10.1016/j.ijhydene.2020.10.146>. URL: <https://www.sciencedirect.com/science/article/pii/S036031992033994X>.
- [35] M. Vrlić, D. Pernsteiner, A. Schirrer, C. Hametner, and S. Jakubek. “Reduced-dimensionality nonlinear distributed-parameter observer for fuel cell systems”. In: *Energy Reports* 10 (2023), pp. 1–14. DOI: [10.1016/j.egy.2023.06.006](https://doi.org/10.1016/j.egy.2023.06.006). URL: <https://doi.org/10.1016/j.egy.2023.06.006>.
- [36] J. Luna, A. Husar, and M. Serra. “Nonlinear distributed parameter observer design for fuel cell systems”. In: *International Journal of Hydrogen Energy* 40.34 (2015), pp. 11322–11332. DOI: [10.1016/j.ijhydene.2015.05.132](https://doi.org/10.1016/j.ijhydene.2015.05.132). URL: <http://dx.doi.org/10.1016/j.ijhydene.2015.05.132>.
- [37] Y. Tian, Q. Zou, and J. Han. “Data-Driven Fault Diagnosis for Automotive PEMFC Systems Based on the Steady-State Identification”. In: *Energies* 14.7 (2021). DOI: [10.3390/en14071918](https://doi.org/10.3390/en14071918). URL: <https://www.mdpi.com/1996-1073/14/7/1918>.
- [38] V. M. Nagulapati, S. S. Kumar, V. Annadurai, and H. Lim. “Machine learning based fault detection and state of health estimation of proton exchange membrane fuel cells”. In: *Energy and AI* 12 (2023), p. 100237. DOI: <https://doi.org/10.1016/j.egyai.2023.100237>. URL: <https://www.sciencedirect.com/science/article/pii/S2666546823000095>.

- [39] Y. Xing, B. Wang, Z. Gong, Z. Hou, F. Xi, G. Mou, Q. Du, F. Gao, and K. Jiao. “Data-Driven Fault Diagnosis for PEM Fuel Cell System Using Sensor Pre-Selection Method and Artificial Neural Network Model”. In: *IEEE Transactions on Energy Conversion* 37.3 (2022), pp. 1589–1599. DOI: 10.1109/TEC.2022.3143163.
- [40] B. Kang, W. Na, and H. Lee. “Model-Based Fault Analysis and Diagnosis of PEM Fuel Cell Control System”. In: *Applied Sciences* 12.24 (2022). DOI: 10.3390/app122412733. URL: <https://www.mdpi.com/2076-3417/12/24/12733>.
- [41] J. Wang, B. Yang, C. Zeng, Y. Chen, Z. Guo, D. Li, H. Ye, R. Shao, H. Shu, and T. Yu. “Recent advances and summarization of fault diagnosis techniques for proton exchange membrane fuel cell systems: A critical overview”. In: *Journal of Power Sources* 500 (2021), p. 229932. DOI: <https://doi.org/10.1016/j.jpowsour.2021.229932>. URL: <https://www.sciencedirect.com/science/article/pii/S037877532100464X>.
- [42] Y. Wang, X. Yang, Z. Sun, and Z. Chen. “A systematic review of system modeling and control strategy of proton exchange membrane fuel cell”. In: *Energy Reviews* 3.1 (2024), p. 100054. DOI: <https://doi.org/10.1016/j.enrev.2023.100054>. URL: <https://www.sciencedirect.com/science/article/pii/S277297022300041X>.
- [43] J. Zhao, X. Li, C. Shum, and J. McPhee. “A computationally efficient and high-fidelity 1D steady-state performance model for PEM fuel cells”. In: *Journal of Physics: Energy* 5.1 (Jan. 2023), p. 015003. DOI: 10.1088/2515-7655/acafa3. URL: <https://dx.doi.org/10.1088/2515-7655/acafa3>.
- [44] C.-Y. Lee, F.-B. Weng, C.-Y. Yang, C.-W. Chiu, and S.-M. Nawale. “Real-Time Monitoring of HT-PEMFC”. In: *Membranes* 12.1 (2022). DOI: 10.3390/membranes12010094. URL: <https://www.mdpi.com/2077-0375/12/1/94>.
- [45] A. K. Prajapati and R. Prasad. “Model Reduction Using the Balanced Truncation Method and the Padé Approximation Method”. In: *IETE Technical Review* 39.2 (2022), pp. 257–269. DOI: 10.1080/02564602.2020.1842257.
- [46] D. Ritzberger, C. Hametner, and S. Jakubek. “A real-time dynamic fuel cell system simulation for model-based diagnostics and control: Validation on real driving data”. In: *Energies* 13.12 (2020). DOI: 10.3390/en13123148.
- [47] M. Vrlic, D. Ritzberger, and S. Jakubek. “Efficient and life preserving power tracking control of a proton exchange membrane fuel cell using model predictive control”. In: *Proceedings of 2020 SICE International Symposium on Control Systems, SICE ISCS 2020* (2020), pp. 77–84. DOI: 10.23919/SICEISCS48470.2020.9083653.

Chapter 2

Publications

List of Selected Journal Publications

Publication A

Martin Vrlić, Daniel Ritzberger, and Stefan Jakubek.

Safe and efficient polymer electrolyte membrane fuel cell control using successive linearization based model predictive control validated on real vehicle data.

Energies 13 (2020)

DOI: 10.3390/en13205353

Publication B

Martin Vrlić, Daniel Ritzberger, and Stefan Jakubek.

Model-predictive-control-based reference governor for fuel cells in automotive application compared with performance from a real vehicle.

Energies 14 (2021)

DOI: 10.3390/en14082206

Publication C

Martin Vrlić, Dominik Pernsteiner, Alexander Schirrer, Christoph Hametner, and Stefan Jakubek.

Reduced-dimensionality nonlinear distributed-parameter observer for fuel cell systems.

Energy Reports 10 (2023) pp. 1–14.

DOI: 10.1016/j.egyrs.2023.06.006

2.1 Publication A

M. Vrlić, D. Ritzberger, and S. Jakubek. “Safe and efficient polymer electrolyte membrane fuel cell control using successive linearization based model predictive control validated on real vehicle data”. In: *Energies* 13.20 (2020). DOI: 10.3390/en13205353

Applicant’s Contribution [†]

- Martin Vrlić: Conceptualization, Methodology, Investigation, Software, Visualization, Writing - Original Draft
- Daniel Ritzberger: Conceptualization, Methodology, Investigation, Writing - Review & Editing
- Stefan Jakubek: Writing - Review & Editing, Supervision, Project administration, Funding acquisition

[†]According to the Elsevier CRediT author statement: <https://www.elsevier.com/authors/policies-and-guidelines/credit-author-statement>

Article

Safe and Efficient Polymer Electrolyte Membrane Fuel Cell Control Using Successive Linearization Based Model Predictive Control Validated on Real Vehicle Data

Martin Vrlíć *, Daniel Ritzberger and Stefan Jakubek

Institut für Mechanik und Mechatronik, Technische Universität Wien, Getreidemarkt 9, 1060 Vienna, Austria; daniel.ritzberger@tuwien.ac.at (D.R.); stefan.jakubek@tuwien.ac.at (S.J.)

* Correspondence: martin.vrljic@tuwien.ac.at

Received: 9 September 2020; Accepted: 8 October 2020; Published: 14 October 2020



Abstract: In this paper, a polymer electrolyte membrane fuel cell (PEMFC) stack control study is presented. The goal is to track the transient power demand of a real fuel cell (FC) vehicle while ensuring safe and efficient operation. Due to the dynamically changing power demand, fast transients occur in the internal states of the fuel cell (e.g., pressure, humidity, reactant mass) leading to degradation effects (e.g., high/low membrane overpressure, reactants starvation) which are avoided by imposing safety constraints. Efficiency is considered in terms of internal voltage losses minimization as well as minimization of the power of the compressor used to pressurize the cathode. For solving the optimization problem of power demand tracking, adhering to safety constraints, and maximizing efficiency, model predictive control (MPC) has been chosen. Due to the nonlinearity of the FC system, a successive linearization based MPC (SLMPC) is used to control the FC throughout its operating region. Simulation results show that the power demand can be fulfilled while at the same time ensuring safe operation in terms of adhering to constraints and that the minimization of internal voltage losses and compressor power lead to an approximate 9.5% less hydrogen consumption than in the actual reference vehicle.

Keywords: fuel cell; automotive; model predictive control; successive linearization; safe operation; efficient operation

1. Introduction

In the ongoing world-scale mission of replacing fossil fuels with clean energy, the technology of hydrogen-powered fuel cells (FC) may come as a promising candidate for supplying power in both stationary and automotive applications [1], the latter being in the focus of this work. Quite a few types of fuel cells exist, but the polymer electrolyte membrane fuel cell (PEMFC) seems to be the technology of choice when it comes to automotive application. This is because PEMFCs have a high power density, high efficiency, and fast start-up ability [1]. Obviously, for the fuel cell technology to compete with combustion engines, it must perform at least as good as them. This requirement poses several challenges in terms of FC stack lifetime and safety restrictions [2]. To increase the lifetime of the stack as well as operate it safely, an appropriate control strategy is of crucial importance. Throughout the last years and even decades, the topic of fuel cell control has inspired the work of many scientists and engineers.

Different approaches can be found in literature dealing with the challenge of fuel cell modeling and control. One can reduce the complex problem and control only one subsystem of the fuel cell (e.g., cathode or anode) [3–6] or examine the whole system [7,8], depending on the problem that

needs to be solved. An important and commonly encountered issue that needs to be addressed in fuel cell control is starvation avoidance, usually formulated as imposing a limit on the stoichiometry of hydrogen and/or oxygen [4]. A common way of controlling the fuel cell system is by setting reference values for the cathode/anode pressure, hydrogen/oxygen stoichiometries, voltage, etc. as seen in [4,9,10].

To increase the practical usability of the fuel cell control test results in an automotive application, it is important to conduct the research on a vehicle drive cycle. Much of the research considering power demand tracking done in the past is not based on a vehicle drive cycle, but instead, on a step reference power trajectory generated to demonstrate a certain effect of the control task (e.g., stoichiometry control, pressure constraints, battery/FC interaction, etc.) [11,12].

In the context of this study, the control of the fuel cell subject to a dynamic drive cycle is of much greater practical relevance. Various test scenarios have recently been reported which rely on the New European Driving Cycle (NEDC) as the validation drive cycle for the control of a fuel cell vehicle [13–15]. The Worldwide Harmonised Light Vehicles Test Procedure (WLTP) also developed in 2015 has been used as the validation drive cycle for several studies concerning fuel cell control [16,17].

In this work, the power demand measured from a real fuel cell vehicle (The vehicle has been built by AVL List GmbH as part of the Keytech4EV project (no. 855237) funded by the Austrian Research Promotion Agency (FFG).) has been used for validation of the proposed control concept. A simulation study has been conducted on the measured power demand using a nonlinear mass-driven zero-dimensional transient fuel cell model. The control goal is to track the power demand from the acquired data of the real vehicle while ensuring safe operation in terms of starvation avoidance as well as respecting the cathode and anode pressure safety limits along with the pressure difference across the membrane safety limit. Also, efficiency is to be maximized by minimizing the internal voltage drop due to the activation, ohmic, and concentration losses, as well as the power, needed to run the compressor used to provide air for the cathode. To fulfill the goals of power tracking and efficiency maximization, while adhering to the mentioned constraints, the model predictive control (MPC) approach has been chosen which is quite popular in fuel cell control [18–22], mainly because of its ability to handle constraints. A common approach of using MPC is to linearize the system around a steady-state operating point (OP) and use one of the few simple standard formulations of MPC for linear systems. This method works fine for regions relatively close to the OP around which the model has been linearized, but fails if the system operates in a region too far from the OP. The power demand used in the study ranges from 0 to 60 kW so an MPC developed for the system linearized around a single OP would fail to fulfill all the control goals. To cope with the nonlinearity, a successive linearization based MPC (SLMPC) [23–26] is used meaning that the system is continuously linearized every time step during the simulation and a linear MPC developed for that particular point in the state-space ensuring the validity of the MPC at all times. However, the linearization point is not a steady-state one and the treatment of this is described in Section 4. In terms of PEMFC vehicle control, to the best of the authors' knowledge, there is no research conducted on a real data drive cycle using successive linearization based model predictive control.

The paper is organized as follows: In Section 2 the zero-dimensional model used for the simulation study is presented. In Section 3 the vehicle description is brought forth while in Section 4 the methodology of the SLMPC is shown. The results consisting of the simulation outcome and its comparison with the data measured from the real vehicle are presented in Section 5. Finally, Section 6 brings the conclusions of this paper along with the direction of future research.

2. Fuel Cell Model

In this section, the FC model used for the control study is presented. The schematics are shown in Figure 1. The focus of the work is not in the model itself, therefore, not all the details will be brought forth, but rather the model structure. For further information on the model equations, the reader is referred to [27].

Modeling assumptions:

- The operating temperature is assumed constant at a value of 70 °C.
- The anode is operated in “dead-end” mode, no recirculation is considered in the present model setup.
- Inlet humidities are assumed to be constant.
- The effect of liquid water on the voltage is not considered.

The whole system model can be viewed as a collection of submodels describing different parts of the fuel cell:

- Cathode
- Anode
- Gas diffusion layer (GDL) on the cathode side
- Electrochemical model

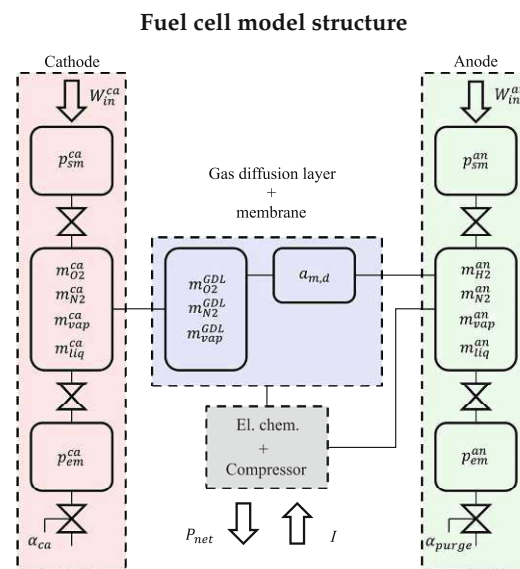


Figure 1. Structure of the fuel cell model. All the submodels(cathode, anode, electrochemical model, compressor, gas diffusion layer, and membrane) are enclosed in dashed lines.

2.1. Cathode Submodel

The cathode side of the fuel cell is assumed to be a series of 3 interconnected zero-dimensional (0D) volumes meaning that there is no spatial distribution along or across the channel leading to valuable numerical benefits while maintaining a decent level of accuracy. Air supply coming from the compressor enters the first volume referred to as the cathode supply manifold (sm) and its state is described by the cathode supply manifold pressure (p_{sm}^{ca}) which is modeled using the ideal gas law. The second volume is the cathode main manifold. The flow of air from the supply manifold to the cathode main manifold is described using a linearized nozzle equation. In the second volume, the states describing the system are the masses of oxygen, nitrogen, water vapor, and liquid water ($m_{O_2}^{ca}$, $m_{N_2}^{ca}$, m_{vap}^{ca} , m_{liq}^{ca}). Finally, the third volume is the cathode exit manifold (em) described by the corresponding cathode exit manifold pressure (p_{em}^{ca}) which leads the exhaust air into the atmosphere. At the end of the exit manifold, there is a backpressure valve. On the cathode side, the actuating variables used by the controller during operation are the mass-flow of air entering the supply manifold (W_{in}^{ca}) and the backpressure valve opening (α_{ca}).

2.2. Anode Submodel

Just like the cathode side, the anode is modeled as a series of three interconnected 0D volumes. The states describing the supply and exit manifold of the anode are analogously the supply and exit manifold pressures (p_{sm}^{an} and p_{em}^{an}). The anode is supplied by hydrogen coming from a highly pressurized tank. In the main manifold, the states describing the system are the masses of hydrogen, nitrogen, water vapor, and liquid water ($m_{H_2}^{an}$, $m_{N_2}^{an}$, m_{vap}^{an} , m_{liq}^{an}). The valve connecting the exit manifold to the ambient is called the purge valve and it is normally closed during operation leading to a so-called “dead-end anode” operating mode. In real systems, the unused hydrogen is usually recirculated and fed back to the anode inlet. In this simulation study, the anode is modeled as dead-end. The actuating variable on the anode side is the hydrogen mass-flow entering the anode supply manifold (W_{in}^{an}) whereas the opening of the purge valve (α_{purge}) is considered to be a disturbance.

2.3. Gas Diffusion Layer Submodel

In this model, the GDL on the cathode side is viewed as an additional 0D volume containing the masses of oxygen, nitrogen, and water vapor ($m_{O_2}^{GDL}$, $m_{N_2}^{GDL}$ and m_{vap}^{GDL}). The dynamics of the oxygen mass in the GDL is due to the diffusion of oxygen from the cathode, as well as the consumption of oxygen due to the reaction. The nitrogen mass in the GDL changes because of the nitrogen diffusion from the cathode as well as the permeation of nitrogen through the membrane to the anode side. As for the water vapor mass, there is the diffusion from the cathode, water formation from the reaction, membrane water flux (electroosmotic drag and backdiffusion), and water condensation. On the anode side, the GDL proved to be unnecessary to include in the model as hydrogen is very diffusive so the dynamics of the potential hydrogen mass in the GDL could be neglected.

2.4. Electrochemical Model

To couple the thermodynamical part of the model described in the above subsections to the actual output of the system that is of primal interest for this work (voltage and power), an electrochemical model is needed and its implementation is based on [28]. The actuating variable regarding the electrochemical part of the model is the stack current (I).

2.5. Power and Efficiency

The power produced by the fuel cell stack $P_{st} = VI$ is defined as the product of the stack voltage V and the stack current I . The net system power is then defined as the difference between the stack power, compressor power P_{cp} , and the power of all the other auxiliary components P_{aux} :

$$P_{net} = P_{st} - P_{cp} - P_{aux}. \quad (1)$$

As only the compressor power is part of the model and it is the dominant parasitic loss, the power of the other auxiliary components is neglected leading to $P_{aux} = 0$:

$$P_{net} = P_{st} - P_{cp}. \quad (2)$$

This assumption is justified by the fact that the difference between the measured net power and the net power calculated assuming $P_{aux} = 0$ is small, only 3%. Fuel cell efficiency is defined as the ratio between the power produced by the stack P_{st} and the power of the fuel $P_{H_2} = E_0 N_{cells} I$ [1]:

$$\eta_{fc} = \frac{P_{st}}{P_{H_2}} = \frac{P_{st}}{E_0 N_{cells} I} = \frac{V}{E_0 N_{cells}} \quad (3)$$

where E_0 is the open-circuit voltage (see Figure 2) and N_{cells} is the number of cells in the stack. However, as the compressor power must be taken into account, it makes sense to define the system efficiency η_{sys} :

$$\eta_{sys} = \frac{P_{net}}{P_{H_2}} = \frac{P_{st} - P_{cp}}{E_0 N_{cells} I} = \frac{VI - P_{cp}}{E_0 N_{cells} I}. \quad (4)$$

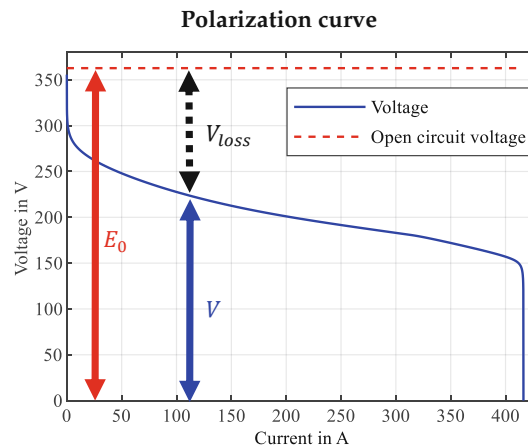


Figure 2. Polarization curve obtained by simulation. The current is ramped up from zero until voltage breakdown. The red dashed line shows the open-circuit voltage, the blue solid line shows the operating voltage. The difference between the two are the losses due to reaction kinetics (activation, ohmic, and concentration) V_{loss} .

2.6. Overview

Combining all of the above-mentioned submodels in which the dynamics of the states are described using first-order differential equations, one obtains a nonlinear state-space model of the form:

$$\dot{x} = f(x, u) \quad (5)$$

$$y = h(x, u) \quad (6)$$

with x being the state vector, u being the input vector and y being the output vector, as defined below:

$$x = \begin{bmatrix} p_{sm}^{ca} \\ m_{O_2}^{ca} \\ m_{N_2}^{ca} \\ m_{vap}^{ca} \\ m_{liq}^{ca} \\ p_{em}^{ca} \\ p_{sm}^{an} \\ m_{H_2}^{an} \\ m_{N_2}^{an} \\ m_{vap}^{an} \\ m_{liq}^{an} \\ p_{em}^{an} \\ a_{m,d} \\ m_{O_2}^{GDL} \\ m_{N_2}^{GDL} \\ m_{vap}^{GDL} \end{bmatrix} \quad u = \begin{bmatrix} W_{in}^{ca} \\ W_{in}^{an} \\ \alpha_{ca} \\ I \end{bmatrix} \quad y = \begin{bmatrix} P_{net} \\ \Delta p \\ \eta_{sys} \end{bmatrix} \quad (7)$$

where $a_{m,d}$ is an additional state describing the dynamic membrane wetting and drying, whereas the outputs of the system are

- Net power of the system (P_{net})
- Pressure difference across the membrane ($\Delta p = p_{sm}^{an} - p_{sm}^{ca}$)
- System efficiency (η_{sys})

3. Vehicle as Validation Data Generator

In this section, the vehicle from which the validation data for the controller has been obtained is presented. To realize the goal of building an FC car, an already existing hybrid construction has been used. The combustion engine from the vehicle was removed and replaced with the fuel cell system while the battery is kept from the original configuration. For the new architecture, an electric motor from another vehicle was used. The vehicle is powered by a 300 cell fuel cell stack with a maximum power output of 68.4 kW. There are three hydrogen tanks in the vehicle that provide the necessary fuel. The actual vehicle is shown in Figure 3a. Its construction was part of the so-called Keytech4EV project, a collaboration initiated in the year 2016 between AVL List GmbH, ElringKlinger AG (Germany) (EK), Magna Steyr Engineering AG & Co KG (MAGNA), HOERBIGER Ventilwerke GmbH & Co KG (HOERBIGER), HyCentA Research GmbH (HyCentA), Institute of Mechanics and Mechatronics, Vienna University of Technology (IMM), Institute of Chemical Engineering and Environmental Technology, Graz University of Technology (CEET) and Institut für Innovative Energie- & Stoffaustauschsysteme (IESTA) with a successful conclusion in 2020 [29].

For demonstration purposes, the vehicle V-I trajectory has been shown in Figure 3b superimposed to the polarization curve obtained by simulation from Figure 2. The vehicle seems to operate in the linear part of the V-I curve, avoiding regions close to the open-circuit voltage or the limiting current.

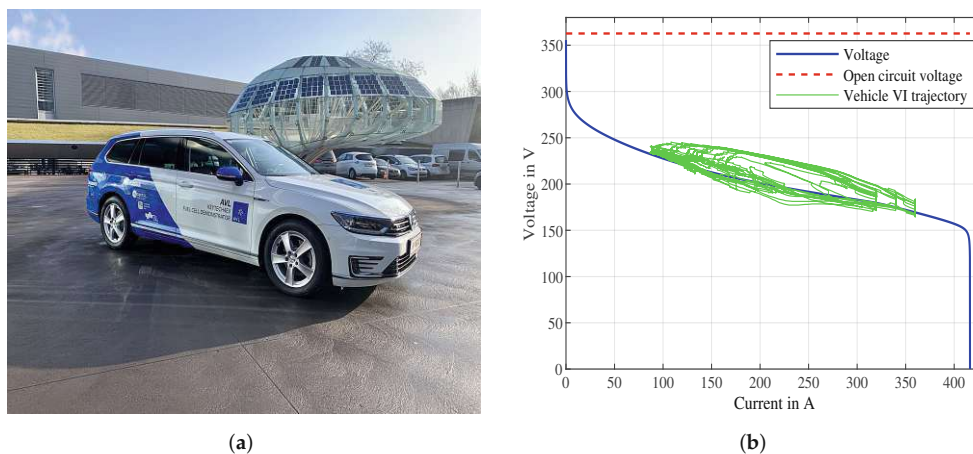


Figure 3. Keytech4EV research vehicle and its measured V-I trajectory superimposed to the simulated polarization curve brought for visualization of the operating range. **(a)** Vehicle developed by AVL List GmbH from which the data has been acquired for the validation of this study. **(b)** Measured V-I trajectory of the vehicle.

4. SLMPC Design

In this section, the controller design will be presented, however, a few key-points are to be mentioned before presenting the mathematical formalism of the SLMPC.

It is important to clearly visualize the end goal of this study which is:

- Fulfill the power demand trajectory from the real vehicle shown in Figure 3a

- Safe operation
- Efficient operation

Each of these points is explained as follows:

Fulfill the power demand

In a fuel cell–battery hybrid configuration, there always exists a so-called energy management system (EMS) which splits the power demand between the battery and the fuel cell stack always following certain rules (e.g., respecting the limit on the state of charge (SoC) of the battery, etc.). The power demand for each of the components gets forwarded to their respective low-level controllers which then generate the signal for the actuators such as the inlet mass-flows of air and hydrogen or the position of the backpressure valves. The measured power demand for the fuel cell coming from the EMS of the vehicle is used to validate the control concept shown in this paper.

Safe operation

There is a number of conditions that degrade and/or destroy the fuel cell system. In this paper, some of them are directly considered:

- Cathode/Anode absolute pressure—During operation, the pressures might rise or drop to a value which would, in a real setup, cause irreversible damage. If the pressure in either channel is too high, the components experience mechanical stress which can lead to fuel cell destruction. On the other hand, if the pressure is too low, starvation may occur, which is described in more detail below. Naturally, the controller must “know” that it cannot allow the system to operate outside the safe pressure range.
- Starvation—Power is mainly provided by drawing a certain amount of current from the fuel cell stack. Current is generated by the reaction of hydrogen and oxygen, the basic principle of how does a fuel cell work. The higher the current, the faster the reactants get consumed. The task of the controller becomes obvious—a sufficient amount of reactant mass must be supplied at all times. If that would not be the case, the electrons which create the current would then come from the platinum in the catalyst layer or the carbon from the gas diffusion layer. Because of starvation, the catalyst or the GDL can be consumed in a matter of seconds destroying the fuel cell [30]. In our setup, a minimum amount of oxygen/hydrogen mass is required to always be present to avoid starvation.
- Pressure difference across the membrane—Similar to the problem of absolute pressures, it is crucial to control the pressure difference between the anode and cathode at all times. Too big of a pressure difference causes stress on the membrane and if the pressure difference becomes negative i.e., the pressure on the cathode side becomes greater than on the anode side, other unfavorable effects can occur, such as pushing the water (generated on the cathode side) over to the anode.
- Purging—As there is air on the cathode side instead of pure oxygen, the effect of nitrogen which does not participate in the reaction must be taken into account. It diffuses through the membrane to the anode side, accumulating and effectively lowering the availability of hydrogen for the reaction potentially causing local starvation. If, in turn, the controller would want to keep a sufficient reserve of hydrogen, it would pump in more and more hydrogen, potentially violating the pressure restriction. Therefore, the necessity of clearing (purging) the anode of nitrogen is obvious. Purging is done by opening the purge valve for a short period of time and then closing it again to not waste hydrogen into the environment. The opening is commonly triggered by a Coulomb counting strategy.

Efficient operation

Two effects should be minimized to achieve efficient operation: voltage losses and compressor power.

- Voltage losses—Due to the reaction kinetics, there are inevitable voltage losses in fuel cell operation [1]. To increase efficiency, these voltage losses should be minimized which suggests operating at higher voltages as it is obvious from Equation (3) and Figure 2.
- Compressor power—To supply the air needed for the operation, a compressor is used which uses the power generated by the fuel cell. One of the goals of the controller is to minimize the usage of the compressor which would increase system efficiency as is visible from Equation (4).

Summary

Control engineering-wise, the above restrictions on the system are formulated as state constraints for the SLMPC. The fact that having constraints provides safe operation is one of the reasons for choosing an MPC approach since coping with constraints is one of the strong points of the model predictive control concept in general. The purge signal is considered to be a disturbance sent to the MPC.

Since the fuel cell system summarized in Equation (7) is nonlinear, a simple linear method would not be sufficient to successfully control it, thus, in this work, a successive linearization based model predictive control approach is used. The advantage of the SLMPC over nonlinear MPC is in the guaranteed existence and uniqueness of a global minimum since the cost function is quadratic. The basic idea is to linearize and discretize the system every sample and develop a linear MPC for that particular instantaneously linearized system. That way, the linear model represents the nonlinear system well throughout the prediction horizon provided that the predicted sequence of optimal control moves does not take the system too far from the linearization point. However, the mentioned problem was not observed in this research. The steps of developing the SLMPC can be found in detail in [23] and here we bring forth the most important components of the algorithm.

4.1. Linearization of the Nonlinear System

At each sample, the model is linearized around the current point (x_k, u_k) . The current sample instant is denoted by the index k . The linearization is carried out by evaluating the Jacobian matrix of the function f defined as

$$A_c = \frac{\partial f}{\partial x} = \begin{bmatrix} \frac{\partial f_1}{\partial x_1} & \frac{\partial f_1}{\partial x_2} & \dots & \frac{\partial f_1}{\partial x_{nx}} \\ \frac{\partial f_2}{\partial x_1} & \frac{\partial f_2}{\partial x_2} & \dots & \frac{\partial f_2}{\partial x_{nx}} \\ \vdots & \vdots & \ddots & \vdots \\ \frac{\partial f_{nx}}{\partial x_1} & \frac{\partial f_{nx}}{\partial x_2} & \dots & \frac{\partial f_{nx}}{\partial x_{nx}} \end{bmatrix} \quad (8)$$

at every point. With an equivalent notation, we define $B_c = \frac{\partial f}{\partial u}$, $C_c = \frac{\partial h}{\partial x}$ and $D_c = \frac{\partial h}{\partial u}$ and arrive at the definition of the linearized system:

$$\dot{x} = f(x_k, u_k) + A_c(x - x_k) + B_c(u - u_k) \quad (9)$$

$$y = h(x_k, u_k) + C_c(x - x_k) + D_c(u - u_k) \quad (10)$$

Since the linearization point is not a steady-state one, the expression $f(x_k, u_k)$ is different from zero. By introducing the following definition:

$$K_x = f(x_k, u_k) - A_c x_k - B_c u_k \quad (11)$$

$$K_y = h(x_k, u_k) - C_c x_k - D_c u_k \quad (12)$$

the linearized system can be written as follows:

$$\dot{x} = A_c x + B_c u + K_x \quad (13)$$

$$y = C_c x + D_c u + K_y \quad (14)$$

4.2. Discretization of the Linearized System

After the system has been linearized, it is discretized using zero-order hold discretization as shown below. Let \mathcal{A} be defined as $\mathcal{A} = \left[\begin{array}{c|c} A_c & [B_c \ K_x] \\ \hline 0 & 0 \end{array} \right]$, then

$$\left[\begin{array}{c|c} A_d & [B_d \ K_{x_d}] \\ \hline 0 & I \end{array} \right] = e^{\mathcal{A}T_s} \quad (15)$$

holds with T_s being the sampling time and I being the identity matrix of appropriate size. Here,

$$C_d = C_c \quad (16)$$

$$D_d = D_c \quad (17)$$

$$K_{y_d} = K_y \quad (18)$$

also holds. By appropriately extracting the system matrices A_d , B_d , C_d , and D_d as well as the equilibrium offset terms K_{x_d} and K_{y_d} , one obtains the system:

$$x_{i+1} = A_d x_i + B_d u_i + K_{x_d} \quad (19)$$

$$y_i = C_d x_i + D_d u_i + K_{y_d} \quad (20)$$

for which the system matrices A_d , B_d , C_d and D_d obtained at every sample instant k are assumed constant throughout the prediction. Here the index i is used to denote the prediction steps. It ranges from 1 to N_p with N_p being the prediction horizon. By taking a difference operation on both sides of Equation (19), one obtains

$$x_{i+1} - x_i = A_d(x_i - x_{i-1}) + B_d(u_i - u_{i-1}) + K_{x_d} - K_{x_d}. \quad (21)$$

By defining $\Delta x_i = x_i - x_{i-1}$ and $\Delta u_i = u_i - u_{i-1}$, then Equation (21) becomes:

$$\Delta x_{i+1} = A_d \Delta x_i + B_d \Delta u_i \quad (22)$$

It has to be noted that the affine term K_{x_d} vanishes when the difference operator is applied since the linearized model used for prediction is unchanged throughout the prediction. Standard procedure for linear MPC is now applied and after the control move Δu has been calculated, the process of linearization, discretization, and linear MPC formulation is reiterated. This formulation is not bound to the system configuration at hand and can be generally applied.

4.3. Control Goals

The goal is to track the power demand from the vehicle while ensuring safe and efficient operation. Outputs to be controlled:

$$y = \begin{bmatrix} P_{net} \\ \Delta p \\ \eta_{sys} \end{bmatrix} \quad (23)$$

Reference values:

- The reference value for the power is actually the power demand acquired from the vehicle.
- The membrane pressure difference is, if possible, kept at 200 mbar.
- The efficiency is maximized, having a reference value of 1.

In the SLMPC formulation, the controller minimizes the cost function:

$$J = \sum_{i=1}^{N_p} \|y_{ref}(k+i) - \hat{y}(k+i)\|_{\mathcal{Q}_y}^2 + \sum_{j=1}^{N_c} \|\Delta u(k+j)\|_{\mathcal{R}}^2 \quad (24)$$

with \mathcal{Q}_y and \mathcal{R} being the output and input weighting matrices, respectively. N_c is the control horizon, $\hat{y}(k+i)$ is the output prediction.

4.4. Constraints

To ensure safe operation, the following state constraints are applied

$$m_{O_2}^{ca} \geq 1 \text{ g} \quad (25)$$

$$m_{H_2}^{an} \geq 0.5 \text{ g} \quad (26)$$

$$1 \text{ bar} \leq p_{ca} \leq 2.4 \text{ bar} \quad (27)$$

$$1 \text{ bar} \leq p_{an} \leq 2.4 \text{ bar} \quad (28)$$

$$100 \text{ mbar} \leq \Delta p \leq 300 \text{ mbar} \quad (29)$$

Because of physical limitations, constraints on the actuating variables have to be imposed as well:

$$W_{in}^{ca} \geq 0 \quad (30)$$

$$W_{in}^{an} \geq 0 \quad (31)$$

$$I \geq 0 \quad (32)$$

$$0 \leq \alpha_{ca} \leq 1 \quad (33)$$

The vector of control moves

$$\Delta \mathbf{U} = \begin{bmatrix} \Delta u_{k+1} \\ \Delta u_{k+2} \\ \vdots \\ \Delta u_{k+N_c} \end{bmatrix} \quad (34)$$

is the solution of the optimization

$$\Delta \mathbf{U} = \arg \min_{\Delta \mathbf{U}} J \text{ s.t. Equations (25)–(33)} \quad (35)$$

Following the receding horizon principle, only the first step Δu_{k+1} is applied to the system.

4.5. SLMPC Numerical Values

The sampling time for the SLMPC was $T_s = 20$ ms and the prediction horizon was $N_p = 50$ (1 s). The control horizon was $N_c = 25$. The output weighting matrix has been brought in Equation (36).

$$\mathcal{Q}_y = \begin{bmatrix} 1 & 0 & 0 \\ 0 & 0.01 & 0 \\ 0 & 0 & 0.01 \end{bmatrix} \quad (36)$$

The weighting matrix shows that the controller tries to follow the power demand and to keep the pressure difference at 200 mbar as well as operate efficiently. To solve the optimization problem (Equation (35)) at every time step, qpOASES was used, an open-source QP solver. Software info: qpOASES v3.0, Hans Joachim Ferreau et al., ABB Corporate Research, Switzerland [31].

5. Results and Discussion

In this section, the vehicle power demand tracking while ensuring safe and efficient operation is presented.

5.1. Power Demand Tracking

In Figure 4a the tracking of the system power demand is shown along with the actual net power measured from the vehicle. The part of the drive cycle before 400 s is omitted because the vehicle was not in its normal operating state during that time, but rather, it experienced a few emergency shut-down events which are not representable by the model at this point. From the presented drive cycle fraction, it is obvious that the controller can fulfill the power demand as shown in Figure 4a. In Figure 4c a detail of the power demand tracking is brought for demonstration purposes.

5.2. Safe Operation

The controller shows its capability of ensuring safe operation in various aspects. Firstly, it can keep the pressure difference across the membrane between its bounds Equation (29) as shown in Figure 4b. Examining the segment of the drive cycle shown in Figure 4d, a few key points should be mentioned. The power demand during the shown segment is the highest (60 kW) so purging events happen more often than at other instances. The SLMPC can react and keep the pressure difference within the safety limits due to the knowledge of the upcoming purging event and thus proving to be a promising concept for fuel cell dynamic control. The conventional control procedure in the vehicle was not able to maintain the pressure difference value within the safety range. Secondly, the controller can keep the system from operating in starvation conditions by always having a reserve of reactant mass as shown in Figure 4e,f. It is worth noting that the oxygen and hydrogen masses shown in Figure 4e,f are not measured, but are the internal states of the fuel cell given by the model. In future work, if the model is validated and proven to represent reality accurately, the knowledge of internal states can be of great importance, as shown in this work.

No results were shown regarding the absolute pressure safety limits (Equations (27) and (28)) as they were not at risk of being violated throughout the simulation.

5.3. Efficient Operation

The system efficiency comparison between the proposed control concept and the actual vehicle operation is shown in Figure 5a. The SLMPC operates usually at higher efficiencies, except during the periods of high power demand where both cannot be achieved. The authors acknowledge that the reason for higher efficiency in most of the drive cycle is partly due to the predictive capability of the controller which is not available in real life as the future power trajectory is generally not known. Further investigation considering that fact is currently underway.

Examining Equation (4), one can deduce that increasing efficiency implies operation at lower currents as well as higher voltages. In addition, the compressor power should be as small as possible. As already mentioned, except for the high power demand periods, i.e., from 565 s to 590 s, the current (Figure 5b) and compressor power (Figure 5c) are lower and the voltage (Figure 5d) is higher, as it should be. The temperature is not controlled in this simulation study and is assumed constant with a value of 70 °C. The measured stack temperature in the vehicle has been observed to be between 60 °C and 75 °C as seen in Figure 5e. The voltage of the fuel cell is increased when the ohmic losses are decreased. The ohmic resistance is inversely proportional to the protonic conductivity σ :

$$\sigma(T, \lambda_m) = (e_0 \lambda_m + e_1) \exp \left[e_2 \left(\frac{1}{303} - \frac{1}{T} \right) \right] \quad (37)$$

which increases with the membrane water content λ_m :

$$\lambda_m = 0.043 + 17.18a_{m,d} - 39.85a_{m,d}^2 + 36a_{m,d}^3. \quad (38)$$

The values of e_0 , e_1 , and e_2 are parameters taken from the literature and through fitting. The effect of the membrane water content is included in the electrochemical model, thus, the SLMPC “knows” that efficiency is high under conditions of higher humidity and acts accordingly. Even though humidity is not actively manipulated, it is controlled with the available control inputs presented in Equation (7). To increase the membrane water content and by extension, the efficiency, the controller can, for example, close the cathode backpressure valve and/or reduce the air inflow to keep the water vapor from flowing out, preventing membrane dryout. The explained implicit consideration of the membrane water content is exactly what happens as seen in Figure 5f, keeping the membrane hydrated. The problem of flooding is currently not included in the model, but research in that respect is underway. However, as visible from the measured voltage in Figure 5d, no serious breakdown happened which could be attributed to the effects of liquid water. The authors have also been informed by the vehicle manufacturers that draining events happen quite often, thus, the quantity of liquid water present during operation is minimized.

Hydrogen saving

The rate of hydrogen consumption \dot{m}_{H_2} is given by Faraday’s law:

$$\dot{m}_{H_2} = \frac{I}{2F} N_{cells} M_{H_2} \quad (39)$$

with I being the stack current, F the Faraday constant, N_{cells} the total number of cells, and M_{H_2} the hydrogen molar mass. As already described above, from the equation alone is obvious that saving hydrogen implies operation at lower currents as is exactly the case as shown in Figure 5b. To calculate the actual consumed hydrogen, it is necessary to integrate Equation (39) over time. The results are shown in Table 1:

Table 1. Consumed hydrogen.

Vehicle operation	218.60 g
Simulation	197.70 g

The results indicate potential hydrogen savings of 9.54%.

System power tracking and safe operation

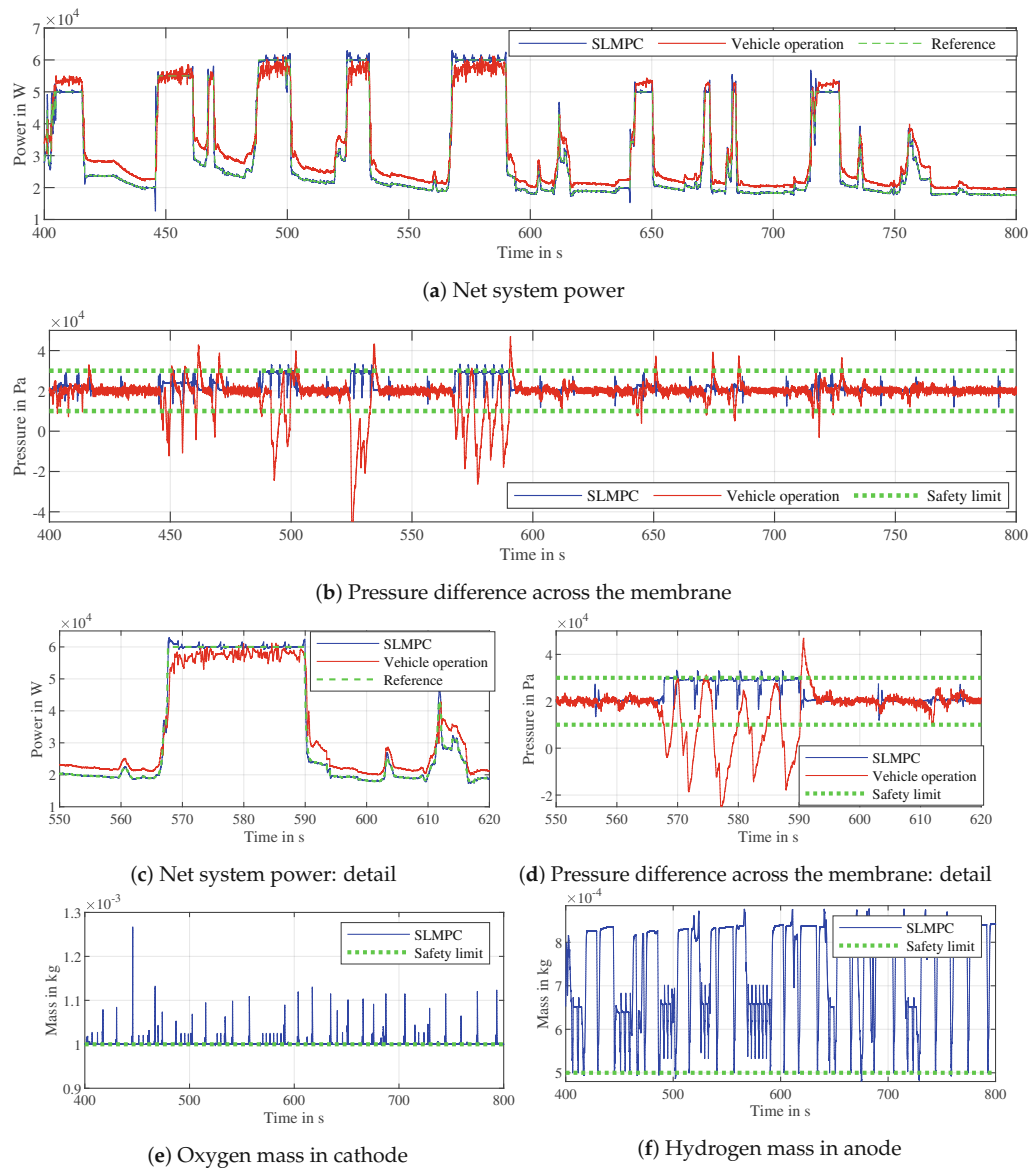


Figure 4. The blue line shows the successive linearization based model predictive control (SLMPC) performance, whereas the red line shows the vehicle operation. In plots (a,c) the green line shows the reference power while in plots (b,d–f) it shows the safety limit for the presented variables.

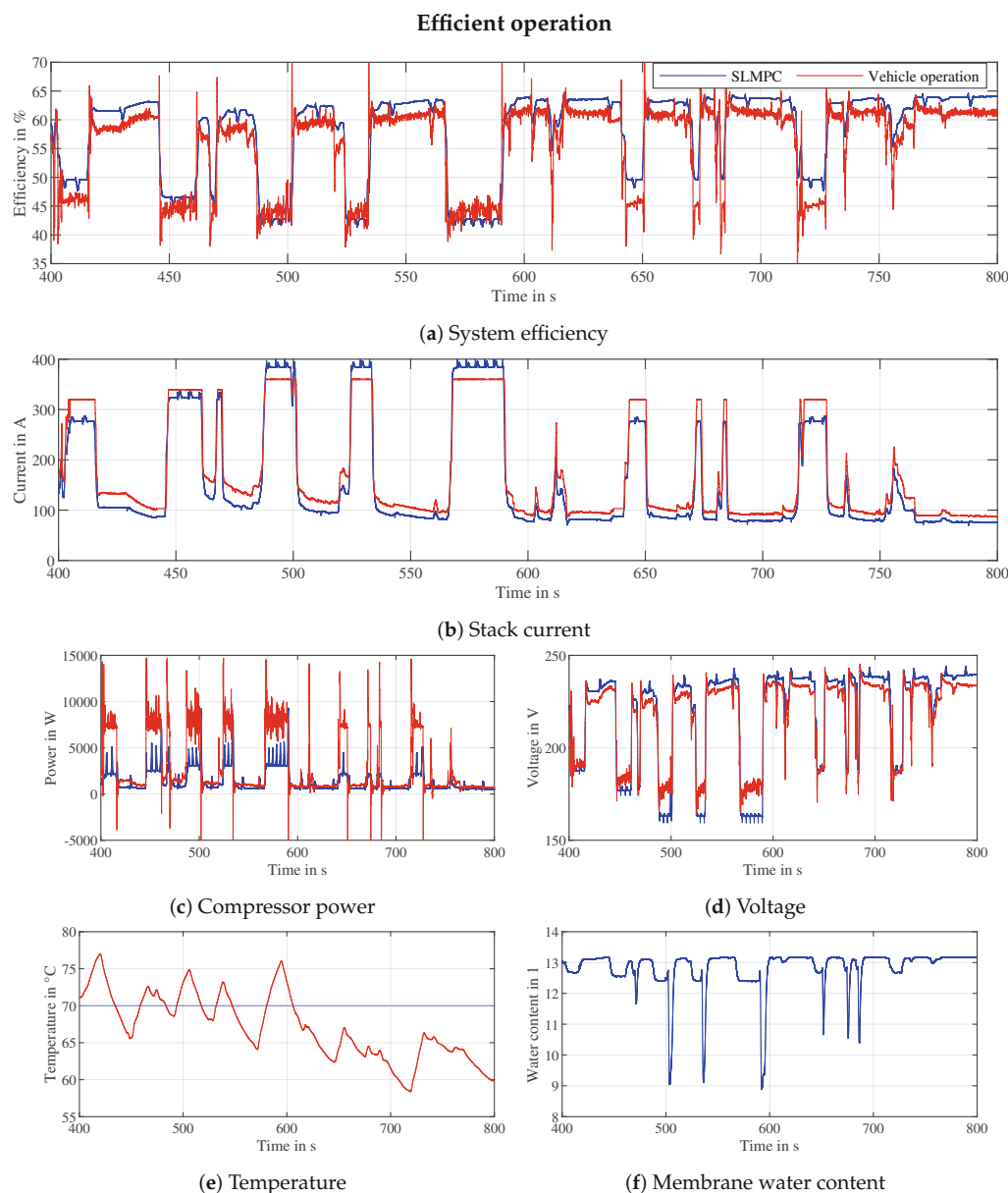


Figure 5. The blue line shows the SLMPC performance, whereas the red line shows the vehicle operation.

6. Conclusions

In this paper, a simulation study using successive linearization based model predictive control has been presented. The proposed control concept was able to track the power demand of a hydrogen-powered fuel cell vehicle while ensuring safe and efficient operation. Comparison with the actual vehicle controlled by a set of PI controllers showed that the SLMPC approach is a promising one in the future of control of fuel cells in automotive applications.

Author Contributions: Conceptualization and methodology, M.V., D.R. and S.J.; software development and investigation, M.V., D.R.; data curation and visualization, M.V.; writing—original draft, M.V.; writing—review and editing, D.R., S.J.; supervision and project administration, S.J. All authors have read and agreed to the published version of the manuscript.

Funding: This research was funded by the Austrian Research Promotion Agency (Österreichische Forschungsförderungsgesellschaft) grant number 865181. The APC was funded by TU Wien Bibliothek.

Acknowledgments: Special thanks to the engineers from AVL List GmbH for providing the data of the vehicle drive cycle as well as for all the useful advice and explanations. The authors acknowledge TU Wien Bibliothek for financial support through its Open Access Funding Program.

Conflicts of Interest: The authors declare no conflict of interest.

References

1. Barbir, F. *PEM Fuel Cells: Theory and Practice*, 2nd ed.; Elsevier Inc.: Amsterdam, The Netherlands, 2013.
2. Pukrushpan, J.T.; Peng, H.; Stefanopoulou, A.G. Control-oriented modeling and analysis for automotive fuel cell systems. *J. Dyn. Syst. Meas. Control. Trans. ASME* **2004**, *126*, 14–25. [\[CrossRef\]](#)
3. Danzer, M.A.; Wilhelm, J.; Aschemann, H.; Hofer, E.P. Model-based control of cathode pressure and oxygen excess ratio of a PEM fuel cell system. *J. Power Sources* **2008**, *176*, 515–522. [\[CrossRef\]](#)
4. Da Fonseca, R.; Bideaux, E.; Gerard, M.; Jeanneret, B.; Desbois-Renaudin, M.; Sari, A. Control of PEMFC system air group using differential flatness approach: Validation by a dynamic fuel cell system model. *Appl. Energy* **2014**, *113*, 219–229. [\[CrossRef\]](#)
5. Chen, J.; Member, S.; Liu, Z.; Wang, F.; Ouyang, Q.; Su, H. Optimal Oxygen Excess Ratio Control for PEM Fuel Cells. *IEEE Trans. Control. Syst. Technol.* **2018**, *26*, 1711–1721. [\[CrossRef\]](#)
6. Ebadighajari, A.; Devaal, J.; Golnaraghi, F. Multivariable control of hydrogen concentration and fuel over-pressure in a polymer electrolyte membrane fuel cell with anode re-circulation. In Proceedings of the 2016 American Control Conference, Boston, MA, USA, 6–8 July 2016; pp. 4428–4433. [\[CrossRef\]](#)
7. Pukrushpan, J.T.; Stefanopoulou, A.G.; Peng, H.; Berlin, S.; Newyork, H.; Kong, H.; Milan, L.; Tokyo, P. *Control of Fuel Cell Power Systems Principles, Modeling, Analysis, and Feedback Design-Monograph*; Springer: Berlin/Heidelberg, Germany, 2004.
8. Li, Q.; Chen, W.; Wang, Y.; Jia, J.; Han, M. Nonlinear robust control of proton exchange membrane fuel cell by state feedback exact linearization. *J. Power Sources* **2009**, *194*, 338–348. [\[CrossRef\]](#)
9. Liu, Z.; Chen, J.; Chen, H.; Yan, C. Air supply regulation for PEMFC systems based on uncertainty and disturbance estimation. *Int. J. Hydrog. Energy* **2018**, *43*, 11559–11567. [\[CrossRef\]](#)
10. Vahidi, A.; Stefanopoulou, A.; Peng, H. Current management in a hybrid fuel cell power system: A model-predictive control approach. *IEEE Trans. Control. Syst. Technol.* **2006**, *14*, 1047–1057. [\[CrossRef\]](#)
11. Meidanshahi, V.; Karimi, G. Dynamic modeling, optimization and control of power density in a PEM fuel cell. *Appl. Energy* **2012**, *93*, 98–105. [\[CrossRef\]](#)
12. Hähnel, C.; Aul, V.; Horn, J. Power Control for Efficient Operation of a PEM Fuel Cell System by Nonlinear Model Predictive Control. *IFAC PapersOnLine* **2015**, *48*, 174–179. [\[CrossRef\]](#)
13. Han, X.; Li, F.; Zhang, T.; Zhang, T.; Song, K. Economic energy management strategy design and simulation for a dual-stack fuel cell electric vehicle. *Int. J. Hydrog. Energy* **2017**, *42*, 11584–11595. [\[CrossRef\]](#)
14. Luna, J.; Usai, E.; Husar, A.; Serra, M. Enhancing the efficiency and lifetime of a proton exchange membrane fuel cell using nonlinear model-predictive control with nonlinear observation. *IEEE Trans. Ind. Electron.* **2017**, *64*, 6649–6659. [\[CrossRef\]](#)
15. Rodatz, P.; Paganelli, G.; Sciarretta, A.; Guzzella, L. Optimal power management of an experimental fuel cell/supercapacitor- powered hybrid vehicle. *Control Eng. Pract.* **2005**, *13*, 41–53. [\[CrossRef\]](#)
16. Shen, D.; Lim, C.C.; Shi, P. Robust fuzzy model predictive control for energy management systems in fuel cell vehicles. *Control Eng. Pract.* **2020**, *98*, 104364. [\[CrossRef\]](#)
17. Kerviel, A.; Pesyridis, A.; Mohammed, A.; Chalet, D. An evaluation of turbocharging and supercharging options for high-efficiency Fuel Cell Electric Vehicles. *Appl. Sci.* **2018**, *8*, 2474. [\[CrossRef\]](#)
18. Arce, A.; Del Real, A.J.; Bordons, C.; Ramírez, D.R. Real-time implementation of a constrained MPC for efficient airflow control in a PEM fuel cell. *IEEE Trans. Ind. Electron.* **2010**, *57*, 1892–1905. [\[CrossRef\]](#)

19. Gruber, J.K.; Doll, M.; Bordons, C. Design and experimental validation of a constrained MPC for the air feed of a fuel cell. *Control Eng. Pract.* **2009**, *17*, 874–885. [\[CrossRef\]](#)
20. Gruber, J.K.; Bordons, C.; Oliva, A. Nonlinear MPC for the airflow in a PEM fuel cell using a Volterra series model. *Control Eng. Pract.* **2012**, *20*, 205–217. [\[CrossRef\]](#)
21. Amin, B.; Bambang, R.T.; Rohman, A.S.; Dronkers, C.J.; Ortega, R.; Sasongko, A. Energy management of fuel cell/battery/supercapacitor hybrid power sources using model predictive control. *IEEE Trans. Ind. Informatics* **2014**, *10*, 1992–2002. [\[CrossRef\]](#)
22. Puig, V.; Feroldi, D.; Serra, M.; Quevedo, J.; Riera, J. Fault-tolerant MPC control of PEM fuel cells. *IFAC Proc. Vol. (IFAC Papers Online)* **2008**, *17*, 11112–11117. [\[CrossRef\]](#)
23. Zhakatayev, A.; Rakhim, B.; Adiyatov, O.; Baimyshev, A.; Varol, H.A. Successive linearization based model predictive control of variable stiffness actuated robots. In Proceedings of the IEEE/ASME International Conference on Advanced Intelligent Mechatronics, Munich, Germany, 3–7 July 2017; pp. 1774–1779. [\[CrossRef\]](#)
24. Ławryńczuk, M. Nonlinear predictive control of a boiler-turbine unit: A state-space approach with successive on-line model linearisation and quadratic optimisation. *ISA Trans.* **2017**, *67*, 476–495. [\[CrossRef\]](#)
25. Bamimore, A.; Taiwo, O.; King, R. Comparison of two nonlinear model predictive control methods and implementation on a laboratory three tank system. In Proceedings of the IEEE Conference on Decision and Control, Orlando, FL, USA, 12–15 December 2011; pp. 5242–5247. [\[CrossRef\]](#)
26. Goshtasbi, A.; Ersal, T. LQ-MPC design for degradation-conscious control of PEM fuel cells. In Proceedings of the American Control Conference, Philadelphia, PA, USA, 10–12 July 2019; pp. 1555–1560. [\[CrossRef\]](#)
27. Ritzberger, D.; Hametner, C.; Jakubek, S. A real-time dynamic fuel cell system simulation for model-based diagnostics and control: Validation on real driving data. *Energies* **2020**, *13*, 3148. [\[CrossRef\]](#)
28. Kravos, A.; Ritzberger, D.; Tavcar, G.; Hametner, C.; Jakubek, S.; Katrasnik, T. Thermodynamically consistent reduced dimensionality electrochemical model for proton exchange membrane fuel cell performance modelling and control. *J. Power Sources* **2020**, *454*. [\[CrossRef\]](#)
29. KEYTECH4EV Development and Demonstration of Key Technologies for Low-Cost Electric Vehicle Platforms. Available online: <http://iesta.at/keytech4ev/> (accessed on 13 August 2020).
30. Yousfi-Steiner, N.; Moçotéguy, P.; Candusso, D.; Hissel, D. A review on polymer electrolyte membrane fuel cell catalyst degradation and starvation issues: Causes, consequences and diagnostic for mitigation. *J. Power Sources* **2009**, *194*, 130–145. [\[CrossRef\]](#)
31. Ferreau, H.J.; Kirches, C.; Potschka, A.; Bock, H.G.; Diehl, M. qpOASES: A parametric active-set algorithm for quadratic programming. *Math. Program. Comput.* **2014**, *6*, 327–363. [\[CrossRef\]](#)

Publisher's Note: MDPI stays neutral with regard to jurisdictional claims in published maps and institutional affiliations.



© 2020 by the authors. Licensee MDPI, Basel, Switzerland. This article is an open access article distributed under the terms and conditions of the Creative Commons Attribution (CC BY) license (<http://creativecommons.org/licenses/by/4.0/>).

2.2 Publication B

M. Vrlić, D. Ritzberger, and S. Jakubek. “Model-predictive-control-based reference governor for fuel cells in automotive application compared with performance from a real vehicle”. In: *Energies* 14.8 (2021). DOI: 10.3390/en14082206

Applicant’s Contribution [†]

- Martin Vrlić: Conceptualization, Methodology, Investigation, Software, Visualization, Writing - Original Draft
- Daniel Ritzberger: Conceptualization, Methodology, Writing - Review & Editing
- Stefan Jakubek: Writing - Review & Editing, Supervision, Project administration, Funding acquisition

[†]According to the Elsevier CRediT author statement: <https://www.elsevier.com/authors/policies-and-guidelines/credit-author-statement>



Article

Model-Predictive-Control-Based Reference Governor for Fuel Cells in Automotive Application Compared with Performance from a Real Vehicle

Martin Vrljić ^{1,*}, Daniel Ritzberger ² and Stefan Jakubek ¹

¹ Institut für Mechanik und Mechatronik, Technische Universität Wien, Getreidemarkt 9, 1060 Vienna, Austria; stefan.jakubek@tuwien.ac.at

² AVL List GmbH, Hans-List-Platz 1, 8020 Graz, Austria; Daniel.Ritzberger@avl.com

* Correspondence: martin.vrljic@tuwien.ac.at

Abstract: In this paper, a real-time capable reference governor superordinate model predictive controller (RG-MPC) is developed for fuel cell (FC) control suitable for automotive application. The RG-MPC provides reference trajectories for the subordinate proportional-integral (PI) controllers, which act directly on the FC system. Antiwindup and decoupling schemes, which are common problems in multivariable PI control, are unnecessary, given that the RG-MPC can inherently consider constraints and multivariable systems. The PI dynamics are incorporated into the prediction model used for control, ensuring the feasibility of the provided references for the PI controllers. The successive linearization technique is used in the RG-MPC to cope with the model's nonlinear nature in real-time. The concept has been illustrated in a simulation scenario featuring efficient and safe power control of an FC stack in automotive application using real driving data obtained from an in-house-built FC vehicle. This work is the first step towards upgrading an existing, PI-based control scheme without the necessity of completely rebuilding the interface.

Keywords: reference governor; fuel cell; automotive; model predictive control; successive linearization; safe operation; efficient operation



Citation: Vrljić, M.; Ritzberger, D.; Jakubek, S. Model-Predictive-Control-Based Reference Governor for Fuel Cells in Automotive Application Compared with Performance from a Real Vehicle. *Energies* **2021**, *14*, 2206. <https://doi.org/10.3390/en14082206>

Academic Editor: Felix Barreras

Received: 24 March 2021

Accepted: 12 April 2021

Published: 15 April 2021

Publisher's Note: MDPI stays neutral with regard to jurisdictional claims in published maps and institutional affiliations.



Copyright: © 2021 by the authors. Licensee MDPI, Basel, Switzerland. This article is an open access article distributed under the terms and conditions of the Creative Commons Attribution (CC BY) license (<https://creativecommons.org/licenses/by/4.0/>).

1. Introduction

In the ever-increasing public awareness of the presence of accelerated environmental pollution processes in the world, researchers from many fields of expertise have focused their efforts into finding energy sources alternative to fossil fuels and new sources altogether [1,2]. Development of hydrogen-powered fuel cells (FC) is of particular interest due to their zero-emission nature and wide area of applicability such as in portable, mobile, and stationary devices. The fact that there is a vast quantity of hydrogen present on Earth in the form of water, in theory, removes the problem of energy shortage in the world. In this paper, automotive application of fuel cells will be of special interest. In the world's attempt to use clean energy in automotive applications, zero-emission polymer electrolyte membrane (PEM) fuel cells qualify as an interesting solution because of their high power density, fast start-up, and low operating temperature. To deliver the required power demand to the vehicle, an appropriate control strategy must be developed. Apart from the power request, additional objectives have to be considered, namely, safety and efficiency. It is important that, during operation, the FC stack powering the vehicle does not run into degrading operating conditions such as hydrogen/oxygen starvation, excess pressure difference across the membrane, nitrogen accumulation, membrane dryout, flooding, etc. On the economic side, the control strategy should aim to reduce the parasitic power losses (e.g., compressor, recirculation pump) as much as possible as well as increase the FC stack efficiency by operating in favorable voltage regions, i.e., at higher voltages.

Much research has been done regarding fuel cell control. A recent fuel cell control review paper brings forth the most popular control methods used in this field [3]. The well-

known proportional-integral-derivative (PID) control was used in [4,5] for fuel starvation prevention by manipulating the current or air/hydrogen flow. Adaptive control of oxygen stoichiometry in terms of sliding mode control and robust adaptive control was used in [6–8], where the controller's parameters were estimated by closed-loop least square parameter identification algorithms. Neural optimal control (NOC) was used in [9] to control the current demand by training the cerebellar model articulation controller. Its long-term memory would be trained offline, reducing the computational effort needed during operation. Its short-term memory only was trained online, then the controller was compared to a PI controller and showed better results. In addition, another concept superior to PI control is dynamic neural network control (DDNC) used in [10], where the neural network learns continuously. The existence of all mentioned control strategies clearly shows that fuel cells have many interesting problems that can be tackled by different advanced approaches. The question that arises is how to effectively use the control theory knowledge in dynamic practical applications such as a vehicle, as opposed to only partially controlling a certain subsystem. In this work, one way of using advanced control schemes in automotive application will be proposed.

When it comes to vehicle level control, the majority of manufacturers and industries still prefer to use rule-based and/or PI-based control algorithms since they are simple to understand and implement, unlike some of the above reported methods that require advanced implementation techniques or control engineering knowledge.

A more sophisticated control algorithm than PI, but still intuitive enough to be understood easily, is model predictive control (MPC) which uses a model to predict future operating conditions of the fuel cell and act on the plant so that all the control goals are fulfilled. Such an approach is appropriate for fuel cell control since it can inherently deal with multivariable systems due to its knowledge of the whole system dynamics, and incorporate constraints, both of which are drawbacks of PI-based control. Due to the mentioned strong characteristics of MPC, researchers have used this concept in fuel cell control for a variety of objectives. MPC was popularly used in reactant starvation prevention as reported in [11–15]. The membrane pressure difference was controlled by MPC in [16], as well as in [11,12], where protection against compressor surge/choke was the control goal. The concept of MPC was even used in an experimental setup to achieve a power request, however, the reported load profile was in the range of a few kilowatts and stayed at a single steady-state power value for a long time, not representing a real drive cycle [17,18]. A recent paper stands out, showing an interesting approach to using linear time by varying MPC with the goal of controlling the power of the fuel cell in simulated driving conditions while imposing constraints on many critical physical quantities (e.g., pressure, temperature, humidity) ensuring safe operation of the fuel cell, partly sharing the paradigm of this paper [19]. MPC shows the most promise compared to other control strategies in the sense that it exhibits all the elements necessary for safe and efficient operation of multivariable constrained systems [20]. However, even though the advantages of MPC over PI are known and obvious, it is usually not used in industries for a few reasons. Firstly, PI controllers are easily understandable, and secondly, much effort must be invested in designing and tuning the controllers. Both reasons give points to the reluctance of changing the existing setup. In this paper, the concept of reference governor MPC (RG-MPC) is introduced into the world of fuel cell control, serving as a bridge between the sophisticated MPC approach and the well-known, easy-to-use PI concept. The idea of MPC-based reference governors is not new, but their usage is scarce in fuel cell control theory. An RG-MPC provides optimized references for the PI controllers acting directly on the plant [21–24]. This approach gives two major advantages. First, the reference trajectories are given by the RG-MPC so that all the constraints are satisfied, removing the necessity of using any antiwindup scheme or retuning the PI controllers, both of which can deteriorate performance. Second, MPC inherently handles multivariable systems meaning that no decoupling schemes are needed, unlike in a purely PI-based scheme, since an individual controller is not aware of the existence of the other PI controllers. Additionally, if the PI controllers have been already

well tuned and implemented, and if during operation of the RG-MPC something goes wrong, the operating strategy can be easily switched back to the one with PIs only. With that in mind, placing the RG-MPC on top of the existing PI controllers as a superordinate control layer shows more promise towards implementing an optimal control scheme to an industrial plant rather than completely replacing the PIs with MPC. To test and illustrate the above-described control idea in a simulation environment, a nonlinear state-space plant model describing the fuel cell stack was used. The plant model was then augmented with the PI dynamics resulting in the prediction model used by the RG-MPC to provide optimized references for the PIs. The control goal was to deliver the power demand from a research fuel cell vehicle presented in Section 2, while ensuring safe and efficient operating conditions. A schematic illustration of the above explained scenario is shown in Figure 1. Since the model is nonlinear, the successive linearization technique was used [25–28]. For more detail regarding the model and the successive linearization-based MPC, the reader is referred to the authors' previous work [29,30]. The problem of state estimation is not treated in this paper for brevity. The state observer implementation used in this work can be found in [31]. This paper is organized as follows. In Section 2, the vehicle is briefly presented and discussed. In Section 3, the model is shown and the incorporation of PI dynamics into the model is discussed. Also, the development of the RG-MPC is brought, detailing the control goals and constraints, as well as the formulation of the optimization problem. In Section 4, results showing the tracking of a real vehicle's power demand using the RG-MPC are presented. Finally, in Section 5, the paper is concluded with a proposal for future work on implementing optimal control into the control units of fuel cell vehicles.

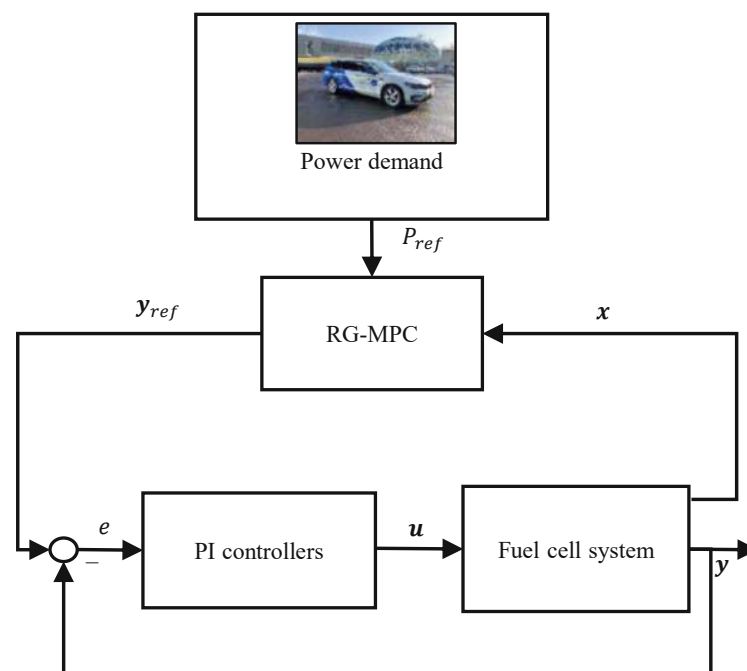


Figure 1. Reference governor model predictive control (MPC) schematics. RG—reference governor; PI—proportional-integral.

2. Vehicle as Validation Data Generator

The RG-MPC was tested in a simulation environment mimicking a real drive cycle performed by a research vehicle developed in the scope of the Keytech4EV project [32]. In the hybrid electric vehicle, the engine bay was replaced with a fuel cell system. The car is shown in Figure 2 and more information on it can be found in [29,30].



Figure 2. AVL List GmbH research demonstrator vehicle.

Vehicle Control Strategy

In the vehicle control unit, the low-level controllers represented by the middle column in Figure 3, receive their setpoints from experimentally obtained and calibrated optimization maps. Clearly, the effort for obtaining the proper set-point calculation strategy is considerable and consists of some important elements:

- Tuning the controllers: it takes a lot of time, especially since decoupling has to be achieved and antiwindup schemes implemented. Further, the number of controllers to be tuned is high.
- Experimental work: to relate the requested power to the current, and then the current to all the other variables, the system has to be identified and a series of experiments with different levels of excitation at multiple operating points need to be conducted. This obviously includes a significant financial investment.
- Recalibration: in the case that a component is replaced (e.g., new compressor), the calibration process has to be repeated to some degree.

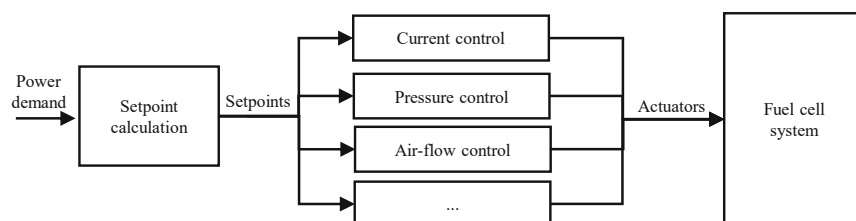


Figure 3. Control scheme of the fuel cell vehicle.

3. Methods

3.1. Plant Model

In this subsection, the model used for the study is briefly presented as the detailed derivation can be found in [29,30]. The model structure is shown in Figure 4.

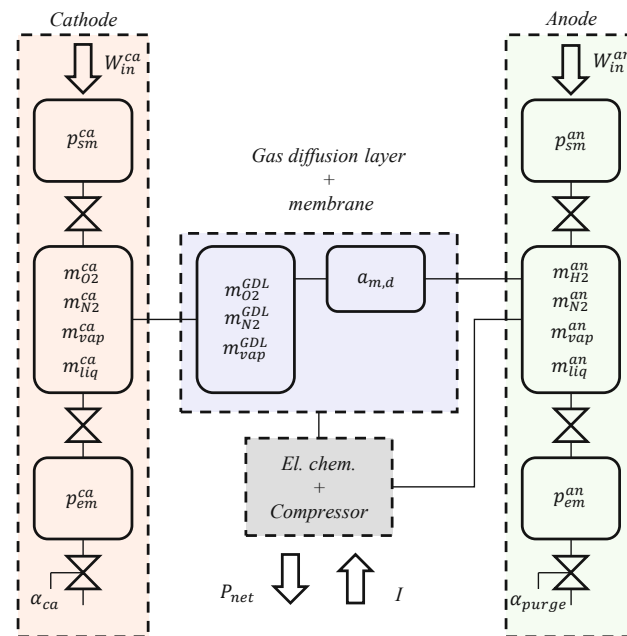


Figure 4. Fuel cell model structure used in the paper. Different colors denote different submodels.

3.1.1. Cathode Submodel

Three interconnected zero-dimensional manifolds represent the cathode channel of the fuel cell. The first in the series, called the supply manifold, is described by a single dynamic state, the supply manifold pressure p_{sm}^{ca} . The center manifold is described by four states, namely, the masses of oxygen, nitrogen, water vapor, and liquid water: $m_{O_2}^{ca}$, $m_{N_2}^{ca}$, m_{vap}^{ca} , m_{liq}^{ca} , respectively. The exit manifold is described by one state, the exit manifold pressure p_{em}^{ca} .

Entering the cathode channel is the inlet air mass-flow W_{in}^{ca} , and at the end of the channel is a backpressure valve characterized by its opening position α_{ca} . Oxygen stoichiometry is defined as the ratio between the inlet oxygen flow and the rate of oxygen consumption in the reaction. It is denoted as λ_{O_2} .

3.1.2. Anode Submodel

Similar with the cathode side, the anode channel is described by three interconnected zero-dimensional manifolds. The first of the three is described by the anode supply manifold pressure p_{sm}^{an} . The center manifold is described by the masses of hydrogen, nitrogen, water vapor, and liquid water: $m_{H_2}^{an}$, $m_{N_2}^{an}$, m_{vap}^{an} , m_{liq}^{an} , respectively. The exit manifold pressure p_{em}^{an} describes the last volume.

Hydrogen entering the anode supply manifold is quantified with the inlet mass-flow W_{in}^{an} . At the end of the channel, there exists a purge valve, the opening of which is described with α_{purge} . Hydrogen stoichiometry is defined as the ratio between the inlet hydrogen flow and the rate of hydrogen consumption in the reaction. It is denoted as λ_{H_2} .

3.1.3. GDL Submodel

The dynamics of the GDL on the anode side are neglected due to hydrogen being a highly diffusive gas, but on the cathode, they are described by 3 states—the masses of oxygen, nitrogen, water vapor: $m_{O_2}^{GDL}$, $m_{N_2}^{GDL}$, m_{vap}^{GDL} , respectively. The mass exchange between the GDL and the cathode channel is through the diffusion law.

3.1.4. Power and Efficiency

The electrochemical submodel, i.e., the dependence of the FC voltage V on the current I and internal states, is adopted from [33]. The power produced by the FC stack is defined as $P_{st} = VI$. The power used by the compressor P_{cp} is defined as in [34]:

$$P_{cp} = C_p \frac{T_{atm}}{\eta_{cp}} \left[\left(\frac{p_{sm}^{ca}}{p_{atm}} \right)^{\frac{\gamma-1}{\gamma}} - 1 \right] W_{in}^{ca}, \quad (1)$$

where $C_p = 1004 \text{ J kg}^{-1} \text{ K}^{-1}$ is the specific heat capacity of air, $T_{atm} = 25 \text{ °C}$ is the temperature of inlet air, $\eta_{cp} = 0.62$ is the compressor efficiency, $p_{atm} = 101,325 \text{ Pa}$ is the pressure of air entering the compressor, and $\gamma = 1.4$ is the ratio of the specific heats of air. The net power is then the difference between the produced power and the parasitic compressor power: $P_{net} = P_{st} - P_{cp}$. The consumed hydrogen power is defined as

$$P_{H_2} = E_0 N_{cells} I, \quad (2)$$

where E_0 is the open circuit voltage of a single cell and N_{cells} is the total number of cells in the stack. The system efficiency η_{sys} is defined as the ratio between the net power and the consumed hydrogen power

$$\eta_{sys} = \frac{P_{net}}{P_{H_2}}. \quad (3)$$

Inserting the expressions for P_{net} and P_{H_2} into Equation (3), one obtains the expression for the system efficiency:

$$\eta_{sys} = \frac{VI - P_{cp}}{E_0 N_{cells} I}. \quad (4)$$

Analyzing the above equation, one can conclude that in order to maximize efficiency, the FC stack should operate at higher voltages and lower compressor powers.

3.1.5. Surge and Choke Margin

A major concern in FC operation control is keeping the compressor operation in a safe area, namely, far from the surge and choke lines, preventing compressor damage. In this work, a hand-tuned reference is given to the controller to track so it has the drive to operate far from dangerous regions. The reference is a linear relation between the pressure ratio of the air exiting and entering the compressor p_{ratio} and the corrected air mass-flow exiting the compressor W_{cr} , shown in Figure 5.

$$p_{ratio} = 22.74 W_{cr} + 0.5885. \quad (5)$$

The distance between the current operating point and the closest point on the reference line is denoted as d and defined as

$$d = \frac{|22.74 W_{cr} + 0.5885 - p_{ratio}|}{\sqrt{1 + (22.74)^2}}. \quad (6)$$

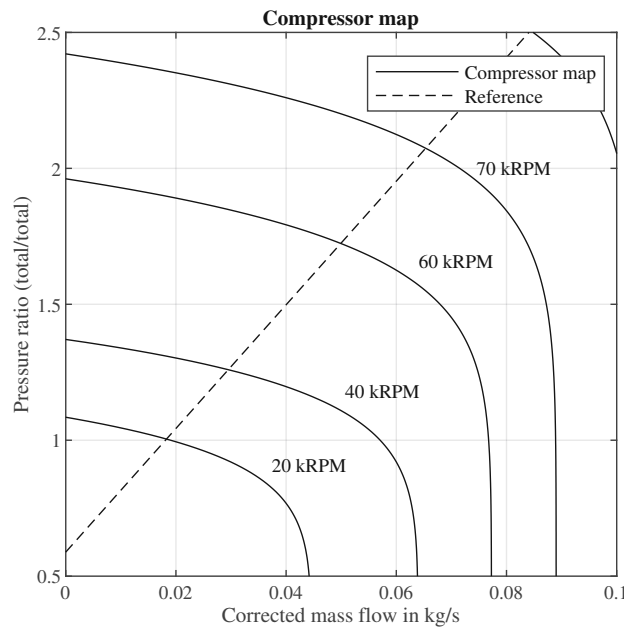


Figure 5. Compressor map. The vicinity of the dashed line is chosen as the desired operation region.

3.1.6. Plant Model Summary

In summary, the FC model is described with the state vector x_{FC} , the input vector u_{FC} , and the output vector y_{FC} :

$$x_{FC} = [p_{sm}^{ca} \ m_{O_2}^{ca} \ m_{N_2}^{ca} \ m_{vap}^{ca} \ m_{liq}^{ca} \ p_{em}^{ca} \ p_{sm}^{an} \ m_{H_2}^{an} \ m_{N_2}^{an} \ m_{vap}^{an} \ m_{liq}^{an} \ p_{em}^{an} \ a_{m,d} \ m_{O_2}^{GDL} \ m_{N_2}^{GDL} \ m_{vap}^{GDL}]^T \quad (7)$$

$$u_{FC} = [W_{in}^{ca} \ W_{in}^{an} \ I \ \alpha_{ca} \ \alpha_{purge}]^T \quad (8)$$

$$y_{FC} = [P_{net} \ \eta_{sys} \ \Delta p \ d \ \lambda_{O_2} \ \lambda_{H_2}]^T, \quad (9)$$

where $a_{m,d}$ is a state describing the dynamic wetting and drying of the membrane and $\Delta p = p_{sm}^{an} - p_{sm}^{ca}$ is the pressure difference across the membrane.

Finally, the nonlinear state-space model reads

$$\dot{x}_{FC} = f(x_{FC}, u_{FC}) \quad (10)$$

$$y_{FC} = h(x_{FC}, u_{FC}). \quad (11)$$

3.2. Prediction Model

In Figure 1, it is shown that the PI controllers provide the signals for the control inputs. The inputs in question are the hydrogen mass-flow and cathode backpressure valve position:

$$W_{in}^{an} = K_{p,an}(p_{sm,ref}^{an} - p_{sm}^{an}) + K_{i,an} \int_0^t (p_{sm,ref}^{an} - p_{sm}^{an}) d\tau \quad (12)$$

$$\alpha_{ca} = K_{p,ca}(p_{sm,ref}^{ca} - p_{sm}^{ca}) + K_{i,ca} \int_0^t (p_{sm,ref}^{ca} - p_{sm}^{ca}) d\tau. \quad (13)$$

For simplicity, the following definitions are introduced:

$$e_{an} = p_{sm,ref}^{an} - p_{sm}^{an} \quad (14)$$

$$e_{ca} = p_{sm,ref}^{ca} - p_{sm}^{ca} \quad (15)$$

$$\dot{I}_{an} = e_{an} \quad (16)$$

$$\dot{I}_{ca} = e_{ca}, \quad (17)$$

leading to a more readable expression for the PI outputs:

$$W_{in}^{an} = K_{p,an}e_{an} + K_{i,an}I_{an} \quad (18)$$

$$\alpha_{ca} = K_{p,ca}e_{ca} + K_{i,ca}I_{ca}. \quad (19)$$

To obtain a model capable of predicting the dynamics of the system, including the PI controllers, it is necessary to augment the plant model with the integrator states of said controllers:

$$\mathbf{x}_{pred} = \begin{bmatrix} \mathbf{x}_{FC} \\ I_{an} \\ I_{ca} \end{bmatrix}. \quad (20)$$

Furthermore, the inputs for the prediction model are different from the ones for the plant model in the following way:

$$\mathbf{u}_{FC} = \begin{bmatrix} W_{in}^{ca} \\ W_{in}^{an} \\ I \\ \alpha_{ca} \\ \alpha_{purge} \end{bmatrix} \rightarrow \mathbf{u}_{pred} = \begin{bmatrix} W_{in}^{ca} \\ p_{sm,ref}^{an} \\ I \\ p_{sm,ref}^{ca} \\ \alpha_{purge} \end{bmatrix}. \quad (21)$$

The outputs of the prediction model are divided into the ones to be controlled, constrained, and observed. The latter refers to those outputs neither controlled nor constrained, but needed for the evaluation of the PI output, namely, the cathode and anode supply manifold pressure.

$$\mathbf{y}_{pred} = \begin{bmatrix} \mathbf{y}_{pred,controlled} \\ \mathbf{y}_{pred,constrained} \\ \mathbf{y}_{pred,observed} \end{bmatrix} = \begin{bmatrix} P_{net} \\ \eta_{sys} \\ \Delta p \\ d \\ \lambda_{O_2} \\ \lambda_{H_2} \\ W_{in}^{an} \\ \alpha_{ca} \\ p_{sm}^{an} \\ p_{sm}^{ca} \end{bmatrix}. \quad (22)$$

Specific values of the constrained inputs and output will be discussed in Section 3.6, where the MPC design is addressed.

3.3. Successive Linearization

In this subsection, the successive linearization framework will be presented and later on used by the controller. This way, nonlinear systems can be easily controlled using the concept of the successive-linearization-based MPC [19,25,27,28,30]. An illustration of the concept can be seen in Figure 6.

The nonlinear prediction model is linearized around the current state $(\mathbf{x}_k, \mathbf{u}_k)$ at each time step k . The linearized model is then discretized using zero-order-hold and a discrete time prediction model is obtained. Since the linearization point is typically not stationary, off-equilibrium terms have to be accounted for. This is done by using the velocity form or

so-called “delta formulation” of the MPC, where the off-equilibrium terms cancel out. The full derivation of the concept can be found in [30], here, only the end result is shown here. The prediction model is

$$\Delta \mathbf{x}_{i+1} = \mathbf{A}_{d,k} \Delta \mathbf{x}_i + \mathbf{B}_{d,k} \Delta \mathbf{u}_i, \quad (23)$$

where \mathbf{x} is the state vector; \mathbf{u} is the input vector; i is the prediction index; and \mathbf{A}_d and \mathbf{B}_d are the current system and input matrix, respectively, which are updated at every time step k . The subscript d denotes that the matrices are in discrete time.

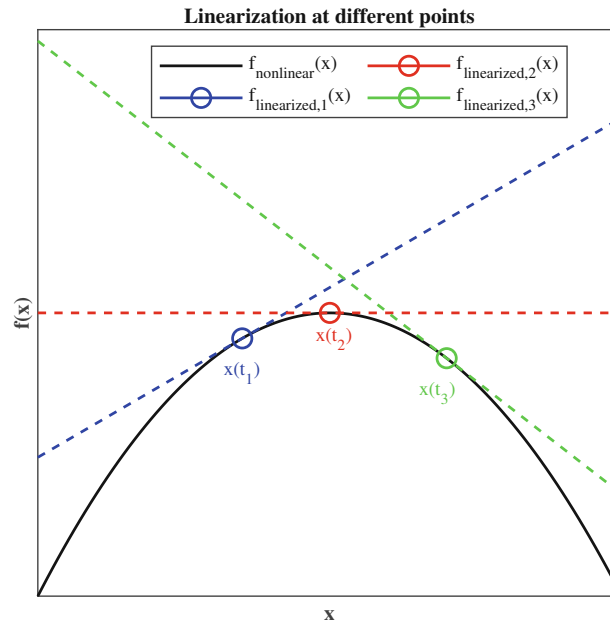


Figure 6. Successive linearization concept. The system function $f(\mathbf{x})$ is linearized around the state vector $\mathbf{x}(t)$ at every time step. The linearized system is used to develop the MPC at that time step.

3.4. MPC Formulation

In the previous subsection, the method of obtaining a linear prediction model each time step has been explained. In this subsection, the formulation of the MPC using the obtained linear model is presented. Firstly, it is important to emphasize that in this work, as already stated, the velocity form MPC is used, having $\Delta \mathbf{x}_i = \mathbf{x}_i - \mathbf{x}_{i-1}$ as its state vector and $\Delta \mathbf{u}_i = \mathbf{u}_i - \mathbf{u}_{i-1}$ as its input vector, where i is the running index in the prediction. In some literature, this is referred to as the “delta formulation” MPC. To obtain offset-free reference tracking, an integrator is added for every output. Following the algorithm, the differential state vector $\Delta \mathbf{x}$ is augmented with the output vector:

$$\mathbf{x}_{aug} = \begin{bmatrix} \Delta \mathbf{x}_{pred} \\ \mathbf{y}_{pred} \end{bmatrix}. \quad (24)$$

The augmented system instantaneously linearized at time k is then as follows:

$$\begin{bmatrix} \Delta \mathbf{x}_{pred} \\ \mathbf{y}_{pred} \end{bmatrix}_{i+1} = \begin{bmatrix} \mathbf{A}_k & \mathbf{0} \\ \mathbf{C}_k \mathbf{A}_{d,k} & \mathbf{I} \end{bmatrix} \begin{bmatrix} \Delta \mathbf{x}_{pred} \\ \mathbf{y}_{pred} \end{bmatrix}_i + \begin{bmatrix} \mathbf{B}_{d,k} \\ \mathbf{C}_{d,k} \mathbf{B}_{d,k} \end{bmatrix} \Delta \mathbf{u}_i + \begin{bmatrix} \mathbf{0} \\ \mathbf{D}_{d,k} \end{bmatrix} \Delta \mathbf{u}_{i+1} \quad (25)$$

$$\mathbf{y}_{pred,i} = [\mathbf{0} \quad \mathbf{I}] \begin{bmatrix} \Delta \mathbf{x}_{pred} \\ \mathbf{y}_{pred} \end{bmatrix}_i. \quad (26)$$

Due to present direct-feedthrough in the model, the D_k matrix shows up in Equation (25). To address this issue, the optimal control move is calculated for the next time step $i + 1$, incorporating the last solution Δu_i as a predicted disturbance and rendering the system causal.

3.5. Objective Formulation

The reference values of the controlled outputs are as follows:

- System net power—the reference is taken from the vehicle in Section 2.
- System efficiency—the reference value is 1.
- Pressure difference across the membrane—the reference value is 200 mbar.
- Distance from optimal line in the compressor map—the reference value is 0.

The goal of the controller is the minimization of the cost function J :

$$J = \sum_{i=1}^{N_p} \|y_{ref_{k+i}} - \hat{y}_{k+i}\|_{\mathcal{Q}_y}^2 + \sum_{j=1}^{N_c} \|\Delta u_{k+j}\|_{\mathcal{R}}^2, \quad (27)$$

where N_p and N_c are the prediction and control horizon; $y_{ref_{k+i}}$, \hat{y}_{k+i} , and Δu_{k+j} are the reference output, prediction output, and control move value i and j steps into the prediction from the linearization instant k , respectively; and \mathcal{Q}_y and \mathcal{R} are the outputs and inputs weighing matrices, respectively.

The outputs are weighted as follows:

$$\mathcal{Q}_y = \begin{bmatrix} \frac{1}{100kW^2} & 0 & 0 & 0 \\ 0 & 1 & 0 & 0 \\ 0 & 0 & \frac{1}{bar^2} & 0 \\ 0 & 0 & 0 & \frac{1}{20} \end{bmatrix}. \quad (28)$$

The values in this matrix suggest that following the net power trajectory has highest priority, where the other two tracking control goals, system efficiency and membrane overpressure, are lower in priority. This choice of priorities coincides with real life operation, where it is important to achieve a certain power while specific control of another quantity (e.g., membrane overpressure) and efficiency are to be achieved if possible, but are not mandatory.

3.6. Constraints

Two types of constraints are present in this study: input and output constraints. One should be careful not to mix the notion of input and actuator constraints. It should be kept in mind that the prediction model has as its inputs, among others, the reference values for the PI controllers, whereas the plant itself has actuators as its inputs. The actuators W_{in}^{an} and α_{ca} are actually part of the output vector of the prediction model. From this point forward, constraints are always given with reference to the prediction model.

Input constraints are as follows:

$$0 \leq W_{in}^{ca} \leq 0.1 \text{ kg s}^{-1} \quad (29)$$

$$1 \text{ bar} \leq p_{sm,ref}^{an} \leq 3 \text{ bar} \quad (30)$$

$$40 \text{ A} \leq I \leq 360 \text{ A} \quad (31)$$

$$1 \text{ bar} \leq p_{sm,ref}^{ca} \leq 3 \text{ bar}. \quad (32)$$

Output constraints are as follows:

$$0.1 \text{ bar} \leq \Delta p \leq 0.3 \text{ bar} \quad (33)$$

$$1 \leq \lambda_{O_2} \leq \infty \quad (34)$$

$$0 \leq \lambda_{H_2} \leq \infty \quad (35)$$

$$0 \leq W_{in}^{an} \leq \infty \quad (36)$$

$$0 \leq \alpha_{ca} \leq 1. \quad (37)$$

The vector of control moves

$$\Delta \mathbf{U} = \begin{bmatrix} \Delta u_{k+1} \\ \Delta u_{k+2} \\ \vdots \\ \Delta u_{k+N_c} \end{bmatrix} \quad (38)$$

is the solution of the optimization

$$\Delta \mathbf{U} = \arg \min_{\Delta \mathbf{U}} J \quad (39)$$

subject to the constraints

Equations (29)–(37)

Only the first step Δu_{k+1} is applied to the system, according to the receding horizon principle.

4. Results and Discussion

In this section, the results of a simulation scenario of tracking the power demand measured from the vehicle and comparison between the RG-MPC and vehicle operation are presented. Moreover, the benefits of the RG-MPC approach are discussed.

4.1. Simulation Results

The end goal of designing the controller described above is to control an FC system in an automotive application. This entails delivering the required net power as efficiently as possible while taking into consideration all the safety requirements. Clearly, in a real vehicle, a vast number of details have to be considered and rigorous testing of the control system has to be done for it to function properly. Therefore, the results of the simulation tests mimicking the vehicle operation in which the RG-MPC tries to deliver the measured power demand compared to the performance of the PID-controlled vehicle are presented in this section. The RG-MPC fulfills the delivery of the required net power in the vehicle shown in Figure 7, except in the region of high power demand of 60 kW, where the performance limitation is hit, since the current is constrained at 360 A (Figure 8d) and the compressor power (Figure 8a) cannot be further reduced, as it would cause operating in dangerous regions—as it will be demonstrated later on. It can be seen in Figure 7 that the power demand on regions of lower power is not followed correctly in the vehicle, presumably because of some other requirement in the vehicle at the time of operation.

As defined in Equation (4), the system efficiency is evaluated and compared to the vehicle. In Figure 8b, one can see that the RG-MPC matches the vehicle efficiency in the region of high power demand, but the compressor power (Figure 8a) and stack voltage (Figure 8c) do not match the ones measured by the vehicle sensors. The RG-MPC is driven to maximize efficiency, as defined in its cost function (Equation (27)), but not explicitly instructed in which state to operate. Obviously, since the voltage is lower, the stack power will be lower as well, but the compressor power is also lower, leading to an equal net power as already discussed and operating at the same current as the vehicle; the efficiencies match.

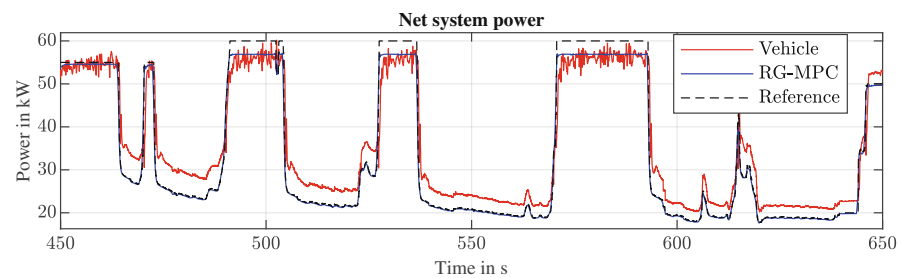


Figure 7. Net system power. Comparison between the vehicle operation and RG-MPC.

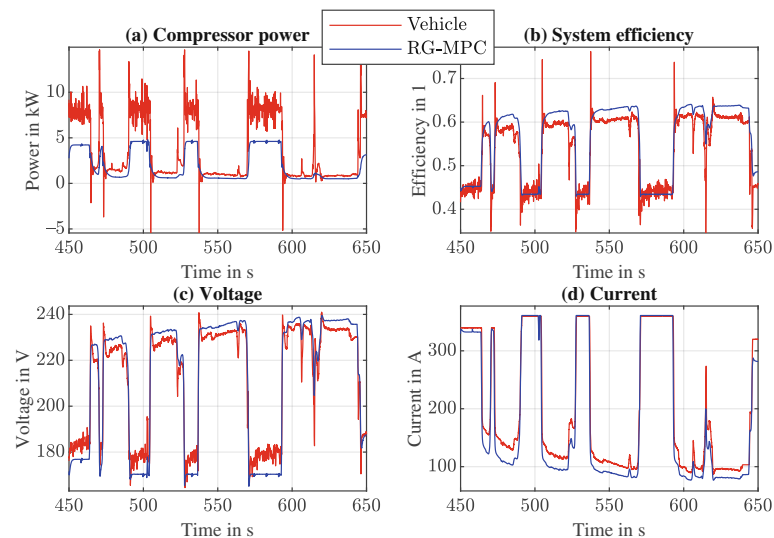


Figure 8. (a) Compressor power, (b) system efficiency, (c) stack voltage, (d) current.

With the goal of preventing oxygen starvation, the controller is keeping the oxygen stoichiometry above its limit of 1 (Figure 9a) and thanks to the anode-to-cathode pressure difference requirement, the hydrogen stoichiometry implicitly takes the value of 1, except during transients of power demand and during purging events, visible as spikes in Figure 9b. The controller could easily incorporate a stricter constraint on the oxygen stoichiometry, leading to an operation in regions of higher compressor power, since the air-flow entering the cathode should be higher. The decision on the exact number would be left to experts operating the actual system.

An important safety requirement is keeping the pressure difference across the membrane inside a safety bandwidth. The predictive capability of the RG-MPC gives the system the opportunity to counteract disturbances such as purging events. In Figure 10a, purging events in the performance of the RG-MPC can be clearly seen as regular small spikes, whereas in the vehicle operation, they are even more visible as large deviations from the setpoint of 0.2 bar. A big absolute value of the pressure difference can cause irreversible damage by rupturing the membrane of the fuel cell. It is important, therefore, for the controller to have a good strategy of keeping the pressure difference inside safety limits. In the RG-MPC, it is done by simply imposing a constraint on it (Equation (33)). In Figure 10b, the sudden burst of inlet hydrogen-flow is the result of the controller's requirement to keep the pressure difference between constraints and the same conclusion goes for the cathode backpressure valve position (Figure 10c), but to a smaller degree, since the cathode pressure would not be abruptly changed by an encountered purging event. A major concern in the safe operation of fuel cells is the compressor's behavior. One would want the compressor to operate far

from the surge and choke lines, the far-left and far-right region of the solid black lines in Figure 11c, respectively. In the RG-MPC setup, the normal distance of the operating state to the reference black dashed line in Figure 11c is minimized (Equation (6)), leading to an operation far from the unsafe region. In the vehicle setup, a series of experimentally obtained optimization maps was used to determine the best operating state. In Figure 11a,b, the cathode inlet pressure and air inlet mass-flow are shown for comparison purposes. The reference control setup that was used on the vehicle tends to operate at higher pressures and mass-flows than the RG-MPC, increasing the used compressor power as already seen in Figure 8a; since the pressure is higher, the voltage is higher as well (Figure 8c), leading to an overall net power and efficiency matching the one obtained by the RG-MPC.

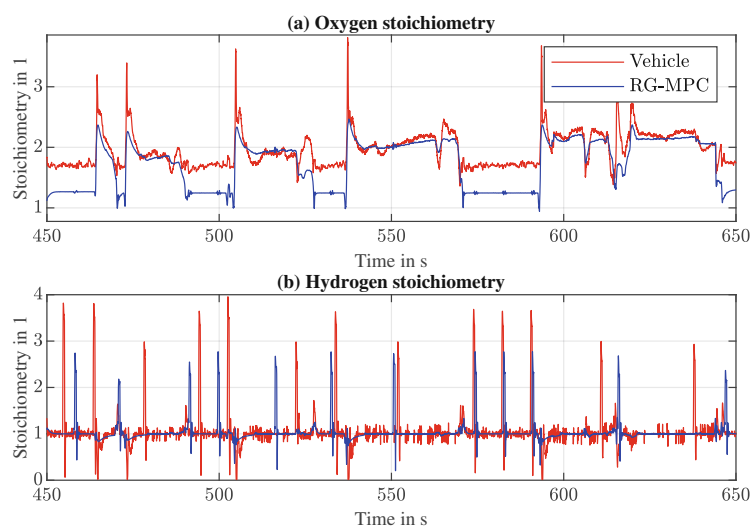


Figure 9. (a) Oxygen stoichiometry, (b) hydrogen stoichiometry.

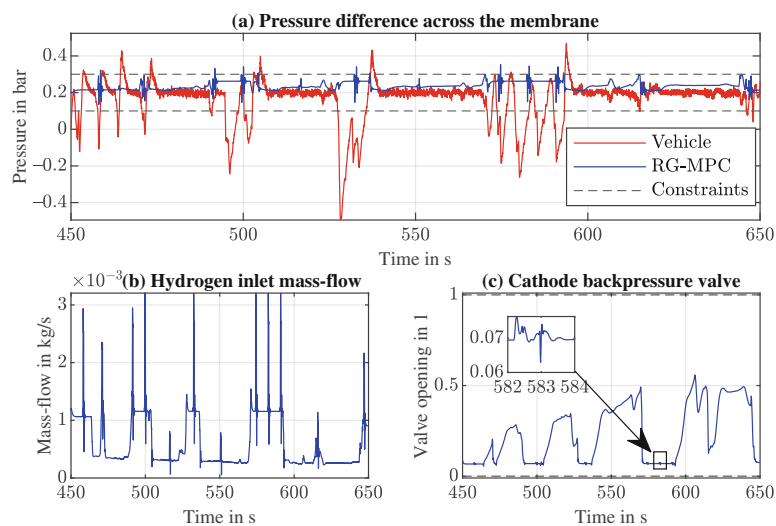


Figure 10. (a) Pressure difference across the membrane, (b) hydrogen inlet mass-flow, (c) cathode backpressure valve.

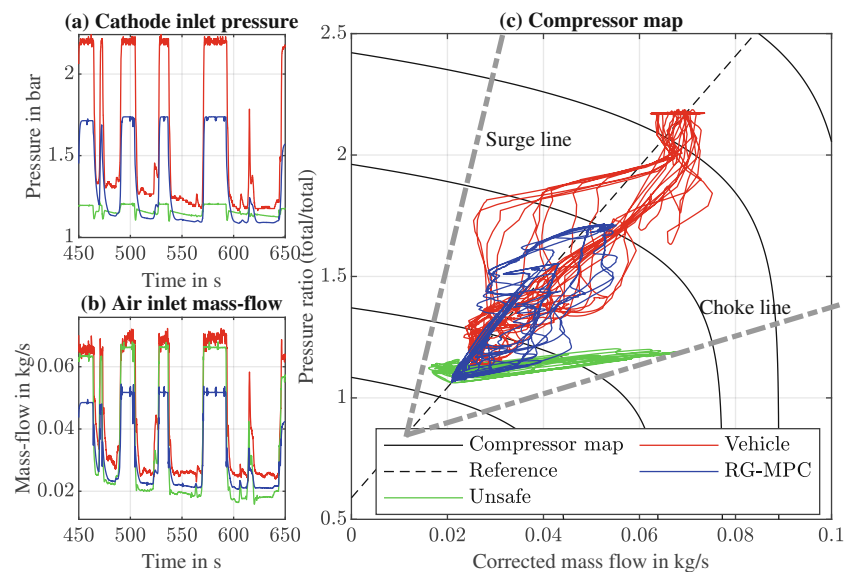


Figure 11. (a) Cathode inlet pressure, (b) air inlet mass-flow, (c) compressor map.

The RG-MPC was tested without the compressor safety requirement, only with the efficiency requirement, which drives the compressor power to be as small as possible. The result is shown in green in Figure 11. Mathematically, the difference between the blue line and the green line is in the weighting matrix from Equation (28). The weight on the minimization of the distance between the current state and the compressor reference line is set to a very low value, effectively meaning that it is not considered by the controller.

$$\mathbf{Q}_y = \begin{bmatrix} \frac{1}{100 \text{ kW}^2} & 0 & 0 & 0 \\ 0 & 1 & 0 & 0 \\ 0 & 0 & \frac{1}{\text{bar}^2} & 0 \\ 0 & 0 & 0 & \frac{1}{2000} \end{bmatrix}. \quad (40)$$

In this case, the controller reduces the cathode inlet pressure (Figure 11a) to reduce the work done by the compressor and thus reducing the effort to provide a certain air-flow needed to get the desired power and keeping the other safety requirements fulfilled. This simulation experiment was conducted to highlight the importance of including the compressor's safe operating strategy into the controller. In the case of the operation shown with the green lines, the compressor would not properly work.

4.2. Benefits and Possible Applications of RG-MPC

The RG-MPC could be used in two different ways. The first one is by replacing the "Setpoint calculation" box in Figure 3 with the RG-MPC. This effectively means that during operation, the RG-MPC provides optimal reference trajectories for the lower-level controllers and tuning, further, the addition of new criteria can be done intuitively as is the case regularly with MPC based controllers.

The second way the RG-MPC could be used is more plausible with the gap between the concept and actual implementation being much smaller than in the first case. In essence, the RG-MPC would be used as an offline optimization map generator. A series of different values of the power demand would be given to the RG-MPC to drive the system to and the controller would optimize all the other values (pressures, current, etc.) based on the criteria given in the cost function. The number of experiments that would have to be run to calibrate the system would be smaller, gaining a financial advantage. Next, the actuator

constraints and the decoupling of all the variables would already be implicitly contained in the RG-MPC. In the case of a change in the system, instead of recalibrating the setpoint calculation algorithm, the model is simply updated. For example, in the case of a new compressor, its new efficiency and other characteristics are passed to the prediction model and the generation of the setpoints for a certain power demand is easily recalculated. The mentioned benefits are systematically shown in Figure 12.

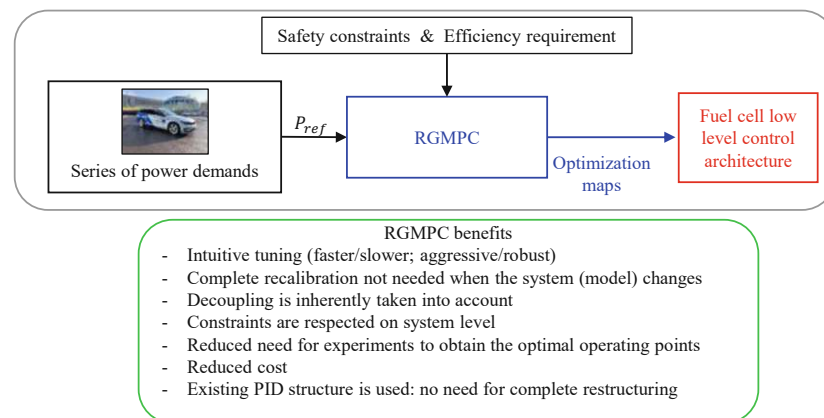


Figure 12. Advantages of using the RG-MPC as a tool for generating optimization maps. PID—proportional-integral-derivative.

5. Conclusions

In this paper, we proposed using the reference governor model predictive controller approach for controlling fuel cell systems, especially vehicles. Instead of acquiring the optimal operational setpoints and/or trajectories by numerous experimental runs, a more intuitive approach would be of benefit, such as the MPC concept. Every safety and efficiency requirement can easily be made part of the optimization criterion used by the controller. In case a system component is added, removed, or its properties changed, the model can simply be updated and the RG-MPC tuning redone in minimal time. In contrast, in the conventional way, numerous time- and money-consuming experiments have to be run. Since there are various complex effects present in fuel cells such as the fact that there is a gas mixture in the channels, electrochemical processes, or compressor dynamics, the model describing the system is unsurprisingly nonlinear. In this work, the authors resorted to the commonly known successive linearization technique to overcome this challenge. To illustrate the performance of the controller, a real vehicle power demand has been used as reference. In addition, safety constraints such as starvation prevention or pressure difference limits have been imposed to the controller, showing its capability of dealing with multiobjective problems. The reference values for the PI controllers produced by the RG-MPC were inherently optimized in such a way that no decoupling or antiwindup schemes were necessary. The main benefit of the RG-MPC concept lies in the fact that it is simply an upgrade and not a replacement to an existing PI controller setup, bringing the concept closer to actual industrial application. The way in which the RG-MPC would be implemented in real life is an open question. We propose two main ways. First, it can be used online to generate the optimal references for the underlying PI controllers during operation. The second way would be to use the RG-MPC to generate trajectories or setpoints for the system before operation and store those results in a form of optimization maps, which would then be called back during operation. The approach described in this paper is not system- or model-dependent and can be a way of optimizing the operation of any system, not just fuel cells. Hopefully, the research done here provides some direction in improving fuel cell control algorithms and reducing the cost barrier that hydrogen power vehicles have in reaching the end user.

Author Contributions: M.V., D.R., and S.J. developed the concept and methodology. M.V. and D.R. developed the software and conducted the analysis. M.V. performed the data curation and visualization. M.V. wrote the original draft. D.R. and S.J. edited and reviewed the original draft. S.J. supervised the work and did all the project administration. All authors have read and agreed to the published version of the manuscript.

Funding: This research was funded by the Austrian Research Promotion Agency (Österreichische Forschungsförderungsgesellschaft) grant number 865181. The APC was funded by TU Wien Bibliothek.

Institutional Review Board Statement: Not applicable.

Informed Consent Statement: Not applicable.

Acknowledgments: The authors would like to thank all the experts from AVL List GmbH for providing the data of the vehicle drive cycle and the insights which helped to solve many research problems. Many thanks to the reviewers for their constructive comments, which have improved this paper. The authors acknowledge TU Wien Bibliothek for financial support through its Open Access Funding Program.

Conflicts of Interest: The authors declare no conflict of interest.

Abbreviations

The following abbreviations are used in this manuscript:

FC	Fuel cell
PEM	Polymer electrolyte membrane
MPC	Model predictive controller
RG-MPC	Reference governor model predictive controller
PI	Proportional-integral
PID	Proportional-integral-derivative

References

- Liang, M.; Liu, Y.; Xiao, B.; Yang, S.; Wang, Z.; Han, H. An analytical model for the transverse permeability of gas diffusion layer with electrical double layer effects in proton exchange membrane fuel cells. *Int. J. Hydrogen Energy* **2018**, *43*, 17880–17888. [\[CrossRef\]](#)
- Liang, M.; Fu, C.; Xiao, B.; Luo, L.; Wang, Z. A fractal study for the effective electrolyte diffusion through charged porous media. *Int. J. Heat Mass Transf.* **2019**, *137*, 365–371. [\[CrossRef\]](#)
- Daud, W.R.; Rosli, R.E.; Majlan, E.H.; Hamid, S.A.; Mohamed, R.; Husaini, T. PEM fuel cell system control: A review. *Renew. Energy* **2017**, *113*, 620–638. [\[CrossRef\]](#)
- Woo, C.H.; Benziger, J.B. PEM fuel cell current regulation by fuel feed control. *Chem. Eng. Sci.* **2007**, *62*, 957–968. [\[CrossRef\]](#)
- Iqbal, M.T. Modeling and control of a wind fuel cell hybrid energy system. *Renew. Energy* **2003**, *28*, 223–237. [\[CrossRef\]](#)
- Garcia-Gabin, W.; Dorado, F.; Bordons, C. Real-time implementation of a sliding mode controller for air supply on a PEM fuel cell. *J. Process Control* **2010**, *20*, 325–336. [\[CrossRef\]](#)
- Dalvi, A.; Guay, M. Control and real-time optimization of an automotive hybrid fuel cell power system. *Control Eng. Pract.* **2009**, *17*, 924–938. [\[CrossRef\]](#)
- Zhang, J.; Liu, G.; Yu, W.; Ouyang, M. Adaptive control of the airflow of a PEM fuel cell system. *J. Power Sources* **2008**, *179*, 649–659. [\[CrossRef\]](#)
- Almeida, P.E.; Simões, M.G. Neural optimal control of PEM fuel cells with parametric CMAC networks. *IEEE Trans. Ind. Appl.* **2005**, *41*, 237–245. [\[CrossRef\]](#)
- Hatti, M.; Tioursi, M. Dynamic neural network controller model of PEM fuel cell system. *Int. J. Hydrogen Energy* **2009**, *34*, 5015–5021. [\[CrossRef\]](#)
- Vahidi, A.; Stefanopoulou, A.; Peng, H. Current management in a hybrid fuel cell power system: A model-predictive control approach. *IEEE Trans. Control Syst. Technol.* **2006**, *14*, 1047–1057. [\[CrossRef\]](#)
- Vahidi, A.; Greenwell, W. A decentralized model predictive control approach to power management of a fuel cell-ultracapacitor hybrid. In Proceedings of the American Control Conference, New York, NY, USA, 9–13 July 2007; pp. 5431–5437. [\[CrossRef\]](#)
- Luna, J.; Jemei, S.; Yousfi-Steiner, N.; Husar, A.; Serra, M.; Hissel, D. Nonlinear predictive control for durability enhancement and efficiency improvement in a fuel cell power system. *J. Power Sources* **2016**, *328*, 250–261. [\[CrossRef\]](#)
- Danzer, M.A.; Wittmann, S.J.; Hofer, E.P. Prevention of fuel cell starvation by model predictive control of pressure, excess ratio, and current. *J. Power Sources* **2009**, *190*, 86–91. [\[CrossRef\]](#)
- Hähnel, C.; Aul, V.; Horn, J. Power Control for Efficient Operation of a PEM Fuel Cell System by Nonlinear Model Predictive Control. *IFAC-PapersOnLine* **2015**, *48*, 174–179. [\[CrossRef\]](#)

16. Ebadighajari, A.; Homayouni, H.; Devaal, J.; Golnaraghi, F. Model Predictive Control of Polymer Electrolyte Membrane fuel cell with dead-end anode and periodic purging. In Proceedings of the 2016 IEEE Conference on Control Applications, CCA, Buenos Aires, Argentina, 19–22 September 2016; pp. 1500–1505. [\[CrossRef\]](#)
17. Ziogou, C.; Pistikopoulos, E.N.; Georgiadis, M.C.; Voutetakis, S.; Papadopoulou, S. Empowering the performance of advanced NMPC by multiparametric programming—An application to a PEM fuel cell system. *Ind. Eng. Chem. Res.* **2013**, *52*, 4863–4873. [\[CrossRef\]](#)
18. Ziogou, C.; Papadopoulou, S.; Georgiadis, M.C.; Voutetakis, S. On-line nonlinear model predictive control of a PEM fuel cell system. *J. Process Control* **2013**, *23*, 483–492. [\[CrossRef\]](#)
19. Goshtasbi, A.; Ersal, T. Degradation-conscious control for enhanced lifetime of automotive polymer electrolyte membrane fuel cells. *J. Power Sources* **2020**, *457*, 227996. [\[CrossRef\]](#)
20. Chen, H.; Chen, J.; Lu, H.; Yan, C.; Liu, Z. A Modified MPC-Based Optimal Strategy of Power Management for Fuel Cell Hybrid Vehicles. *IEEE/ASME Trans. Mechatron.* **2020**, *25*, 2009–2018. [\[CrossRef\]](#)
21. Klaučo, M.; Kalúz, M.; Kvasnica, M. Real-time implementation of an explicit MPC-based reference governor for control of a magnetic levitation system. *Control Eng. Pract.* **2017**, *60*, 99–105. [\[CrossRef\]](#)
22. Klaučo, M.; Kvasnica, M. Control of a boiler-turbine unit using MPC-based reference governors. *Appl. Therm. Eng.* **2017**, *110*, 1437–1447. [\[CrossRef\]](#)
23. Garone, E.; Di Cairano, S.; Kolmanovsky, I. Reference and command governors for systems with constraints: A survey on theory and applications. *Automatica* **2017**, *75*, 306–328. [\[CrossRef\]](#)
24. Klaučo, M.; Kvasnica, M. *MPC-Based Reference Governors*; Springer: Cham, Switzerland, 2019.
25. Zhakatayev, A.; Rakhim, B.; Adiyatov, O.; Baimyshev, A.; Varol, H.A. Successive linearization based model predictive control of variable stiffness actuated robots. In Proceedings of the IEEE/ASME International Conference on Advanced Intelligent Mechatronics, AIM, Munich, Germany, 3–7 July 2017; pp. 1774–1779. [\[CrossRef\]](#)
26. Ławryńczuk, M. Nonlinear predictive control of a boiler-turbine unit: A state-space approach with successive on-line model linearisation and quadratic optimisation. *ISA Trans.* **2017**, *67*, 476–495. [\[CrossRef\]](#) [\[PubMed\]](#)
27. Goshtasbi, A.; Ersal, T. LQ-MPC design for degradation-conscious control of PEM fuel cells. In Proceedings of the American Control Conference, Philadelphia, PA, USA, 10–12 July 2019; pp. 1555–1560. [\[CrossRef\]](#)
28. Bamimore, A.; Taiwo, O.; King, R. Comparison of two nonlinear model predictive control methods and implementation on a laboratory three tank system. In Proceedings of the IEEE Conference on Decision and Control, Orlando, FL, USA, 12–15 December 2011; pp. 5242–5247. [\[CrossRef\]](#)
29. Ritzberger, D.; Hametner, C.; Jakubek, S. A real-time dynamic fuel cell system simulation for model-based diagnostics and control: Validation on real driving data. *Energies* **2020**, *13*, 3148. [\[CrossRef\]](#)
30. Vrlc, M.; Ritzberger, D.; Jakubek, S. Fuel Cell Control Using Successive Linearization Vehicle Data. *Energies* **2020**, *13*, 5353. [\[CrossRef\]](#)
31. Böhler, L.; Ritzberger, D.; Hametner, C.; Jakubek, S. Constrained Extended Kalman Filter Design and Application for On-Line State Estimation of High-Order Polymer Electrolyte Membrane Fuel Cell Systems. *Int. J. Hydrogen Energy* **2021**. [\[CrossRef\]](#)
32. KEYTECH4EV—Development and Demonstration of Key Technologies for Low-cost Electric Vehicle Platforms. Available online: <http://iesta.at/keytech4ev/> (accessed on 1 February 2021).
33. Kravos, A.; Ritzberger, D.; Tavčar, G.; Hametner, C.; Jakubek, S.; Katrašnik, T. Thermodynamically consistent reduced dimensionality electrochemical model for proton exchange membrane fuel cell performance modelling and control. *J. Power Sources* **2020**, *454*, 227930. [\[CrossRef\]](#)
34. Pukrushpan, T.; Peng, H. Dynamics of Low-Pressure and High-pressure Fuel Cell Air Supply Systems. In Proceedings of the 2003 American Control Conference, Denver, CO, USA, 4–6 June 2003; pp. 2049–2054.

2.3 Publication C

M. Vrlić, D. Pernsteiner, A. Schirrer, C. Hametner, and S. Jakubek. “Reduced-dimensionality nonlinear distributed-parameter observer for fuel cell systems”. In: *Energy Reports* 10 (2023), pp. 1–14. DOI: 10.1016/j.egyr.2023.06.006. URL: <https://doi.org/10.1016/j.egyr.2023.06.006>

Applicant’s Contribution [†]

- Martin Vrlić: Conceptualization, Methodology, Investigation, Software, Visualization, Writing - Original Draft
- Dominik Pernsteiner: Conceptualization, Methodology, Investigation, Software, Visualization, Writing - Original Draft
- Alexander Schirrer: Conceptualization, Methodology, Writing - Review & Editing, Supervision
- Christoph Hametner: Conceptualization, Methodology, Writing - Review & Editing, Supervision, Project administration, Funding acquisition
- Stefan Jakubek: Conceptualization, Methodology, Writing - Review & Editing, Supervision, Project administration, Funding acquisition

[†]According to the Elsevier CRediT author statement: <https://www.elsevier.com/authors/policies-and-guidelines/credit-author-statement>



Contents lists available at ScienceDirect

Energy Reports

journal homepage: www.elsevier.com/locate/egyr

Research paper

Reduced-dimensionality nonlinear distributed-parameter observer for fuel cell systems

Martin Vrlić^{a,*}, Dominik Pernsteiner^{a,b}, Alexander Schirrer^a, Christoph Hametner^{a,b}, Stefan Jakubek^a^a Institute of Mechanics and Mechatronics, TU Wien, Austria^b CD Laboratory for Innovative Control and Monitoring of Automotive Powertrain Systems, TU Wien, Austria

ARTICLE INFO

Article history:

Received 29 January 2023

Received in revised form 31 May 2023

Accepted 2 June 2023

Available online xxxx

Keywords:

Fuel cell

Balanced truncation

Distributed state estimation

Extended kalman filter

ABSTRACT

To ensure reliable and efficient operation of fuel cell systems, it is important to monitor them online. However, placing sensors inside the fuel cell is often challenging, so virtual sensing using an efficient state observer is used in this study. Detecting local internal phenomena, such as reactants' starvation, membrane dryout/flooding, and nitrogen accumulation, requires knowledge of the spatial distribution of internal states. Lumped-parameter models are not suitable for this, as they use a single variable to describe parameters such as hydrogen concentration. Instead, a high-order distributed-parameter fuel cell model is used to predict the spatial profiles of various internal states. An observer algorithm is employed to correct the predicted quantities using a few measurements taken at the system boundary. This update step only considers dominant dynamics from a reduced model to adjust all system states accordingly, making it computationally efficient and robust. The observer algorithm's performance was verified against a high-fidelity model through detailed simulations.

© 2023 The Author(s). Published by Elsevier Ltd. This is an open access article under the CC BY license (<http://creativecommons.org/licenses/by/4.0/>).

1. Introduction

The share of hydrogen in the overall energy sector is expected to increase due to the transition to renewable energy sources. Fuel cells play an important role in converting hydrogen back into power. The application of fuel cells is envisaged both in transport (cars, trucks, railways, and aviation) and in stationary systems (industry and buildings) (IEA, 2019, 2021).

Polymer electrolyte membrane fuel cells (PEMFC) are an attractive zero-emission power source due to their high efficiency and other benefits such as low operating temperature, and fast startup (İnci et al., 2021). Fuel cells in automotive applications are of particular interest, and their development is a challenging and wide research area. One of the major topics still not fully resolved and under investigation is onboard system monitoring and diagnostics of fuel cell electric vehicles (FCEV). Evidently, good system observation is crucial for safe and efficient operation under highly dynamic conditions which are usually present in FCEVs. Measurement signals commonly available on FCEVs such as system voltage, anode/cathode inlet/outlet pressures and humidity are of course necessary, but not sufficient to detect critical conditions that may occur inside the system during operation. Information about internal states such as species concentrations

in gas channels (GC) and gas diffusion layers (GDL), species densities and membrane water content, to name a few, gives more profound insight necessary for proper system monitoring and diagnostics. Methods for measuring the internal states of the system have been developed in the past. For example, neutron imaging and magnetic resonance imaging have been commonly used to measure water concentration inside a fuel cell (Wang et al., 2021; Lee et al., 2021). Furthermore, nitrogen and oxygen concentrations have been measured using gas chromatography analysis (Dobrokhotoev and Larin, 2019). Temperature at certain points inside the cell has been determined using distributed fibre optic sensors (Zaghloul et al., 2021). However, measuring devices for such quantities are expensive, relatively big, hard to implement even under laboratory conditions, and outright impossible in vehicles. These methods have been summarised in Table 1.

A promising alternative, which is explored in this paper, is virtual sensing using a state observer. The state observer uses a model and uses available measurement signals to estimate the internal states of the system. An observer generally works as follows: a model is used to predict the same signals that are being measured by the available sensors, called outputs. In doing so, the internal states are estimated. The states are controlled using an algorithm to match the measured outputs. When the outputs are matched and if the system is observable, the internal states of the model match the unmeasurable reality. It is to be noted that for this to hold, the plant-model mismatch must be minimal.

* Corresponding author.

E-mail address: martin.vrlic@tuwien.ac.at (M. Vrlić).<https://doi.org/10.1016/j.egyr.2023.06.006>2352-4847/© 2023 The Author(s). Published by Elsevier Ltd. This is an open access article under the CC BY license (<http://creativecommons.org/licenses/by/4.0/>).

Nomenclature**State variables of the fuel cell quasi-2D model**

γ_{H_2}	Hydrogen mole fraction
γ_{N_2}	Nitrogen mole fraction
γ_{O_2}	Oxygen mole fraction
λ	Membrane water content
ρ	Gas density
ξ_{H_2}	Hydrogen mass fraction
ξ_{N_2}	Nitrogen mass fraction
ξ_{O_2}	Oxygen mass fraction
i	Local current density
p	Gas pressure
V	Cell voltage
v	Gas velocity

Number of discretisation nodes

N_{ca}	Number of discretisation nodes in the anode channel
N_{ca}	Number of slices
N_{cc}	Number of discretisation nodes in the cathode channel
N_{ga}	Number of discretisation nodes in the anode gas diffusion layer
N_{gc}	Number of discretisation nodes in the cathode gas diffusion layer
N_{mem}	Number of discretisation nodes in the membrane

State space model

\mathbf{x}	State vector of the whole system
\mathbf{x}_{ca}	State vector of the anode channel
\mathbf{x}_{cc}	State vector of the cathode channel
\mathbf{x}_{ga}	State vector of the anode gas diffusion layer
\mathbf{x}_{gc}	State vector of the cathode gas diffusion layer
\mathbf{x}_{mem}	State vector of the membrane
\mathbf{A}	System matrix
\mathbf{b}	Right-hand side vector
\mathbf{u}	Input vector
\mathbf{x}	State vector of the whole system including past states
\mathbf{y}	Output vector
k	Current time step

Observer

$\tilde{\mathbf{Q}}$	Reduced order process noise covariance
\mathbf{Q}	Process noise covariance
\mathbf{R}	Measurement noise covariance
$\Delta\hat{\mathbf{x}}$	State correction
$\hat{\mathbf{x}}^-$	Predicted state vector
$\hat{\mathbf{y}}^-$	Predicted output vector
\mathcal{T}	Transformation matrix from full state-space to reduced state-space
\mathbf{y}_{meas}	Measurement vector
$\hat{\mathbf{A}}_r$	Reduced order Jacobian matrix
$\hat{\mathbf{C}}_r$	Reduced order output matrix
\mathbf{K}	Kalman gain

$\tilde{\mathbf{P}}$	Updated error covariance matrix
$\hat{\mathbf{P}}^-$	Predicted error covariance matrix
$\hat{\mathbf{S}}$	Innovation covariance

Balanced truncation

\mathbf{x}_s	Scaled state vector
$\tilde{\mathbf{T}}$	Transformation matrix from physical state-space to balanced realisation
$\tilde{\mathbf{x}}$	State vector in the balanced realisation
\tilde{n}_r	Number of modes
$\tilde{\mathbf{x}}_e$	Eliminated states
$\tilde{\mathbf{x}}_r$	State vector in the reduced state-space
n_x	Number of states

Therefore, before the model can be used as a state observer, it must first be validated. In this work, however, as it is explained later on, the simulated reality and the model used as basis for the observer have the same underlying structure, but different number of discretisation points. For that reason, the validation of the model used by the observer is considered to be fulfilled.

Fuel cell models which are appropriate for observer design can be categorised on the basis of their underlying system dynamics (Hidayat et al., 2011) into:

- Lumped-parameter models, whose dynamics are described by ordinary differential equations.
- Distributed-parameter models, whose dynamics are described by partial differential equations.

The vast majority of fuel cell system observers were developed with lumped-parameter models with aggregated states. However, pressure, gas concentration etc. are non-uniformly distributed inside the cell. Distributed-parameter models are, therefore, necessary to describe along-the-channel effects and local phenomena.

Literature on observers for distributed states in fuel cells is scarce, as evident from a recent review on the topic of fuel cell observers (Yuan et al., 2020). A simplified, 10-element model for observing the water distribution profile is reported in Sarmiento-Carnevali et al. (2017). However, the focus of that paper is developing the controller. Concerning publications with a detailed description of the observer development, to the best of our knowledge, only Luna et al. tackled this topic in their work (Luna et al., 2015, 2016b,a, 2017). Their fuel cell observer employs a finite volume model and is based on assumed measurements of species concentration at the system boundary. In their paper, they only show the time-evolution of the species at the middle point of the channels.

In their work they use a sliding mode observer, a discontinuous type of observer that uses some input variable as corrective action. This input variable does not have a clear meaning and it is not seen in the results section of the paper, making it difficult to grasp the overall result. The complexity of an observer, such as the one proposed by Luna et al. naturally increases with the number of discretisation volumes (system resolution). This problem is resolved in the present work by using dominant-modes-only Jacobians for the update step of the observer (explained later on), resulting in an efficient observer algorithm. The observer is based on easily attainable measurements at the system boundary such as the cell voltage as a measured output and other commonly known quantities, namely the inlet/outlet pressures, the inlet gas composition, and the current density demand as boundary conditions. The actual distribution of the internal states of the system is presented in the figures in Section 6. The time evolution

Table 1
Measurement techniques for fuel cell internal states.

Ref	Measurement	Method
Wang et al. (2021), Lee et al. (2021)	Water concentration	Neutron imaging, magnetic resonance
Dobrokhotoy and Larin (2019)	N ₂ and O ₂ concentrations	Gas chromatography
Zaghoul et al. (2021)	Local temperature	Distributed fibre optic sensors

Table 2
Existing observers for estimation of the internal states of fuel cell systems.

Ref	Observer type	Model type	Performance object(s)
Yuan et al. (2020) (Review paper)	Extended Kalman filter	Single phase, 8th order, lumped	Oxygen partial pressure
	Unscented Kalman filter	Single phase, 4th order, lumped	Nitrogen partial pressure at anode
	Luenberger	Two-phase, 6th order, lumped	Current density difference
	First-order sliding mode	Single phase, 6th order, lumped	Manifold pressure and mass flow
	High order sliding mode	Two-phase, 13th order, lumped	Hydrogen and oxygen partial pressures
Luna et al. (2015, 2016b,a, 2017)	High order sliding mode	Single phase, distributed	Hydrogen and oxygen partial pressures along the channel

Table 3
Reduction techniques for Extended Kalman Filters with high-order models as its basis.

Ref	Observer purpose	Reduction approach
Farrell and Ioannou (2001)	Storm track forecasting	Balanced truncation
Khodadadi and Jazayeri-Rad (2011)	Joint state and parameter estimation of a continuous stirred tank reactor	Dual EKF
Lee et al. (2007)	Li-ion battery SOC estimation	Equivalent circuit model simplification
Park et al. (2013)	Estimation of internal states of permanent magnet synchronous motors	Parallel structure of simplified models
Pernsteiner et al. (2021)	Temperature estimation of a latent heat storage	Balanced truncation

of the whole distribution is shown in the videos found in the supplementary material. In the present paper, a detailed quasi-2D fuel cell model from Murschenhofer et al. (2018) is used as the basis for a newly developed distributed-parameter fuel cell observer. The representative observer types have been collected in Table 2.

The observer algorithm chosen in this work is based on the well-known extended Kalman filter (EKF) (Jazwinski, 1970; Wishner et al., 1969).

When applying an EKF to high-order models, such as the discretised quasi-2D fuel cell model, two major problems can arise: (1) the problem becomes infeasible to be solved in real time due to its computational complexity, and (2) the system becomes (almost) unobservable when the entire state dimension is considered. To overcome these challenges, different types of reduced-order EKFs have been investigated, see for example Farrell and Ioannou (2001), Khodadadi and Jazayeri-Rad (2011), Lee et al. (2007), Park et al. (2013), Pernsteiner et al. (2021). Model reduction methods in observer design can be used to compute reduced-order system Jacobians necessary for the update step in the EKF, explained in Section 4. In Table 3, different methods of dealing with the problem of high-dimensionality are shown.

Model reduction approaches are applied to efficiently reduce the system dynamics' complexity while maintaining their dominant behaviour. Especially model reduction in linear systems is well established, and the research topic has been broadly covered in literature, see for example the review paper (Benner et al., 2015). An example for linear model reduction is the balanced truncation introduced by Moore (1981) where the modes of the system showing the smallest Hankel singular values are eliminated. For nonlinear systems, data-based approaches such as the proper orthogonal decomposition (Brunton and Kutz, 2019) or the dynamic mode decomposition (Schmid, 2010) can be an appropriate choice. The main idea behind these approaches is the empirical investigation of data representative for a relevant operating range. The data are decomposed into orthonormal basis

vectors using singular value decomposition (SVD). Few basis vectors that describe the most characteristic system behaviour can be extracted, and the system properties can be projected onto these so-called *modes*.

In this work, the model reduction technique applied to obtain the reduced-order system Jacobians is Balanced truncation. Only the most dominant modes, whose Hankel singular values exceed a defined threshold, are chosen to be reflected in the Jacobians, the others are discarded. Particularly, the system is being successively linearised, ensuring the validity of the Jacobian matrix used in the observer. A simulation study is performed to test the aforementioned approach. Measurements are taken at the system boundary with the goal of estimating the unmeasurable internal states. The full order quasi-2D model is used for prediction and validation, but these two versions of the model differ in grid sizes. Despite this model mismatch, the observer algorithm works well. For the update step of the EKF, the reduced order system Jacobians are used. The described procedure is depicted in Fig. 1. All details and results are discussed in Section 6. The identified research gap is to detect the distributed internal states of a fuel cell in an efficient way with realistic measurements. The fuel cell observer proposed for this purpose, which is based on a high-fidelity model with distributed parameters and a dominant-modes-only correction, has not yet been reported in the fuel cell community. In particular, the temporal evolution of the internal states' spatial distribution is shown, highlighting the extent of such an observer's capabilities.

In summary, this paper shows an internal state estimation framework using an on-board commonly available measurement signal, i.e. system voltage. Moreover, the estimated states are not lumped as in the majority of the literature, but their distribution is shown. In literature (Luna et al., 2015), crucial simplifying assumptions were made which were not made in this paper. These include: no nitrogen crossover, availability of outlet concentrations measurements and assuming the fluxes between the cathode channel and gas diffusion layer to be known.

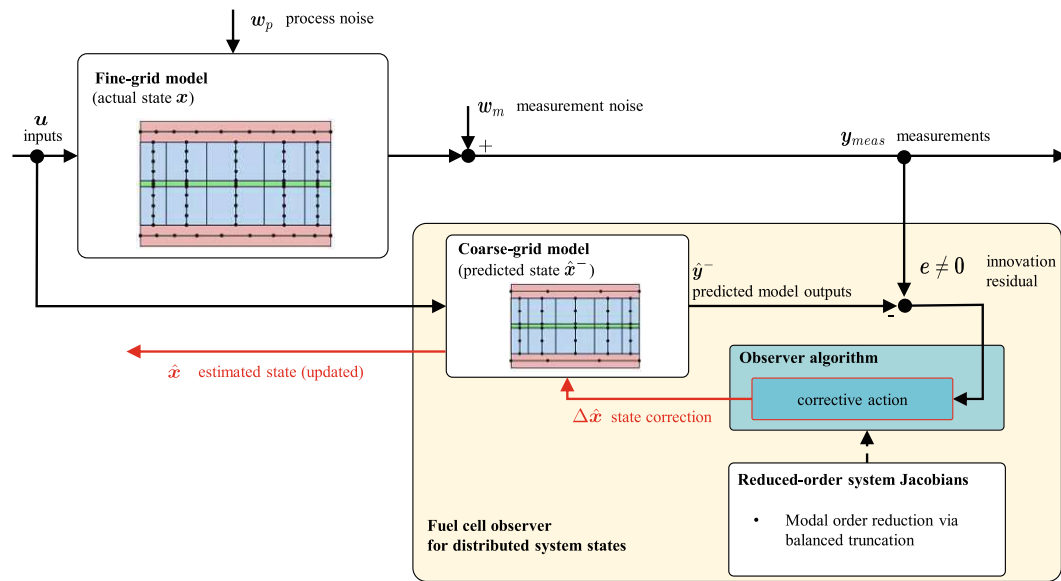


Fig. 1. Scheme of the fuel cell observer for estimating the distributed system state.

The paper is organised as follows. In Section 2 the observation task is explained in more detail, in Section 3 the quasi-2D model is presented, in Section 4 the observer algorithm and model reduction technique are shown, in Section 5 the case study simulation experiment is explained, in Section 6 the results are shown and discussed and the reader is referred to the videos in the supplementary material, and the paper is finally concluded in Section 7.

2. Observation task

The observation task is to estimate the unmeasurable internal states of the system by means of a model, available measurement signals and an appropriate algorithm. The mentioned internal states include: local current density, membrane water content and species concentrations. The model used in this paper is a straight channel isothermal distributed parameter fuel cell model, developed and validated against detailed Computational Fluid Dynamics (CFD) simulations in Murschenhofer et al. (2018). The model overview is given in Section 3. It is important to emphasise that the methodology used in this paper can be applied to practically any type of high-dimensional distributed model, not only to the one used in this work.

The premise is as follows. A fine-grid version of the model is used as simulated reality, against which the observer will be validated. This is necessary as in reality, the validation of an observer can never fully be done as it is not possible to measure the internal states. The fine-grid model provides the measured output signal, in this case, the voltage only. Of course, the input boundary conditions are also known. These include the inlet/outlet pressures, the inlet gas composition, and the current density demand. There is no assumption, however, about the availability of the species concentrations at the system outlet.

Next, a coarse-grid version of the model is used by the observer for the prediction of the internal states. The reason for using a different granularity for the simulated reality and the observer's prediction model is to take into account the plant-model mismatch which is generally always present.

The observer takes in the measured voltage from the simulated reality fine-grid model and at the same time, predicts the

voltage using the coarse-grid model. The difference between the two signals, called *innovation residual* is to be minimised. This is done by correcting the internal states of the system. Once that has been achieved, if the system is observable, one can conclude that the internal states computed by the coarse-grid model match reality provided that the model has been validated beforehand so the plant-model mismatch is minimal.

However, a problem arises for a system with many (several hundred or more) states, such as in this case. It is not plausible that all states can freely be corrected for the observer to match the measured voltage. For example, the pressure distribution along the channel should not be in a zig-zag shape just because the observer “thinks” that would be best for minimising the innovation residual. In addition, tuning the observer, i.e. choosing how strongly should each state be available for correction, might become an impossible task for systems with this many states.

It is not plausible that all individual internal states are observable with the available information. For that reason, a model reduction is performed, to detect only the dominant dynamics. Only a few principal *modes* of the system are extracted (see Section 4.2) and the observer makes its correction in the direction of the modes. As a result, the possibly disproportional update of each individual node is avoided. The whole idea described above is visualised in Fig. 1.

In this work, only the voltage is assumed to be a measured output. No additional assumptions of measurements available are made, such as the species concentrations at the system boundaries. The whole procedure results in the estimation of the distribution of internal states of the system.

3. Fuel cell quasi-2D model

This section describes the distributed parameter fuel cell model (Murschenhofer et al., 2018) used as basis for the observer as well as the validation model. The model domain (see Fig. 2) consists of five sections:

1. Cathode gas channel
2. Cathode gas diffusion layer
3. Membrane

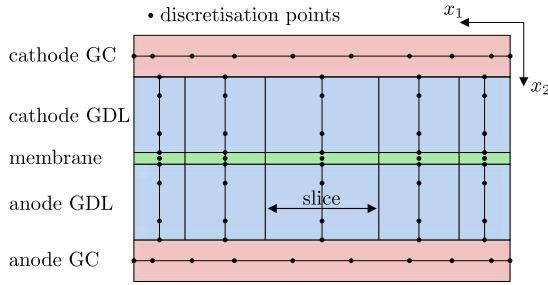


Fig. 2. Spatial discretisation of the quasi-2D fuel cell model.

4. Anode gas diffusion layer
5. Anode gas channel

Every section is coupled via the system equations and appropriate boundary conditions. For modelling details the reader is referred to Murschenhofer et al. (2018). The model is spatially discretised in direction x_1 along-the-channel, and in direction x_2 across the GDL. Therefore, the model is classified as a quasi-2D model.

Some important assumptions are made in the model. First, the model is considered to be isothermal, meaning that the temperature is assumed to be controlled and kept at a constant value of 70 °C. Second, the model does not include liquid water states, but regardless of this fact, membrane dryout/flooding could be avoided if constraints on the membrane water content would be imposed in some control application. Therefore, the information on the membrane water content can be sufficient for practical applications, even if there is no liquid water present in the model.

3.1. Gas channels

Each node in the gas channels is described with the following state variables: gas velocity v , oxygen mass fraction ξ_{O_2} (cathode only), hydrogen mass fraction ξ_{H_2} (anode only), nitrogen mass fraction ξ_{N_2} , water vapour mass fraction ξ_{H_2O} , gas pressure p and gas density ρ . If the number of nodes in the cathode and anode gas channel is N_{cc} and N_{ca} , respectively, then the corresponding state vectors χ_{cc} and χ_{ca} are defined as

$$\chi_{cc} = \begin{bmatrix} v_1 \\ \vdots \\ v_{N_{cc}} \\ \xi_{O_2,1} \\ \vdots \\ \xi_{O_2,N_{cc}} \\ \xi_{N_2,1} \\ \vdots \\ \xi_{N_2,N_{cc}} \\ \xi_{H_2O,1} \\ \vdots \\ \xi_{H_2O,N_{cc}} \\ p_1 \\ \vdots \\ p_{N_{cc}} \\ \rho_1 \\ \vdots \\ \rho_{N_{cc}} \end{bmatrix} \quad \text{and} \quad \chi_{ca} = \begin{bmatrix} v_1 \\ \vdots \\ v_{N_{ca}} \\ \xi_{H_2,1} \\ \vdots \\ \xi_{H_2,N_{ca}} \\ \xi_{N_2,1} \\ \vdots \\ \xi_{N_2,N_{ca}} \\ \xi_{H_2O,1} \\ \vdots \\ \xi_{H_2O,N_{ca}} \\ p_1 \\ \vdots \\ p_{N_{ca}} \\ \rho_1 \\ \vdots \\ \rho_{N_{ca}} \end{bmatrix}. \quad (1)$$

3.2. Gas diffusion layers

In the GDLs, the nodes are described with the same variables as in the gas channels. Every internal slice j is described with its own state vector. If the number of nodes in each slice is N_{gc} for the cathode GDL and N_{ga} for the anode GDL, then the cathode and anode GDL state vectors, $\chi_{gc,j}$ and $\chi_{ga,j}$, respectively, are defined analogously as in Eq. (1).

3.3. Membrane

The membrane is described simply by its membrane water content λ in all nodes for every slice. If the number of nodes in the membrane is N_{mem} , then the state vector $\chi_{mem,j}$ for each membrane slice j is defined as

$$\chi_{mem,j} = \begin{bmatrix} \lambda_1 \\ \vdots \\ \lambda_{N_{mem}} \end{bmatrix}_j. \quad (2)$$

3.4. Local current density and voltage

In addition to all the system variables mentioned until this point, there is the local current density i_j computed for every slice and the cell voltage V , described as an aggregated state.

3.5. State-space system

The full system state vector χ_k at timestep k is composed of the individual state vectors of the cathode and anode gas channels, N_{sl} slices and the cell voltage. The state vector of every slice is composed of the state vectors of the GDLs and membrane as well as the local current density. The complete system state vector is then

$$\chi_k = \begin{bmatrix} \chi_{cc} \\ \chi_{ca} \\ \chi_{gc,1} \\ \chi_{mem,1} \\ \chi_{ga,1} \\ i_1 \\ \vdots \\ \chi_{gc,N_{sl}} \\ \chi_{mem,N_{sl}} \\ \chi_{ga,N_{sl}} \\ i_{N_{sl}} \\ V \end{bmatrix}_k. \quad (3)$$

The model equations are linearised-in-time (LIT) at every time step.

The LIT technique is explained in detail in Murschenhofer et al. (2018), but for practical reasons, the keypoints of the method are outlined here. The process of discretising the underlying partial differential equations results in a large system of non-linear equations required to be solved each time step. To be computationally efficient, one cannot afford to treat the non-linear terms with numerically expensive iterations. For that reason, the system is successively linearised with respect to the previous time step and only one iteration is necessary to solve the system equations. As a result, the system evolution, i.e. the state vector at time step k , is computed as the solution of a linear system of equations

$$\mathcal{A}(\chi_{k-1}, \chi_{k-2}, \chi_{k-3}, \mathbf{u}_{k-1})\chi_k = \mathbf{b}(\chi_{k-1}, \chi_{k-2}, \chi_{k-3}, \mathbf{u}_{k-1}), \quad (4)$$

where \mathbf{u}_{k-1} is the system input defined as

$$\mathbf{u}_{k-1} = \begin{bmatrix} i_{avg}^{cc} \\ p_{in}^{cc} \\ p_{out}^{cc} \\ p_{in}^{ca} \\ p_{out}^{ca} \\ \xi_{O_2,in}^{cc} \\ \xi_{N_2,in}^{cc} \\ \xi_{H_2O,in}^{cc} \\ \xi_{H_2,in}^{ca} \\ \xi_{N_2,in}^{ca} \\ \xi_{H_2O,in}^{ca} \end{bmatrix}, \quad (5)$$

consisting of all the boundary conditions mentioned in Section 2. However, only the average current density is dynamically changed and all the other inputs are kept constant.

The sparsity pattern of matrix \mathcal{A} is seen in Fig. 3. The dependence of the matrix \mathcal{A} and vector \mathbf{b} on the state vector at times $k-1$, $k-2$ and $k-3$ comes from the necessity of computing the time derivatives for the LIT approach. For brevity, the matrices in Eq. (4) will be denoted as \mathcal{A}_k and \mathbf{b}_k . Taking into account the dependence of the system evolution on not only the current state, but also on the last and second last ones, all three time instances ($k-1$, $k-2$ and $k-3$) must be part of the finally complete state vector $\mathbf{x}_{k-1} = [\mathbf{x}_{k-1}^T \mathbf{x}_{k-2}^T \mathbf{x}_{k-3}^T]^T$. Thus, one obtains the state-space formulation of the system

$$\mathbf{x}_k = \begin{bmatrix} \mathbf{x}_k \\ \mathbf{x}_{k-1} \\ \mathbf{x}_{k-2} \end{bmatrix} = \begin{bmatrix} \mathcal{A}_k^{-1} \mathbf{b}_k \\ \mathbf{x}_{k-1} \\ \mathbf{x}_{k-2} \end{bmatrix}. \quad (6)$$

By defining

$$\mathbf{f}(\mathbf{x}_{k-1}, \mathbf{u}_{k-1}) \equiv \begin{bmatrix} \mathcal{A}_k^{-1} \mathbf{b}_k \\ \mathbf{x}_{k-1} \\ \mathbf{x}_{k-2} \end{bmatrix}, \quad (7)$$

Eq. (6) can be written as

$$\mathbf{x}_k = \mathbf{f}(\mathbf{x}_{k-1}, \mathbf{u}_{k-1}) \text{ with } \mathbf{x}_k \in \mathbb{R}^{n_x \times 1}. \quad (8)$$

The output equation is

$$\mathbf{y}_k = \mathbf{C} \mathbf{x}_k \text{ with } \mathbf{y}_k \in \mathbb{R}^{n_y \times 1}. \quad (9)$$

The entries in the output vector \mathbf{y}_k are the modelled sensor signals that can be measured and depend on the setup. In this particular case, $\mathbf{y}_k = V$, the cell voltage. More detail about the outputs used in this paper are presented in Section 6. Eqs. (8) and (9) describe a nonlinear discrete time state-space model.

3.6. Mole fraction calculation

In the fuel cell community, instead of using the mass fractions ξ , it is more common to represent the species concentrations in mole fractions γ . The oxygen mole fraction is

$$\gamma_{O_2} = \frac{1}{M_{O_2}} \frac{\xi_{O_2}}{\xi_{O_2} + \frac{\xi_{N_2}}{M_{N_2}} + \frac{\xi_{H_2O}}{M_{H_2O}}}, \quad (10)$$

where M is the molar mass of each gas. The expression for calculation of the mole fraction for gases other than oxygen is analogous to Eq. (10).

4. Methods

In this section, the observer design as well as the methods for obtaining the reduced-order system Jacobians are presented. All the equations are written in general form and are then applied

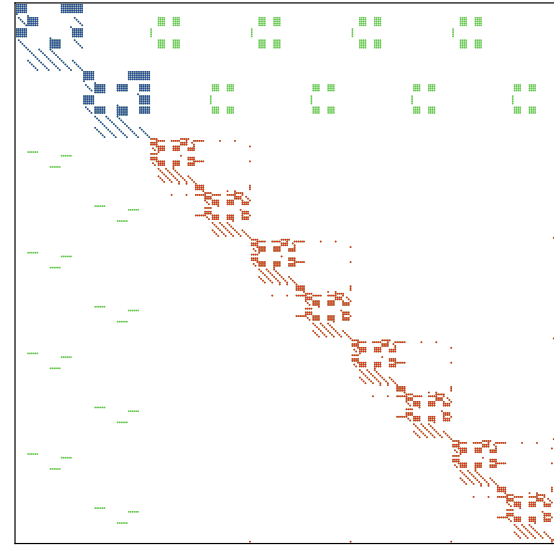


Fig. 3. Sparsity pattern of matrix \mathcal{A} showing the interdependency of the model domains. Every block on the diagonal represents the coupling of the states of one domain. Blue: cathode and anode gas channels; Red: internal slices, every slice is constituted of two GDLs and the membrane in between. The off-diagonal green entries represent the coupling between the slices and gas channels. (For interpretation of the references to colour in this figure legend, the reader is referred to the web version of this article.)

to the model described in the previous section. This shows the modularity of the algorithm, as it can be used with any high-order nonlinear state-space model. This reduced-dimensionality observer algorithm is visualised in Fig. 4.

4.1. Observer design

An efficient observer design is required to estimate the distributed internal fuel cell states in a robust fashion and in real time, see Fig. 1. In the observer design, the high-order quasi-2D fuel cell model (Section 3) predicts/simulates the distributed system states one time step ahead. Measurements are taken from the simulated reality and compared to the predicted model outputs. If a residual arises, the states of the quasi-2D fuel cell model are updated by an observer algorithm, in this work the proposed reduced-order EKF. The update is computed on the basis of system information given by the sensitivities of the states, the so-called Jacobians. To enhance efficiency, robustness, and convergence of the fuel cell observer algorithm, only the dominant system behaviour is to be considered in the update step.

To do so, the system is transformed from a state-space representation to a modal space (modes $\tilde{\mathbf{x}}$), and only the high-energy modes are retained, referred to as $\tilde{\mathbf{x}}_r$. The reduced-order system Jacobians that capture the main behaviour in modal space will be denoted as $\tilde{\mathbf{A}}_r$. The matrix $\tilde{\mathbf{C}}_r$ maps the dominant modes $\tilde{\mathbf{x}}_r$ to the model outputs.

In the following section, the formulation of the EKF from Simon (2006) is briefly recapitulated and applied to the present fuel cell problem. A special focus lies on the computation of the update step in modal space.

4.1.1. Background

The Kalman filter is an optimal estimator for linear systems with additive white Gaussian noise and minimises the mean

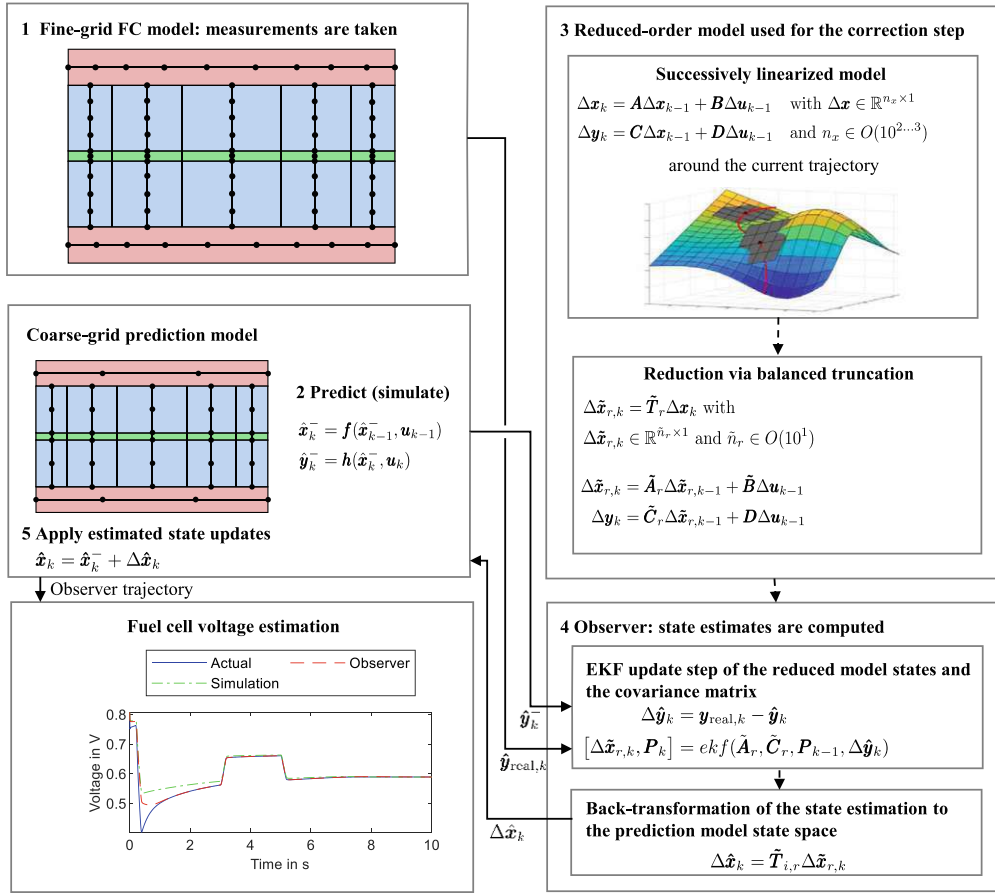


Fig. 4. Reduced-dimensionality observer algorithm.

square errors of the parameters to be estimated. The EKF is one nonlinear extension of it, but the optimality is no longer guaranteed. The discrete-time nonlinear model of the fuel cell (8)–(9) with process noise $\mathbf{w}_{p,k}$ and measurement noise $\mathbf{w}_{m,k}$ has the form

$$\mathbf{x}_k = \mathbf{f}(\mathbf{x}_{k-1}, \mathbf{u}_{k-1}) + \mathbf{w}_{p,k}, \quad (11)$$

$$\mathbf{y}_k = \mathbf{C}\mathbf{x}_k + \mathbf{w}_{m,k}. \quad (12)$$

It is assumed that the zero-mean, Gaussian uncorrelated and white noises,

$$\mathbf{w}_{p,k} \sim \mathcal{N}(\mathbf{0}, \mathbf{Q}) \quad \text{and} \quad \mathbf{w}_{m,k} \sim \mathcal{N}(\mathbf{0}, \mathbf{R}), \quad (13)$$

have the known covariance matrices \mathbf{Q} and \mathbf{R} , respectively.

The EKF for estimating the true system states consists of two steps, the prediction step and the update step. The idea of the EKF implementation in this work is to compute the prediction step using the coarse-grid model, and the update step in the modal space using the reduced order Jacobians ($\tilde{\mathbf{A}}_r$ and $\tilde{\mathbf{C}}_r$).

4.1.2. Prediction step

In the prediction step of the EKF, the predicted state vector, output vector and the error covariance matrix are determined a priori. The predicted state vector $\hat{\mathbf{x}}_k^-$ and the predicted output vector $\hat{\mathbf{y}}_k^-$ result from evolving the coarse-grid model (8)–(9). The predicted error covariance matrix

$$\tilde{\mathbf{P}}_k = \tilde{\mathbf{A}}_r \tilde{\mathbf{P}}_{k-1} \tilde{\mathbf{A}}_r^T + \tilde{\mathbf{Q}} \quad (14)$$

is obtained in the modal space with the corresponding covariance matrix $\tilde{\mathbf{Q}}$. The difference between the predicted output and the measurements \mathbf{y}_{meas} yields the innovation residual,

$$\mathbf{e}_k = \mathbf{y}_{\text{meas},k} - \hat{\mathbf{y}}_k^-, \quad (15)$$

and initiates the update step.

4.1.3. Update step

The update step of the EKF is carried out in the reduced modal space. The estimated (corrected) state vector and error covariance matrix are computed a posteriori based on the innovation residual.

First, the innovation covariance and the Kalman correction gain are determined,

$$\tilde{\mathbf{S}}_k = \tilde{\mathbf{C}}_r \tilde{\mathbf{P}}_k \tilde{\mathbf{C}}_r^T + \mathbf{R}, \quad (16)$$

$$\tilde{\mathbf{K}}_k = \tilde{\mathbf{P}}_k \tilde{\mathbf{C}}_r^T \tilde{\mathbf{S}}_k^{-1}, \quad (17)$$

respectively. Then, the state correction of the fuel cell model

$$\Delta \hat{\mathbf{x}}_k = \tau \tilde{\mathbf{K}}_k \mathbf{e}_k \quad (18)$$

is computed based on the corrective action given by $\tilde{\mathbf{K}}_k \mathbf{e}_k$ and the transformation from the reduced modal space to the original state-space of the fuel cell model τ .

The obtained state correction is applied to the states predicted by the quasi-2D fuel cell model, resulting in the updated

estimated state vector

$$\hat{\mathbf{x}}_k = \hat{\mathbf{x}}_k^- + \Delta \hat{\mathbf{x}}_k. \quad (19)$$

The estimation error covariance matrix is updated for the next time step,

$$\tilde{\mathbf{P}}_k = (\mathbf{I} - \tilde{\mathbf{K}}_k \tilde{\mathbf{C}}_r) \tilde{\mathbf{P}}_k^-, \quad (20)$$

wherein \mathbf{I} is the identity matrix of appropriate size.

The observer's corrective measures are based on the reduced-order system Jacobians (dominant modes only). The high accuracy of the estimated states is achieved through the interaction between the forward simulation of the quasi-2D fuel cell model and the careful measurement-based correction by the observer.

4.2. Reduced-order system Jacobians

The reduced-order system Jacobians capture the main behaviour of the quasi-2D fuel cell model and can be obtained in different ways, one of them being the balanced truncation, which is presented and used in this paper.

4.2.1. Balanced truncation: Background

The balanced truncation is an approach in which the least controllable and observable modes of the system are removed (truncated) and only the dominant behaviour is kept (Moore, 1981). First, the system represented with Eq. (8) is successively linearised around the current point $(\mathbf{x}_{wp}, u_{wp})$. Then, the linearised system is transformed to a balanced realisation, where the controllability and observability Gramians are equal and diagonal (Besselink et al., 2013). Since the diagonal entries of the Gramian reflect the controllability and observability of the modes, those modes with a small Gramian entry can be truncated. Finally, the truncation step is performed, yielding a reduced order model with the most observable modes only.

4.2.2. Successive linearisation and system scaling

The Extended Kalman Filter approach uses the Jacobians of the nonlinear system defined in Eq. (8). To have a valid correction algorithm in place at all times, the system is successively linearised along the state and input trajectory. The successively linearised model is of the form

$$\mathbf{x}_k = \mathbf{A}_{wp} \mathbf{x}_{k-1} + \mathbf{B}_{wp} u_{k-1} + \mathbf{K}_{x,wp}, \quad (21)$$

where

$$\mathbf{A}_{wp} = \left. \frac{\partial \mathbf{f}(\mathbf{x}_{k-1}, \mathbf{u}_{k-1})}{\partial \mathbf{x}} \right|_{\mathbf{x}_{wp}, \mathbf{u}_{wp}}, \quad (22)$$

$$\mathbf{B}_{wp} = \left. \frac{\partial \mathbf{f}(\mathbf{x}_{k-1}, \mathbf{u}_{k-1})}{\partial \mathbf{u}} \right|_{\mathbf{x}_{wp}, \mathbf{u}_{wp}}, \quad (23)$$

$$\mathbf{K}_{x,wp} = \mathbf{f}(\mathbf{x}_{wp}, \mathbf{u}_{wp}) - \mathbf{A}_{wp} \mathbf{x}_{wp} - \mathbf{B}_{wp} \mathbf{u}_{wp}. \quad (24)$$

In order to compute the Gramians and transform the system to its balanced realisation, it is necessary to prescale the system. The scaled state vector \mathbf{x}_s is then defined as $\mathbf{x}_s = \mathbf{X}_s^{-1} \mathbf{x}$, where \mathbf{X}_s is a diagonal square matrix. The same procedure is applied to the input and output vectors: $u_s = U_s^{-1} u$ and $\mathbf{y}_s = \mathbf{Y}_s^{-1} \mathbf{y}$, respectively.

The index “s” stands for “scaled”.

4.2.3. Balanced realisation

Using the scaled system, the balanced realisation can be computed. To cope with the off-equilibrium term $\mathbf{K}_{x,wp,s}$, it is lumped together with the input matrix in the following way,

$$\mathbf{x}_{s,k} = \mathbf{A}_{s,wp} \mathbf{x}_{s,k-1} + [\mathbf{B}_{s,wp} \quad \mathbf{K}_{x,wp,s}] \begin{bmatrix} u_{s,k-1} \\ 1 \end{bmatrix}, \quad (25)$$

formulating the system in a suitable way for the MATLAB command `balreal`, used to compute the balanced realisation.

The state transformation

$$\tilde{\mathbf{x}} = \tilde{\mathbf{T}} \mathbf{x}_s \quad (26)$$

is used to convert system (25) into its balanced realisation, in which the controllability and observability Gramians are equal and diagonal. In Eq. (26), $\tilde{\mathbf{x}} \in \mathbb{R}^{n_x \times 1}$ and $\tilde{\mathbf{T}} \in \mathbb{R}^{n_x \times n_x}$.

The balanced state vector $\tilde{\mathbf{x}}$ is partitioned into two parts: the one that is going to be retained $\tilde{\mathbf{x}}_r$ for the reduced-order system and the other, which is going to be eliminated $\tilde{\mathbf{x}}_e$,

$$\tilde{\mathbf{x}} = \begin{bmatrix} \tilde{\mathbf{x}}_r \\ \tilde{\mathbf{x}}_e \end{bmatrix}, \quad (27)$$

where $\tilde{\mathbf{x}}_r \in \mathbb{R}^{\tilde{n}_r \times 1}$ and $\tilde{\mathbf{x}}_e \in \mathbb{R}^{\tilde{n}_e \times 1}$, with $\tilde{n}_r + \tilde{n}_e = n_x$, the total number of states. The truncation value \tilde{n}_r is chosen upon analysing the Gramian of the system. Following this notation, the state transformation matrix $\tilde{\mathbf{T}}$ and its inverse $\tilde{\mathbf{T}}^{-1}$ are also partitioned into the part which maps the true states to the reduced order ones and the part which maps them to the eliminated ones. Inserting Eq. (27) into (26) and performing the partition of the transformation matrices, the direct mapping between the reduced and eliminated states, and the true states, is obtained,

$$\begin{bmatrix} \tilde{\mathbf{x}}_r \\ \tilde{\mathbf{x}}_e \end{bmatrix} = \begin{bmatrix} \tilde{\mathbf{T}}_r \\ \tilde{\mathbf{T}}_e \end{bmatrix} \mathbf{x}_s, \quad (28)$$

as well as its inverse

$$\mathbf{x}_s = \begin{bmatrix} \tilde{\mathbf{T}}_{i,r} & \tilde{\mathbf{T}}_{i,e} \end{bmatrix} \begin{bmatrix} \tilde{\mathbf{x}}_r \\ \tilde{\mathbf{x}}_e \end{bmatrix}, \quad (29)$$

where $\tilde{\mathbf{T}}_r \in \mathbb{R}^{\tilde{n}_r \times n_x}$, $\tilde{\mathbf{T}}_e \in \mathbb{R}^{\tilde{n}_e \times n_x}$, $\tilde{\mathbf{T}}_{i,r} \in \mathbb{R}^{n_x \times \tilde{n}_r}$ and $\tilde{\mathbf{T}}_{i,e} \in \mathbb{R}^{n_x \times \tilde{n}_e}$.

4.2.4. Truncation

Since they contribute much less to the system behaviour, the states $\tilde{\mathbf{x}}_e$ are simply deleted and the system is described with $\tilde{\mathbf{x}}_r$ only, yielding the following transformation for the reduced states,

$$\tilde{\mathbf{x}}_r = \tilde{\mathbf{T}}_r \mathbf{x}_s. \quad (30)$$

Inverting Eq. (30) and inserting it into Eq. (25) and then left multiplying the whole expression with $\tilde{\mathbf{T}}_r$, one obtains the reduced-order system

$$\tilde{\mathbf{x}}_{r,k} = \underbrace{\tilde{\mathbf{T}}_r \mathbf{A}_{s,wp} \tilde{\mathbf{T}}_{i,r}}_{\tilde{\mathbf{A}}_r} \tilde{\mathbf{x}}_{r,k-1} + \tilde{\mathbf{T}}_r [\mathbf{B}_{s,wp} \quad \mathbf{K}_{x,wp,s}] \begin{bmatrix} u_{s,k-1} \\ 1 \end{bmatrix}. \quad (31)$$

Finally, the Jacobian $\tilde{\mathbf{A}}_r = \tilde{\mathbf{T}}_r \mathbf{A}_{s,wp} \tilde{\mathbf{T}}_{i,r}$ is obtained, with $\tilde{\mathbf{A}}_r \in \mathbb{R}^{\tilde{n}_r \times \tilde{n}_r}$. Also, the new output equation is

$$\mathbf{y}_{s,k} = \tilde{\mathbf{C}}_r \tilde{\mathbf{x}}_{r,k} \text{ with } \tilde{\mathbf{C}}_r \in \mathbb{R}^{n_y \times \tilde{n}_r}, \quad (32)$$

where $\tilde{\mathbf{C}}_r = \mathbf{C}_{s,wp} \tilde{\mathbf{T}}_{i,r}$.

The Jacobian $\tilde{\mathbf{A}}_r$ is used in the update step of the EKF to correct the dominant modes. To obtain the correction in the original states, the modes are projected onto the states using the transformation matrix \mathcal{T} from Eq. (18). For the approach described above, \mathcal{T} is defined as:

$$\mathcal{T} = \mathbf{X}_s \tilde{\mathbf{T}}_{i,r}. \quad (33)$$

4.3. Observability analysis

The observability of the system is approached from two different angles. One is the observability of the modes and the other is the observability of the states. In Table 4, the different model sizes

Table 4
Different model sizes.

Model	N_{cc}	N_{gc}	N_{mem}	N_{ga}	N_{ca}	N_{sl}	$\Delta t/ms$
Fine	30	8	5	8	30	10	2
Coarse	6	4	5	4	6	4	6.25

of the fine-grid and coarse-grid model are shown. Using this data and the state vector structure from Eqs. (1)–(3), one can compute the total number of states n_x in each model:

$$n_x = 3(6N_{cc} + 6N_{sl}N_{gc} + N_{sl}N_{mem} + N_{sl} + 6N_{sl}N_{ga} + 6N_{ca} + 1). \quad (34)$$

The factor 3 comes from the fact that three time instances, $k-1$, $k-2$ and $k-3$ are included in the state vector for the LIT approach, as explained in Section 3. The number of states of the fine-grid model is 4143 and for the coarse-grid model the number of states is 867. However, observability is analysed only for the first third of the state vector and only for the coarse-grid model since the fine-grid model serves the role of simulated reality. Therefore, there are 289 states in the first third of the state vector of the coarse-grid model. The number of modes \tilde{n}_r obtained by balanced truncation is chosen to be 5.

4.3.1. Observability of the modes

The observability of the modes is computed by checking the rank of the observability matrix Q_{ob} at any operating point defined as:

$$Q_{ob} = \begin{bmatrix} \tilde{\mathbf{C}}_r \\ \tilde{\mathbf{C}}_r \tilde{\mathbf{A}}_r \\ \tilde{\mathbf{C}}_r \tilde{\mathbf{A}}_r^2 \\ \vdots \\ \tilde{\mathbf{C}}_r \tilde{\mathbf{A}}_r^{\tilde{n}_r-1} \end{bmatrix} \quad (35)$$

The observability matrix Q_{ob} is shown to have full rank for any tested operating point meaning that the principal modes of the system are observable.

4.3.2. Observability of the states

The observability of the states cannot be easily computed via the observability matrix as in the case for the modes due to the large number of states. One would have to compute high powers of the Jacobian matrix \mathbf{A}_{wp} which becomes numerically unreliable. Instead, the observability of the states is analysed by using the transformation matrix $\tilde{\mathbf{T}}_r$. This matrix maps the states to the modes and by analysing the rows of this matrix, one can see in which direction in the state space all the dominant modes point to. In Fig. 5, one can see the entries of the rows of this matrix from top to bottom, starting with the most dominant mode on the top. Any location on the x-axis corresponds to a certain state and the value on the y-axis is the absolute value of the entry of each row of the matrix $\tilde{\mathbf{T}}_r$. Upon analysing the rows of this matrix, one can see that the modes of the system point in the direction of all domains, but only for the anode channel it is very weak, indicating that all domains except the anode channel are observable. The modes do not point in the direction of all states, but there is neither the need for it, as per the strong coupling between the adjacent states, the profiles will follow the observer's corrective action. To remedy the anode channel observability problem, it must be pointed out that the analysis of the transformation matrix entries must be supplemented with information about the known boundary conditions. Namely, for the anode channel, the inlet gas composition and pressure as well

as the outlet pressure are known which gives enough information for the system to be fully observable, as confirmed by the results in Section 6. To elaborate further, these values at the boundary are also part of the state vector, but the time evolution of these states is not computed, but imposed as an input, and that is the reason why in the transformation matrix entries, they do not show up since the observer will not correct them, but they are, of course, known, providing good observability.

5. Simulation experiment

In this section, the simulation scenario of the case study mentioned in the introduction is explained in detail. The performance of the observer is demonstrated using a more detailed simulation, considered as reality, to evaluate the convergence of all states inside the fuel cell. An evaluation of the observer based on real measurements is currently impossible, as no sensors are available to detect the distributed state inside the fuel cell.

5.1. Setup

The goal of the observer is to estimate all states of the fuel cell given in Eq. (3). In this work, special attention is paid to the along-the-channel spatial distribution of the following quantities:

- Current density i
- Membrane water content λ
- Species mole fractions in the cathode and anode gas channels γ_j , where $j \in \{\text{O}_2, \text{N}_2, \text{H}_2\text{O}\}$ for the cathode and $j \in \{\text{H}_2, \text{N}_2, \text{H}_2\text{O}\}$ for the anode

It is assumed that only a few inexpensive sensors are available to the observer for measurements, namely cell voltage and pressure at the system boundaries. In this experiment, the system is considered pressure-driven, therefore, the pressures at the system boundaries are set as boundary conditions, as seen in Eq. (5). The output of the system, available to the observer as measurement is the cell voltage $\mathbf{y}_{\text{meas}} = V$. If the fuel cell would be operated in a mass-driven mode, then the pressures at the system boundaries would also constitute the output vector. The measurements are subject to Gaussian noise with a standard deviation of 1% of the corresponding quantity. The system is excited with a time-varying input, the average current density, whose signal is seen in Fig. 6.

5.2. Simulation models and their resolution

Three simulation runs are performed:

- Measurement generation using a fine-grid model, referred to as *Actual*
- Reference simulation using a coarse-grid model without the observer, referred to as *Simulation*
- Estimation using a coarse-grid model with observer, referred to as *Observer*

The number of discretisation points, illustrated in Fig. 2, determine the resolution of the model. In the following simulation study, models of different sizes are used. First, a fine-grid model is used to generate the simulated reality that the observer will try to estimate, i.e. the *Actual* states distribution. The information on the internal states of this first simulation run is by no means known to the observer, which receives only information about the system outputs. The model used by the observer is a coarse-grid model, meaning that it has less discretisation points than the reality model, introducing a model error. The models' grid sizes and the time step size Δt are given in Table 4. To show the performance of the observer, it is always interesting to see what

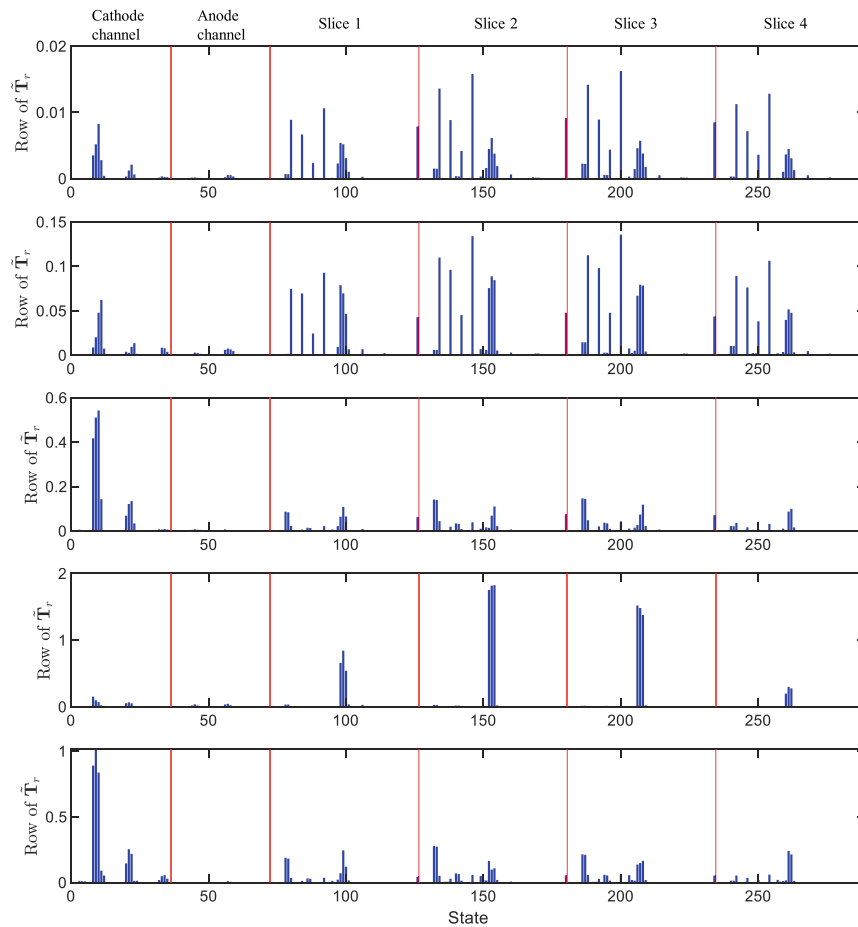


Fig. 5. Entries of the rows of the transformation matrix \tilde{T}_r . The top plot shows the entries for the first dominant mode, and so on until the bottom. The entries show the direction in which the observer corrects the system. The red lines separate the domains in the state vector. (For interpretation of the references to colour in this figure legend, the reader is referred to the web version of this article.)

would happen in a pure simulation, in which the observer is not active. In this *Simulation* run, the system is initialised differently than in the first run, as it is not possible to know the initial state conditions in reality. Also, the observer is not active. If the system is asymptotically stable, as it is the case for this model, the system will eventually converge towards the true state, regardless of the wrong initialisation. However, if the observer is active, it is aware of the error between simulation and reality and tries to match the states accordingly. In this third *Observer* simulation run with wrong initialisation, the system converges towards the true state faster, which is crucial for diagnostics and/or fault detection, especially if the initial error is large or if slow dynamics are present in the system. In Fig. 7, the voltage behaviour in all three simulation runs is shown as demonstration of the explained procedure.

6. Results and discussion

The results of the simulation are presented both in the form of figures in this paper as well as two videos which can be found in the supplementary material. The system is excited with the average current density demand as shown in Fig. 6. The vertical magenta lines in Figs. 6 and 7 mark the times for which the snapshots, i.e., Figs. 8 to 10 are plotted. In these figures, the top

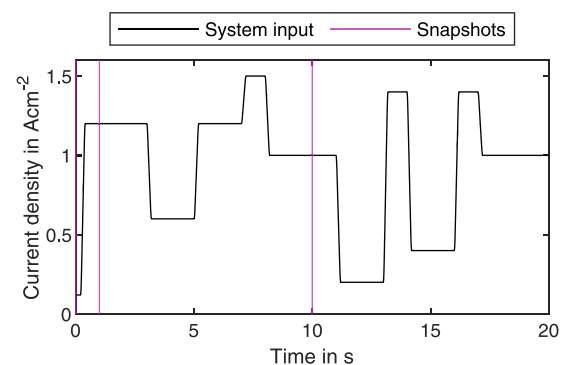


Fig. 6. Excitation signal. The solid black line is the input (average current density) trajectory and the magenta lines indicate the times where snapshots shown in Section 6 are taken. (For interpretation of the references to colour in this figure legend, the reader is referred to the web version of this article.)

plot is the system snapshot at the initial time $t = 0$ s, the middle plot shows the system at time $t = 1$ s and the bottom plot shows the system at time $t = 6$ s. The purpose of the figures is to give

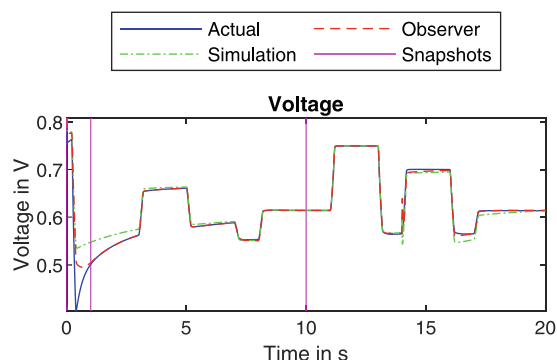


Fig. 7. Cell voltage. The observer (red line) converges towards the true value (blue line) faster than the uncorrected simulation (green line). The magenta lines indicate the times where snapshots shown in Section 6 are taken. (For interpretation of the references to colour in this figure legend, the reader is referred to the web version of this article.)

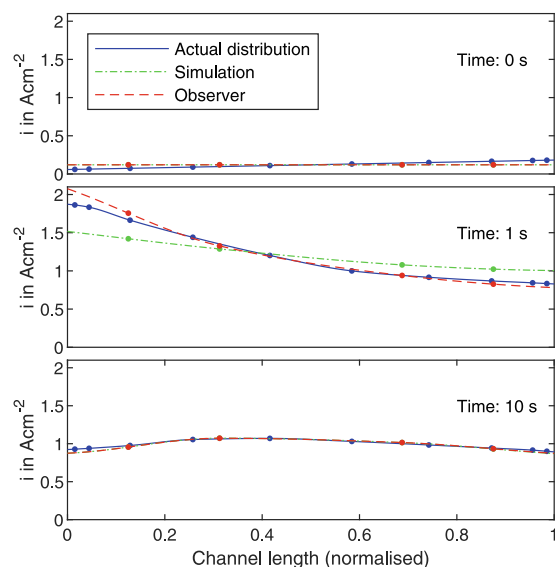


Fig. 8. Local current density distribution along the channel at different times. The reality model has 10 and the simulation model has 4 nodes. (For interpretation of the references to colour in this figure legend, the reader is referred to the web version of this article.)

the opportunity to visualise the procedure at a glance and to point out some interesting details, but the whole richness of the results is found in Videos 1 and 2.

6.1. Local current density and membrane water content

The current density distribution along the channel is shown in Video 1 (top plot) as well as in Fig. 8. The number of plotted nodes for the simulated reality fine-grid model is 10, equal to the number of slices (blue line). The simulation without the observer is plotted in green and the simulation where the observer is active is plotted in red. The number of nodes in the green and red lines is 4, equal to the number of slices of the coarse-grid model. The profile of all the states is interpolated with a Piecewise Cubic Hermite Interpolating Polynomial using the MATLAB `pchip` command. The current density distribution in the simulation model is

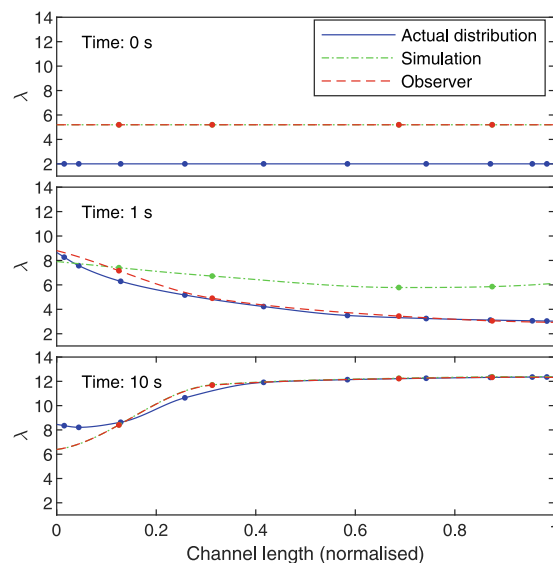


Fig. 9. Membrane water content distribution along the channel at different times. The observer converges towards the true state much faster than the uncorrected simulation.

initialised differently from reality, as it is not realistic to assume the initial distribution in reality to be known. In Video 1, the initialisation can be seen at time $t = 0$ s as well as in the top plot of Fig. 8. At time $t = 1$ s, in the middle plot of Fig. 8, one can see that the local current density distribution estimated by the observer already almost matches the true state. Furthermore, it is to be noted that the whole profile of the local current density distribution matches reality even though the coarse-grid model has fewer nodes and the nodes position is not equal to the ones in the fine-grid model. This highlights the robustness of the algorithm. At time $t = 6$ s, seen in the bottom plot of Fig. 8 both the simulation and the observer have converged towards the true state completely. The membrane water content is shown in Video 1 (middle plot) and Fig. 9. As with the current density, in the simulation, it is initialised differently than reality, as seen in Video 1 at time $t = 0$ s as well as in the top plot of Fig. 9. The main reason for the big voltage offset seen in Fig. 7 at the beginning of the simulation is exactly the membrane water content. The membrane is assumed to be too humid at this point and the observer corrects the error by dehumidifying the membrane quite fast, whereas the pure simulation takes long to dehumidify the membrane due to the slow water transport dynamics. This can be clearly seen in the middle and bottom plot of Fig. 9. In the figures, however, the transition from the initial value to the true state cannot be captured, but in Video 1, the transient can be clearly seen.

6.2. Species mole fractions

The second group of results are the species mole fractions shown in Fig. 10 and in Video 2. Unlike the local current density and membrane water content, the species mole fractions are initialised the same way in the fine-grid and coarse-grid models, but as already stated, the main effect for the voltage deviation is the error in the membrane water content. Since the membrane starts with a significantly higher water content in the simulation and observer than in the fine-grid model, the water is driven towards the channel at different rates because the concentration gradient

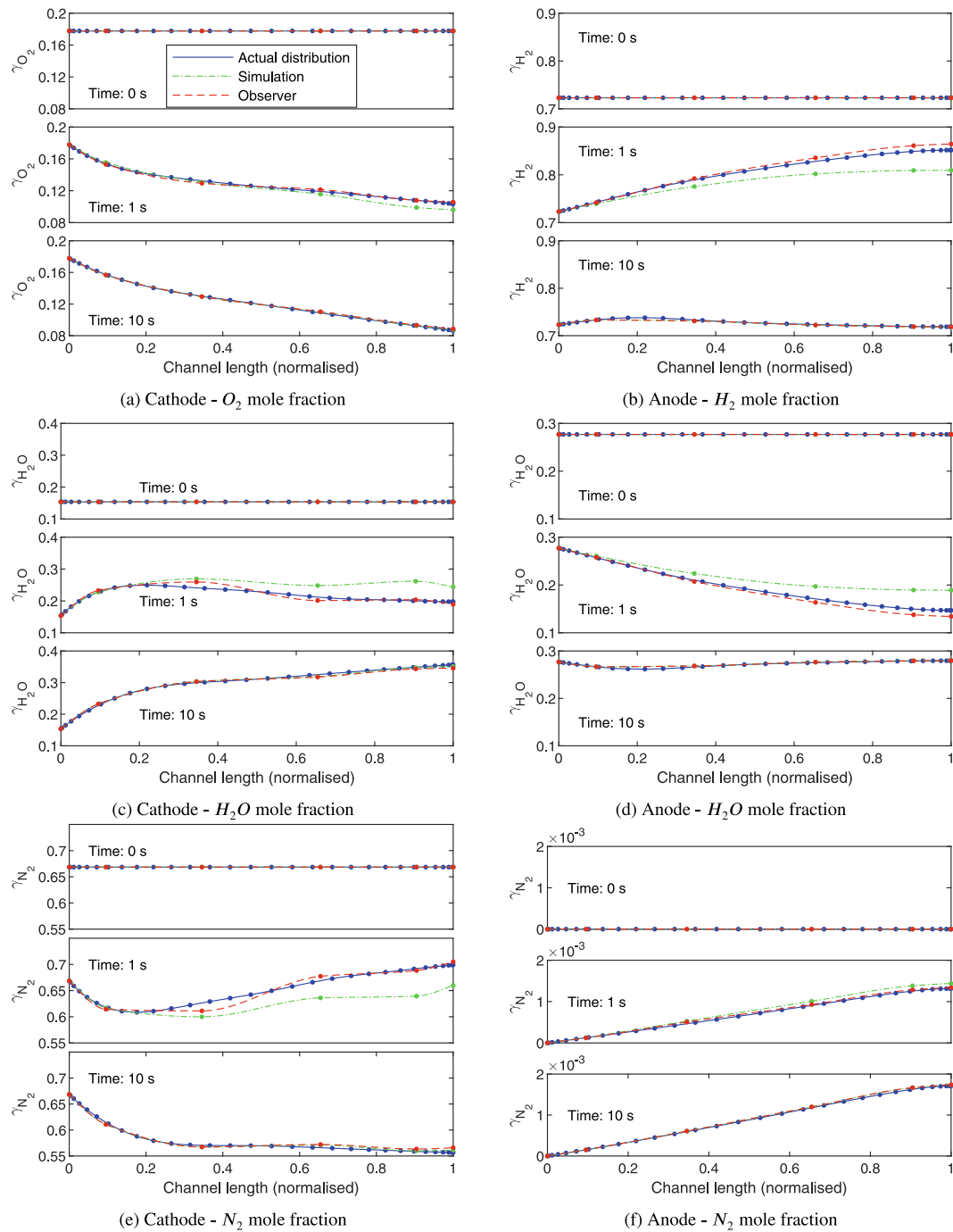


Fig. 10. The distribution of the species mole fractions along the cathode (a, c, e) and anode (b, d, f) channels. The actual distributions, denoted in blue, are generated by a high-fidelity fine-grid model. The green lines denote simulations of a coarse-grid model with no feedback from sensor data. The red lines indicate the distribution estimates generated by the proposed observer. (For interpretation of the references to colour in this figure legend, the reader is referred to the web version of this article.)

is different. In addition, the difference between simulation and observer comes from the corrective action of the observer. Very quickly, though, the observer corrects the mole fractions, visible in the middle and bottom plots of the state triplets in Fig. 10. There are 30 nodes in the gas channels for the reality model

and only 6 for the simulation model. An interesting detail can be observed in this experiment. For example, in the middle plot of Fig. 10(c), the water mole fraction in the cathode is seen. If the mole fraction at the end of the channel could be measured, and no observer existed, one would see that the simulation deviates

at that point by some value, but the actual error is larger than that – a significant portion of the whole profile is wrong. One would be ignorant to this fact from measuring the mole fraction at the outlet only. On the other hand, with an observer in place, one can estimate the distribution better, since by its very nature, the observer pushes the system towards reality.

7. Conclusion

Monitoring the internal states of a fuel cell is challenging but crucial for its safe and lasting operation. While measuring them is almost impossible or only realisable with highly expensive equipment, observers offer a good alternative to estimate the distributed states on the basis of models and a few simple measurements. However, realistic modelling of fuel cells leads to complex high-order systems described by partial differential equations. The implementation of such models in observers is not straightforward when keeping real-time feasibility and robustness in mind. In this work, we have developed an observer that uses a full fuel cell model to predict future states and reduced system Jacobians (dominant modes only) to update the predicted states based on measurements. The method has advantages in terms of good observability and computational efficiency, as only the dominant behaviour is considered in the correction of the predicted states, resulting in well-converging state estimates.

The developed method is tested using a high-fidelity simulated reality to best evaluate the convergence of the distributed system states. A model with wrong initialisation and model errors (coarser discretisation in space and time) is used as a reference simulation and serves as the basis for the observer. Only a few realistic and inexpensive sensors at the inlet and outlet of the fuel cell provide the observer with measurements. It turns out that the observer updates the simulation model correctly and quickly drives all states to their true values. The estimates of the distributed internal states converge well, allowing monitoring of critical states in the fuel cell. A pure simulation without observer correction leads to slow convergence and is not useful to improve the operation of a fuel cell.

The novel fuel cell observer is ready to be implemented in real-world applications, such as the automotive industry, where critical conditions may occur due to transient and dynamic operations and highly expensive laboratory measurement equipment is not available. Currently, the observer algorithm is being extended to include parameter estimation in addition to state estimation. This means that an imperfect model will correct itself, relaxing the need for perfect initial parametrisation, which would require expensive experimental tests. In future work, the observer can be extended with additional functionalities, e.g. estimation of changing parameters due to ageing processes.

CRedit authorship contribution statement

Martin Vrljić: Conceptualization, Methodology, Software, Simulations, Writing – original draft. **Dominik Pernsteiner:** Conceptualization, Methodology, Software, Simulations, Writing – original draft, Visualisation. **Alexander Schirrer:** Writing – reviewing and editing, Supervision. **Christoph Hametner:** Supervision, Funding acquisition. **Stefan Jakubek:** Supervision, Funding acquisition.

Declaration of competing interest

The authors declare that they have no known competing financial interests or personal relationships that could have appeared to influence the work reported in this paper.

Data availability

No data was used for the research described in the article

Acknowledgements

This work was funded by the FFG project AlpeDHues (grant number 884322) and the Christian Doppler Research Association. The authors acknowledge TU Wien Bibliothek for financial support through its Open Access Funding programme.

Appendix A. Supplementary data

Supplementary material related to this article can be found online at <https://doi.org/10.1016/j.egy.2023.06.006>.

References

- Benner, P., Gugercin, S., Willcox, K., 2015. A survey of projection-based model reduction methods for parametric dynamical systems. *SIAM Rev.* 57, 483–531. <http://dx.doi.org/10.1137/130932715>.
- Besselink, B., Tabak, U., Lutowska, A., Wouw, N.V.D., Nijmeijer, H., Rixen, D.J., Hochstenbach, M.E., Schilders, W.H.A., 2013. A comparison of model reduction techniques from structural dynamics, numerical mathematics and systems and control. *J. Sound Vib.* 332, 4403–4422. <http://dx.doi.org/10.1016/j.jsv.2013.03.025>.
- Brunton, S.L., Kutz, J.N., 2019. *Data-Driven Science and Engineering: Machine Learning, Dynamical Systems, and Control*. Cambridge University Press, Cambridge (U.K.), <http://dx.doi.org/10.1017/9781108380690>.
- Dobrokhoto, V., Larin, A., 2019. Multisensory gas chromatography for field analysis of complex gaseous mixtures. *ChemEngineering* 3, 1–18. <http://dx.doi.org/10.3390/chemengineering3010013>.
- Farrell, B.F., Ioannou, P.J., 2001. State estimation using a reduced-order Kalman filter. *J. Atmos. Sci.* 58, 3666–3680. [http://dx.doi.org/10.1175/1520-0469\(2001\)058<3666:SEUARO>2.0.CO;2](http://dx.doi.org/10.1175/1520-0469(2001)058<3666:SEUARO>2.0.CO;2).
- Hidayat, Z., Babuska, R., De Schutter, B., Núñez, A., 2011. Observers for linear distributed-parameter systems: A survey. In: 2011 IEEE International Symposium on Robotic and Sensors Environments. ROSE, pp. 166–171. <http://dx.doi.org/10.1109/ROSE.2011.6058523>.
- IEA, 2019. The future of hydrogen. URL: <https://www.iea.org/reports/the-future-of-hydrogen>. (Accessed 14 January 2022).
- IEA, 2021. Global hydrogen review 2021. URL: <https://www.iea.org/reports/global-hydrogen-review-2021>. (Accessed 14 January 2022).
- Inci, M., Büyük, M., Demir, M.H., Ilbey, G., 2021. A review and research on fuel cell electric vehicles: Topologies, power electronic converters, energy management methods, technical challenges, marketing and future aspects. *Renew. Sustain. Energy Rev.* 137, <http://dx.doi.org/10.1016/j.rser.2020.110648>.
- Jazwinski, A., 1970. *Stochastic Processes and Filtering Theory*. Academic Press, New York (NY, USA) and London (U.K.).
- Khodadadi, H., Jazayeri-Rad, H., 2011. Applying a dual extended Kalman filter for the nonlinear state and parameter estimations of a continuous stirred tank reactor. *Comput. Chem. Eng.* 35, 2426–2436. <http://dx.doi.org/10.1016/j.compchemeng.2010.12.010>.
- Lee, J., Nam, O., Cho, B.H., 2007. Li-ion battery SOC estimation method based on the reduced order extended Kalman filtering. *J. Power Sources* 174, 9–15. <http://dx.doi.org/10.1016/j.jpowsour.2007.03.072>.
- Lee, J., Nguyen, H.D., Escibano, S., Micoud, F., Rosini, S., Tengattini, A., Atkins, D., Gebel, G., Iojoiu, C., Lyonnard, S., Morin, A., 2021. Neutron imaging of operando proton exchange membrane fuel cell with novel membrane. *J. Power Sources* 496, <http://dx.doi.org/10.1016/j.jpowsour.2021.229836>.
- Luna, J., Husar, A., Serra, M., 2015. Nonlinear distributed parameter observer design for fuel cell systems. *Int. J. Hydrogen Energy* 40, 11322–11332. <http://dx.doi.org/10.1016/j.ijhydene.2015.05.132>.
- Luna, J., Jemei, S., Yousfi-Steiner, N., Husar, A., Serra, M., Hissel, D., 2016a. Nonlinear predictive control for durability enhancement and efficiency improvement in a fuel cell power system. *J. Power Sources* 328, 250–261. <http://dx.doi.org/10.1016/j.jpowsour.2016.08.019>.
- Luna, J., Usai, E., Husar, A., Serra, M., 2016b. Nonlinear observation in fuel cell systems: A comparison between disturbance estimation and high-order sliding-mode techniques. *Int. J. Hydrogen Energy* 41, 19737–19748. <http://dx.doi.org/10.1016/j.ijhydene.2016.06.041>.
- Luna, J., Usai, E., Husar, A., Serra, M., 2017. Enhancing the efficiency and lifetime of a proton exchange membrane fuel cell using nonlinear model-predictive control with nonlinear observation. *IEEE Trans. Ind. Electron.* 64, 6649–6659. <http://dx.doi.org/10.1109/TIE.2017.2682787>.
- Moore, B., 1981. Principal component analysis in linear systems: Controllability, observability, and model reduction. *IEEE Trans. Automat. Control* 26, 17–32. <http://dx.doi.org/10.1109/TAC.1981.1102568>.

- Murschenhofer, D., Kuzdas, D., Braun, S., Jakubek, S., 2018. A real-time capable quasi-2D proton exchange membrane fuel cell model. *Energy Convers. Manage.* 162, 159–175. <http://dx.doi.org/10.1016/j.enconman.2018.02.028>.
- Park, B.-G., Kim, J.-M., Kim, J.-W., Lee, K.-C., Koo, D.-H., Hyun, D.-S., 2013. New approach to EKF-based sensorless control using parallel structure for non-salient pole permanent magnet synchronous motors. In: 2013 International Conference on Electrical Machines and Systems. ICEMS, pp. 1099–1104. <http://dx.doi.org/10.1109/ICEMS.2013.6754407>.
- Pernsteiner, D., Schirrer, A., Kasper, L., Hofmann, R., Jakubek, S., 2021. State estimation concept for a nonlinear melting/solidification problem of a latent heat thermal energy storage. *Comput. Chem. Eng.* 153, 107444. <http://dx.doi.org/10.1016/j.compchemeng.2021.107444>.
- Sarmiento-Carnevali, M., Serra, M., Battle, C., 2017. Distributed parameter model-based control of water activity and concentration of reactants in a polymer electrolyte membrane fuel cell. *Int. J. Hydrogen Energy* 42, 26389–26407. <http://dx.doi.org/10.1016/j.ijhydene.2017.08.191>.
- Schmid, P.J., 2010. Dynamic mode decomposition of numerical and experimental data. *J. Fluid Mech.* 656, 5–28. <http://dx.doi.org/10.1017/S0022112010001217>.
- Simon, D., 2006. *Optimal State Estimation: Kalman, H ∞ , and Nonlinear Approaches*. John Wiley & Sons, Hoboken (NJ, USA), <http://dx.doi.org/10.1002/0470045345>.
- Wang, X.R., Ma, Y., Gao, J., Li, T., Jiang, G.Z., Sun, Z.Y., 2021. Review on water management methods for proton exchange membrane fuel cells. *Int. J. Hydrogen Energy* 46, 12206–12229. <http://dx.doi.org/10.1016/j.ijhydene.2020.06.211>.
- Wishner, R.P., Tabaczynski, J.A., Athans, M., 1969. A comparison of three non-linear filters. *Automatica* 5, 487–496. [http://dx.doi.org/10.1016/0005-1098\(69\)90110-1](http://dx.doi.org/10.1016/0005-1098(69)90110-1).
- Yuan, H., Dai, H., Wei, X., Ming, P., 2020. Model-based observers for internal states estimation and control of proton exchange membrane fuel cell system: A review. *J. Power Sources* 468, <http://dx.doi.org/10.1016/j.jpowsour.2020.228376>.
- Zaghloul, M.A.S., Mason, J.H., Wang, M., Buric, M., Peng, Z., Lee, S., Ohodnicki, P., Abernathy, H., Chen, K.P., 2021. High spatial resolution temperature profile measurements of solid-oxide fuel cells. *Appl. Energy* 288, <http://dx.doi.org/10.1016/j.apenergy.2021.116633>.

CURRICULUM VITAE

Personal Information

Name	Martin Vrlić
Date of Birth	8 March 1994
Birthplace	Buenos Aires, Argentina
Citizenship	Croatia



Education

10/2018 -	TU Wien Doctoral Programme in Engineering Sciences Mechanical Engineering
10/2015 - 09/2018	University of Split, Faculty of science Master Programme: Computational Physics Pass with distinction Thesis: "Obtaining high pressure in a diamond anvil cell at the Technical University of Vienna" Advisor: Prof.dr.sc. Ante Bilušić
10/2012 - 09/2015	University of Split, Faculty of science Bachelor Programme: Engineering Physics Pass with distinction Thesis: "Rotation in special theory of relativity" Advisor: Prof.dr.sc. Franjo Sokolić
09/2008 - 06/2012	Franciscan classical gymnasium Sinj (secondary school) Pass with distinction

Professional Work Experience

09/2022 -	Research consultant Founder Research centre RAQUEL
10/2018 - 07/2022	Project Assistant (Prae-Doc) TU Wien Research Unit of Control and Process Automation
03/2015 – 07/2015	Working student University of Split, Faculty of science

IT Skills

Operation Systems	Windows, Linux
Office	Microsoft Office, L ^A T _E X
Programming	MATLAB, Python, C, Arduino
Video editing	Adobe Premiere Pro, Kdenlive

Languages

Croatian	Native language
Spanish	Native language
English	Fluent in written and spoken
Italian	Basics
German	Basics

Leisure Interests

Traveling, Arduino programming, Psychology, Nature

LIST OF SCIENTIFIC PUBLICATIONS

International Journals

1. M. Vrlić, D. Ritzberger, and S. Jakubek. “Safe and efficient polymer electrolyte membrane fuel cell control using successive linearization based model predictive control validated on real vehicle data”. In: *Energies* 13.20 (2020). DOI: 10.3390/en13205353
2. M. Vrlić, D. Ritzberger, and S. Jakubek. “Model-predictive-control-based reference governor for fuel cells in automotive application compared with performance from a real vehicle”. In: *Energies* 14.8 (2021). DOI: 10.3390/en14082206
3. M. Vrlić, D. Pernsteiner, A. Schirrer, C. Hametner, and S. Jakubek. “Reduced-dimensionality nonlinear distributed-parameter observer for fuel cell systems”. In: *Energy Reports* 10 (2023), pp. 1–14. DOI: 10.1016/j.egyr.2023.06.006. URL: <https://doi.org/10.1016/j.egyr.2023.06.006>

International Conferences

1. M. Vrlic, D. Ritzberger, and S. Jakubek. “Efficient and life preserving power tracking control of a proton exchange membrane fuel cell using model predictive control”. In: *Proceedings of 2020 SICE International Symposium on Control Systems, SICE ISCS 2020* (2020), pp. 77–84. DOI: 10.23919/SICEISCS48470.2020.9083653
2. M. Vrlic and S. Jakubek. “Degradation avoiding start up and shut down of fuel cell stacks for automotive application using two plant model predictive control”. In: *2021 6th International Conference on Smart and Sustainable Technologies, SpliTech 2021* (2021), pp. 1–6. DOI: 10.23919/SpliTech52315.2021.9566412